

# Modeling, state observation and control of Compression System.

**Tove Helene Hovd**

Master of Science in Engineering Cybernetics

Submission date: May 2007

Supervisor: Jan Tommy Gravdahl, ITK

Co-supervisor: Erik Korssj en, Kongsberg Maritime



## Problem Description

The thesis covers the topics modeling and control of surge in compressors. Specifically, estimators, models for flow recirculation and a control algorithm is to be developed. The estimators are to be experimentally verified in the compressor lab at the Department of Engineering Cybernetics. The flow recirculation models and the surge avoidance control algorithm are to be simulated in Matlab/Simulink.

## Assignments:

1. A Kalman filter for estimation of mass flow in a compression system is to be formulated.
  - a. Derive Kalman filters for the compressor with and without compressor map.
  - b. Evaluate the pros and cons of estimating mass flow only against estimating both mass flow and pressure.
2. Verify the Kalman filters experimentally in the compressor lab.
3. A recycle loop is to be designed for the compressor lab
  - a. Investigate models for design of such a recycle loop.
  - b. Simulate designs for recycle.
  - c. Discuss pros and cons and practical aspects of the different models.
4. A control law for Surge Avoidance is to be designed
  - a. Define surge margin, and select the measurements needed for this.
  - b. Design a PI control law for Surge avoidance using a recycle loop.

Advisor: PhD-student Bjørnar Bøhagen

Assignment given: 08. January 2007

Supervisor: Jan Tommy Gravdahl, ITK



Modeling, state observation and control of Compression System.



# Preface

This thesis is the final result of a master assignment written at the Norwegian University of Science and Technology, department of Engineering Cybernetics. The report constitutes 100 % of the 10. semester of an MSc-degree. The report covers the theoretical deviations of different compression schemes, kalman filters and a study of industrial solutions for surge avoidance.

Through this assignment I have gained a thorough understanding of centrifugal compressors and how they function in the industry today. I have also learned how important the process of planning and investigation is prior to building a physical system, especially the importance of obtaining a good simulation model and using correct instrumentation. This has been an invaluable experience to me, and I hope I will be able to directly implement the knowledge I have gained in my future work.

I would like to thank Bjørnar Bøhagen for serving as my supervisor throughout this semester. His views, ideas and help have been of great value to the development of my assignment. I also want to thank my supervisor Jan Tommy Gravidahl for coming up with the initial idea to the thesis and helping me in the right direction as the assignment took its course. Erik Schnell and Erik Korssjøen at Kongsberg Maritime has helped me keeping focus on planning and seeing a project through, for this I am thankful. Lastly I would like to thank my office mates for creating a constructive and fun working environment.

Trondheim, May 30, 2007

Tove Helene Hovd



# Contents

	<b>Page</b>
Preface . . . . .	iii
Table of Contents . . . . .	v
List of Figures . . . . .	viii
Abstract . . . . .	xiii
<b>Chapter</b>	
1 Introduction . . . . .	1
2 Theory . . . . .	3
2.1 Compressor modeling . . . . .	3
2.1.1 The centrifugal compressor . . . . .	3
2.1.2 Shaft dynamics . . . . .	4
2.1.3 Mass balance . . . . .	6
2.1.4 Momentum equation . . . . .	7
2.1.5 Energy flow in recycle systems . . . . .	8
2.1.6 Resulting compression system with recycle line . . . . .	9
2.1.7 Model of compression system without feedback . . . . .	9
2.1.8 Downstream pressure measurements . . . . .	11
2.1.9 Generic component simulation model . . . . .	12
2.1.10 The surge phenomenon . . . . .	14
2.2 Compressor Control . . . . .	15
2.2.1 Industrial compression recycling systems . . . . .	17
2.2.2 Surge avoidance control . . . . .	20
2.3 Kalman filter . . . . .	23
2.3.1 Discrete kalman filter . . . . .	23
Extended kalman filter . . . . .	26
2.3.2 Continuous kalman filter . . . . .	28
Extended kalman filter . . . . .	32
3 Development, simulations and implementation . . . . .	33
3.1 Presentation of compressor model and lab set-up. . . . .	33
3.2 Matlab model of compression system . . . . .	36
3.3 Kalman filters . . . . .	37

3.3.1	Kalmanfilter 1 . . . . .	40
3.3.2	Kalmanfilter 2 . . . . .	43
3.3.3	Kalmanfilter 3 . . . . .	44
3.3.4	Kalmanfilter 4 . . . . .	45
3.4	Recycle system modeling . . . . .	46
3.4.1	Recycle directly downstream . . . . .	46
3.4.2	Recycling from plenum . . . . .	50
3.4.3	Simulation of generic component model . . . . .	51
3.5	Implementation and simulations surge avoidance. . . . .	53
4	Results and observations . . . . .	57
4.1	Results simulation of compression system. . . . .	57
4.2	Results simulations of kalman filters with no recycle feedback. . . . .	58
4.2.1	Kalman filter 1 . . . . .	58
4.2.2	Kalman filter 2 . . . . .	60
4.2.3	Kalman filter 3 . . . . .	62
4.2.4	Kalman filter 4 . . . . .	63
4.3	Results implementation of kalman filters on compression system. . . . .	65
4.3.1	Kalman filter 1 . . . . .	65
4.3.2	Kalman filter 2 . . . . .	68
4.3.3	Kalman filter 3 . . . . .	72
4.3.4	Kalman filter 4 . . . . .	73
4.4	Simulations recycling directly downstream . . . . .	75
4.5	Simulations recycling from plenum . . . . .	77
4.6	Simulations of generic component model. . . . .	79
4.7	Simulations surge avoidance schemes . . . . .	79
5	Discussion, conclusions and future work . . . . .	85
5.1	Discussion results of kalman filters . . . . .	85
5.2	Discussion recycle models . . . . .	87
5.2.1	Model recycling directly downstream. . . . .	87
5.2.2	Recycling from plenum . . . . .	88
5.2.3	Generic component model . . . . .	88
5.3	Discussion surge avoidance simulations . . . . .	89
5.4	Discussion practical aspects of building and modeling the recycle loop. . . . .	90
5.5	Conclusions . . . . .	92
5.6	Suggestions to future work . . . . .	93

Bibliography . . . . .	94
<b>Appendix</b>	
A Results implementation, Case 2 . . . . .	97
B Results implementation, Case 3 . . . . .	101
C Results implementation, Case 4 . . . . .	105
D Test plan recycle system . . . . .	109
E Testing of valve characteristics . . . . .	111
F Contents of added disc. . . . .	113

# List of Figures

2.1	Compressor with recycle loop . . . . .	4
2.2	Velocity Triangle . . . . .	5
2.3	Compression system without feedback . . . . .	10
2.4	Basic compression system. From Bøhagen (2007) . . . . .	11
2.5	Compressor characteristics: Stall . . . . .	15
2.6	Compressor characteristics: Deep surge . . . . .	16
2.7	Recycle system . . . . .	18
2.8	Hot recycle . . . . .	19
2.9	CCC recycle system . . . . .	20
2.10	Surge margin . . . . .	21
2.11	Implementation discrete kalman filter . . . . .	27
2.12	Linear continuous kalman filter . . . . .	31
3.1	Compressor map. From Bøhagen (2007). . . . .	35
3.2	Lab set-up of compression system. . . . .	35
3.3	Implementation of compressor. Pressure. . . . .	37
3.4	Implementation of compressor. Mass flow. . . . .	37
3.5	Simulink kalman filters . . . . .	39
3.6	Simulink kalman filter 1 . . . . .	41
3.7	Simulink subsystem "K" . . . . .	42
3.8	Simulink subsystem, kalman filter 2. . . . .	44
3.9	Principal sketch of compression system with recycling , duct and plenum. . . . .	47
3.10	Forcing term $F_{cu}$ in steady state. From (Bøhagen 2007). . . . .	48
3.11	Recycling from plenum. . . . .	50
3.12	Recycle from plenum using model suggested by Murphy et al. (1995). . . . .	52
3.13	Compressor map with surge lines . . . . .	54
4.1	Simulated and measured compressor values. . . . .	57
4.2	Estimates, filter 1 . . . . .	58
4.3	Innovation process, filter 1 . . . . .	59
4.4	Kalman gains, filter 1 . . . . .	59

4.5	Estimate, filter 2 . . . . .	60
4.6	Innovation process, filter 2 . . . . .	61
4.7	Kalman gain, filter 2 . . . . .	61
4.8	Estimates, filter 3 . . . . .	62
4.9	Innovation process, filter 3 . . . . .	62
4.10	Kalman gains, filter 3 . . . . .	63
4.11	Estimates, filter 4 . . . . .	64
4.12	Innovation processes, filter 4 . . . . .	64
4.13	Kalman gains, filter 4 . . . . .	65
4.14	Implementation: Estimates, filter 1 . . . . .	66
4.15	Imp: Innovation process, filter 1 . . . . .	67
4.16	Imp: Kalman gains, filter 1 . . . . .	67
4.17	Implementation: Estimate, filter 2 . . . . .	69
4.18	Imp: Innovation process, filter 2 . . . . .	70
4.19	Imp: Kalman gain, filter 2 . . . . .	70
4.20	Corrected mass flow filter . . . . .	71
4.21	Corrected mass flow filter, case 2 . . . . .	71
4.22	Implementation: Estimates, filter 3 . . . . .	72
4.23	Imp: Innovation process, filter 3 . . . . .	72
4.24	Imp: Kalman gains, filter 3 . . . . .	73
4.25	Implementation: Estimates, filter 4 . . . . .	73
4.26	Imp: Innovation processes, filter 4 . . . . .	74
4.27	Imp: Kalman gains, filter 4 . . . . .	74
4.28	Pressures up- and down-stream when recycling directly downstream 1 . . . . .	75
4.29	Pressures up- and down-stream when recycling directly downstream 2 . . . . .	76
4.30	Inlet mass flow $w_f$ with $L_3 = 50$ cm (top) and $L_3 = 150$ cm (bottom). . . . .	77
4.31	Pressures, feedback from plenum . . . . .	78
4.32	Mass flows, feedback from plenum . . . . .	78
4.33	Surge indication of avoidance scheme 1 . . . . .	80
4.34	Recycle valve . . . . .	80
4.35	Surge indication of avoidance scheme 2 . . . . .	81
4.36	Plenum pressure and mass flow . . . . .	81
4.37	Surge indication of avoidance scheme 3 . . . . .	82
4.38	Plenum pressure and mass flow. . . . .	83
4.39	Plenum pressure and mass flow with step in speed. . . . .	84

5.1	Compressor map . . . . .	87
5.2	T-section, suggest measure point . . . . .	91
A.1	Kalman filter 1: Estimated and measured states . . . . .	97
A.2	Kalman filter 1: Innovation process $p - \hat{p}$ . . . . .	97
A.3	Kalman filter 1: Kalman gains, pressure at top and mass flow at bottom. . . . .	98
A.4	Kalman filter 3: Estimated and measured states. . . . .	98
A.5	Kalman filter 3: Innovation process $p - \hat{p}$ . . . . .	98
A.6	Kalman filter 3: Kalman gains, pressure at top and mass flow at bottom. . . . .	99
A.7	Kalman filter 4: Estimated and measured states. . . . .	99
A.8	Kalman filter 4: Innovation processes $p - \hat{p}$ (top) and $p_c(w, N) - p_c(\hat{w}, N)$ (bottom). . . . .	99
A.9	Kalman filter 4: Kalman gains. . . . .	100
B.1	Kalman filter 1: Estimated and measured states . . . . .	101
B.2	Kalman filter 1: Innovation process $p - \hat{p}$ . . . . .	101
B.3	Kalman filter 1: Kalman gains, pressure at top and mass flow at bottom. . . . .	102
B.4	Kalman filter 3: Estimated and measured states. . . . .	102
B.5	Kalman filter 3: Innovation process $p - \hat{p}$ . . . . .	102
B.6	Kalman filter 3: Kalman gains, pressure at top and mass flow at bottom. . . . .	103
B.7	Kalman filter 4: Estimated and measured states. . . . .	103
B.8	Kalman filter 4: Innovation processes $p - \hat{p}$ (top) and $p_c(w, N) - p_c(\hat{w}, N)$ (bottom). . . . .	103
B.9	Kalman filter 4: Kalman gains. . . . .	104
C.1	Kalman filter 1: Estimated and measured states . . . . .	105
C.2	Kalman filter 1: Innovation process $p - \hat{p}$ . . . . .	105
C.3	Kalman filter 1: Kalman gains, pressure at top and mass flow at bottom. . . . .	106
C.4	Kalman filter 3: Estimated and measured states. . . . .	106
C.5	Kalman filter 3: Innovation process $p - \hat{p}$ . . . . .	106
C.6	Kalman filter 3: Kalman gains, pressure at top and mass flow at bottom. . . . .	107
C.7	Kalman filter 4: Estimated and measured states. . . . .	107
C.8	Kalman filter 4: Innovation processes $p - \hat{p}$ (top) and $p_c(w, N) - p_c(\hat{w}, N)$ (bottom). . . . .	107
C.9	Kalman filter 4: Kalman gains. . . . .	108

E.1	Step in valve, 0 – 100%. . . . .	112
E.2	Step in valve, 100 – 0%. . . . .	112



# Abstract

The need of simulation models for physical systems is essential in all phases of its life-time. During construction better decisions can be made and difficulties discovered. When running observers one can use the model to estimate states. Knowledge of the system is also needed to develop good control strategies.

A compression system without surge avoidance recycling exists, and its mathematical development and simulation model was studied and simulated. Kalman filters were developed in theory, four filters were designed and lastly implemented. A study of industrial solutions for surge avoidance was performed, with attention to practical building, measurements, mathematical modeling and control. The study resulted in three simulation models for recycling that were fitted to the compressor at hand. Lastly a surge avoidance system was implemented on the model most likely to be built.

A good simulation model of the existing compressor is available, and using this three well working kalman filters were implemented. A fourth filter yielded non-unique and sometimes unstable estimates, and emphasized the importance of retrieving enough information from the measurements to estimate the correct state.

All recycle system models used the characteristics of the existing compressor. The solution most likely to be implemented and form basis for a simulation model recycled gas directly downstream of the compressor. The other two models retrieved the recycled gas from the plenum, however this will change the dynamics of the system. These were not considered practical solutions for the specific system. The surge avoidance scheme worked well for production close to the surge line and small set-point changes. It also worked well for large changes in speed, but will surge if the speed becomes too low. The controller scheme did not work well when a large change in plenum throttle occurred, the recycle valve was then too slow. Future work consists of building a recycle loop, develop simulation model and implement surge avoidance scheme for academic purposes.

# Chapter 1

## Introduction

In this assignment an extensive research of centrifugal compressor modeling, state observation and control was performed with the purpose of mounting a surge avoidance recycle system on a laboratory compressor. An investigation of the already existing system was performed, and a simulation model was built and tested based on measurement data available. Four kalman filters were then developed for estimation of mass flow and filtering of pressure measurements. These were simulated and implemented on the existing compressor. A theoretical investigation of industrial standards for gas recycling in compression systems was then performed. Three solutions to building a recycle loop in the existing system were investigated, simulated and evaluated with regards to practical aspects such as available valves, physical room size and combination with already implemented control scheme. Lastly a surge avoidance control scheme was simulated on one of the recycle models.

The importance of being able to run good simulations of physical systems can not be stressed enough. When the plant has started production there is normally not room for changes in variables or set-points unless one is certain of what effect the change will have on the plant and its surroundings. Also when planning and building a system it will be essential to have good simulation models so that design ideas can be tested, and possible problems avoided. It is by far cheaper to put a system into failure in a simulation than in real life where the financial cost may become enormous and threat to health in certain cases can be an even greater danger.

Control and safety systems constitute a major part of industrial plants, including instrumentation, observers and control algorithms. The need to at all time knowing the value of certain states is essential to be able to run the plant efficient and safely. Simulations using realistic data can be invaluable for the development of observers. A centrifugal compressor in the oil and gas industry is an example of a system that would need both observer and control system. They are often of a great size, demanding a large amount of energy to run at requested level. Knowledge of the exact system together with a simulation model are important tools to keep the compressor running safe and optimize

production.

Being that one can not always measure all the states that needs to be controlled in a system such as a compressor, an observer is needed. Kalman filters were first introduced in 1960 and has since then grabbed hold as a state observer being that computer power grew rapidly in the period after its introduction. By using a kalman filter one is able to both filter measured states as well as estimate non-measurable, but observable, states. In a compression system mass flow is often hard to measure, especially when surge occurs and the direction of the mass flow alternates. For control purposes we always want to know the value of states that needs to be controlled, and a kalman filter ensure this.

There exists a centrifugal compressor laboratory at NTNU, and this was the basis for this thesis. Today the system is set up for active surge control, but hopefully in the future the system will be changed in such a manner that also a somewhat different control scheme, surge avoidance control, can be used on the system for academic purposes. This goal has been kept in mind throughout the whole thesis, and results presented take its basis in what will be possible to build on the lab system. Still it was important to investigate different solutions to see how they would affect the already working system, and to fully understand the effects of early decisions in a building process. Hopefully, this report will be used as a guide when the recycle part is being installed.

This document is divided into five chapters. In chapter 2 a theoretical deviation of a centrifugal compressor with recycle feedback using a Greitzer surge model is presented. The equations describing a compressor with duct, plenum and throttle is also presented together with some practical aspects to modeling based on pressure measurements. A generic component model of a recycle system is then presented. The surge phenomena and aspects of industrial compressor systems and control is discussed. Lastly a deviation of the kalman filter is presented, starting with the original discrete-time linear filter and ending with a presentation of the extended continuous kalman filter.

Chapter 3 gives a presentation of all developments, simulations and implementations performed in this assignment. The reader is shortly introduced to the laboratory compressor set-up as well as the simulation model for the existing compressor system. The four kalman filters are then presented. Three simulation models of the known compressor with added recycle line are developed and simulated before one model is chosen for simulation of a surge avoidance control scheme.

In chapter 4 the results from all simulations and implementations are presented and commented upon, before a discussion in chapter 5 leads to the conclusions and suggestions of future work.

# Chapter 2

## Theory

### 2.1 Compressor modeling

Compressors are used in several areas of industry, ranging from turbo jet engines to cooling systems to pressurization of gas in the process industry. There are four general types of compressors: reciprocating, rotary, centrifugal and axial compressors. The two first aims to reduce gas volume while the two latter work to increase the potential energy in the fluid manifested in pressure rise (Egeland & Gravdahl 2003). The focus in this thesis will be on a centrifugal compressor. Three presentations of such a compressor and its surrounding system will here be presented. A compressor with recycle feedback and driven by a drive torque  $\tau_d$  from a motor, is modeled with equations for shaft dynamics, mass balance and momentum. A second model of a compression system without feedback is also presented. Lastly, a model of a compression system with recycling somewhat different from the first is presented. The deviation of the first two compression systems is based on Egeland & Gravdahl (2003), chapter 13, unless otherwise is specified.

#### 2.1.1 The centrifugal compressor

The centrifugal compressor consists mainly of a stationary casing containing a rotating impeller, as well as a diffuser and collector/volute (Bøhagen 2007). It is in the impeller that the fluids are accelerated to increase the kinetic energy. This energy is then converted into potential energy by decelerating the fluid in diverging channels, the diffuser, which also is a fixed part of the casing. This is either vaned or unvaned. The fluids flows from the impeller through the diffuser to a collector/volute before it leaves the compressor. The impeller is mounted either on a drive shaft or a separate shaft driven through couplings (Egeland & Gravdahl 2003). A compressor with one impeller is referred to a single-stage compressor. Multiple stage compressors contain more than one impeller in series, sharing the same drive shaft. This way the pressure rise is increased in stages reaching higher values (Bøhagen 2007).

## 2.1.2 Shaft dynamics

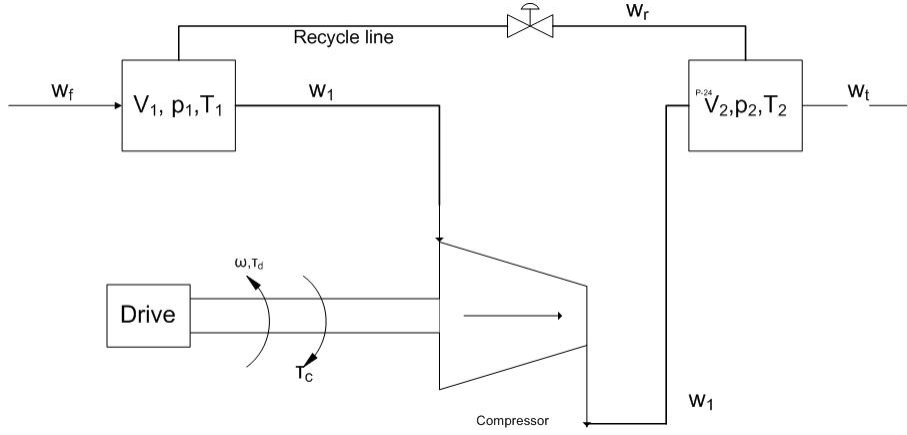


Figure 2.1: A centrifugal compressor with recycle loop and motor.

A principal sketch of a compression system with surge control feedback can be seen in figure 2.1. We assume that the compressor is driven by an electrical motor. The compressor shaft dynamics are given by:

$$J\dot{\omega} = \tau_d - \tau_c \quad (2.1)$$

where  $\tau_d$  is the drive torque from the shaft,  $\tau_c$  is the compressor torque acting on the compressor shaft from the rotor blades. The inertia of the compressor shaft and wheel is  $J$  and finally  $\omega$  is the angular velocity of the shaft.  $\tau_c$  is expressed as the rate of change of angular momentum given by:

$$\tau_c = w_1(r_2 C_{\theta 2} - r_1 C_{\theta 1}) \quad (2.2)$$

Here  $w_1$  is the mass flow into the compressor,  $C_{\theta 1}$  is the tangential velocity of the fluid at the rotor inlet,  $C_{\theta 2}$  is the velocity at the rotor outlet,  $r_1$  and  $r_2$  are the radius of the rotor in- and outlet. Figure 2.2 shows the rotor outlet.  $C_{\theta 1}$  is normally set to zero under the assumption that there is no pre-whirl. The torque can now be written as

$$\tau_c = w_1 r_2 C_{\theta 2} \quad (2.3)$$

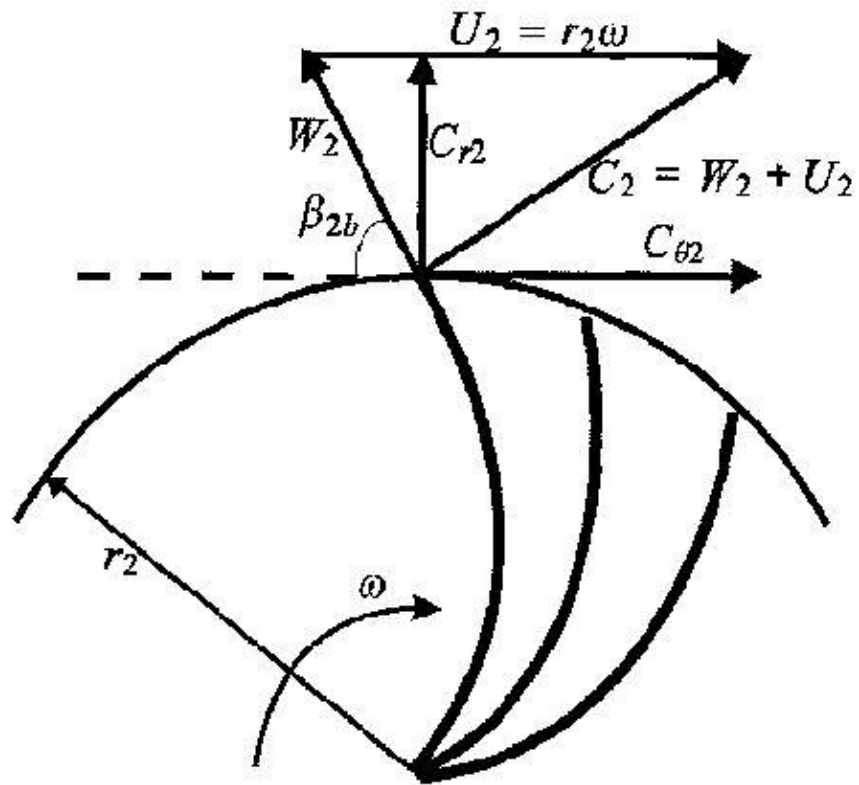


Figure 2.2: Velocity triangle at impeller exit. From Egeland & Gravdahl (2003)

For back swept blades in the impeller, we see from figure 2.2 that a further derivation of  $C_{\theta 2}$  is possible.

$$\begin{aligned}
 C_{\theta 2} &= U_2 - C_{r2} \cot \beta_{2b} \\
 &= (1 - \phi \cot \beta_{2b})U_2 \\
 &= \mu(\phi)U_2
 \end{aligned}
 \tag{2.4}$$

$C_{r2}$  is radial flow velocity and  $U_2$  is the tangential speed of the impeller tip:

$$U_2 = r_2\omega
 \tag{2.5}$$

The tangential speed at the impeller tip is denoted  $\phi$  and written as

$$\phi = \frac{C_{r2}}{U_2} = \frac{w_1}{\rho_1 A_1} \frac{r_2}{\omega}
 \tag{2.6}$$

The energy transfer coefficient is described by

$$\mu(\phi) = 1 - \phi \cot \beta_{2b} \quad (2.7)$$

The torque of the compressor can now be written as

$$\tau_c = w_1 \mu(\phi) r_2^2 \omega \quad (2.8)$$

### 2.1.3 Mass balance

The mass balance of the downstream volume in figure 2.1 is described by

$$V_1 \dot{\rho}_1 = w_f - w_1 + w_r \quad (2.9)$$

where  $V_1$  is the downstream volume,  $w_f$  is mass flow into the downstream volume and  $w_1$  is mass flow through the compressor.  $w_r$  is the recycle mass flow given as

$$w_r = k_r \sqrt{\Delta p_r} \quad (2.10)$$

where  $\Delta p_r$  is the pressure drop across the valve and  $k_r$  is a gain proportional to the opening of the valve in the recycle loop.

Assuming that the gas is ideal and isentropic it can be shown that

$$dp_1 = c_{01}^2 d\rho_1 \quad (2.11)$$

$$c_{01} = \sqrt{\kappa R T_1} \quad (2.12)$$

where  $c_{01}$  is the sonic velocity in the volume. The mass balance of the downstream volume can now be developed from combining the equations 2.9 and 2.11

$$\dot{p}_1 = \frac{c_{01}^2}{V_1} (w_f - w_1 + w_r) \quad (2.13)$$

We assume the same sonic velocity of the gas in the upstream volume, the mass balance can now here be described by

$$\dot{p}_2 = \frac{c_{01}^2}{V_2} (w_1 - w_r - w_t) \quad (2.14)$$

$V_2$  is the upstream volume. The throttle flow  $w_t$  is dependent of the plenum pressure, and can be modeled as a function of the pressure drop over the throttle and the throttle opening as suggested in Gravdahl (1998).

$$w_t(p_2) = k_t \sqrt{p_2 - p_t} \quad (2.15)$$

The pressure outside the throttle is here  $p_t$ .  $k_t$  is the throttle gain proportional to the opening of the throttle.

## 2.1.4 Momentum equation

An expression for mass flow in the duct from the outlet of the compressor to the upstream volume in figure 2.1 is developed based on the momentum balance. A control volume is considered. Assuming the flow is incompressible, the mass flow in the duct will be given as

$$w_1 = \rho AC \quad (2.16)$$

Bøhagen (2007) also assumes one dimensional flow through the duct, and this assumption will also be used here.  $C$  is the velocity of the fluid along the duct, and it is assumed to be constant. The density in the duct is  $\rho$  and  $A$  is the area of the cross-section of the duct. The momentum for the volume is given by

$$\frac{d(LA\rho)C}{dt} \quad (2.17)$$

$L$  is the length of the duct. The velocity of the fluids can be written

$$C = \frac{q}{A} = \frac{w_1}{\rho A} \quad (2.18)$$

where  $q$  is the duct volume flow. By inserting the expression for  $C$  into equation (2.17) the momentum becomes

$$\frac{d}{dt}(Lw_1) = L\dot{w}_1 \quad (2.19)$$

The sum of the forces working on the fluid in the control volume are the surface forces plus the resulting force from the compressor (Bøhagen 2007)

$$\sum F = Ap_1 - Ap_2 + F'_c \quad (2.20)$$

By writing  $F_c = \frac{1}{A}F'_c$  for convenience, the mass flow of the compressor is described by

$$\dot{w}_1 = \frac{A}{L}(p_1 - p_2 + F_c) \quad (2.21)$$

Bøhagen (2007) describes that assumptions of incompressible and one-dimensional flow does not hold in the compressor locally, both density and fluid velocity will vary along the flow path,  $F_c$  may therefore not be expected to behave linearly. The resulting force from the compressor can be described as a function of the mass flow and impeller speed,  $F_c(w_1, \omega)$ , where  $w_1$  reflects the fluid speed and mass.  $F_c(w_1, \omega)$  is normally

described as a nonlinear mapping of the mass flow and the impeller speed in steady-state,  $F_c(w_1, \omega) = p_2 - p_1$ . For notational reasons we now rewrite the mass flow equation by defining  $p_c(w_1, \omega) = F_c(w_1, \omega) + p_1$ . The mass balance is now

$$\dot{w}_1 = \frac{A}{L}(p_c(w_1, \omega) - p_2) \quad (2.22)$$

The power of the compressor is normally described by the compressor characteristic,  $\Psi_c$ , that reflects the steady-state compressor pressure rise as an expression mass flow and impeller speed,  $\Psi(w_1, \omega) = \frac{p_2}{p_1}$ . A relation to the resulting force of the compressor in steady-state can now be drawn

$$\Psi_c = 1 + \frac{F_c(w_1, \omega)}{p_1} \quad (2.23)$$

The compressor characteristic is normally expressed through a compressor map fitted to the specific compressor. An example of such can be seen in figure 3.1, showing the pressure rise for different speeds as an expression of mass flow. For a mathematical description the reader is referred to Egeland & Gravidahl (2003). An expression for mass flow using measured pressures instead of a compressor map will be presented later in this chapter.

### 2.1.5 Energy flow in recycle systems

When the gas is compressed, the temperature rises, and if the gas is recycled the temperature will increase more if not any action is taken. Coolers are commonly used to ensure that the gas recycled does not infer too much with the efficiency of the compressor. A study of the energy flow from Egeland & Gravidahl (2003) follows, deriving an expression for the change in temperature for a volume, for example  $V_2$  in figure 2.1.

Combining the mass balance for a volume  $V_j$

$$\dot{m} = w_{in} - w_{out} \quad (2.24)$$

with the energy balance of the same volume

$$\frac{d}{dt}U = \sum_i w_i h_i - Q \quad (2.25)$$

$U$  is the internal energy and  $h = c_p T$  is the specific enthalpy. We may express  $U = mu = mc_v T$ , where  $u = c_v T$  is the specific internal energy.  $c_p$  and  $c_v$  are the specific heats at

constant pressure and volume. Assuming ideal gas

$$pV = mRT \quad (2.26)$$

the energy balance can be written

$$\frac{d}{dt}(mu) = \sum_i w c_p T_i - Q \quad (2.27)$$

$$(w_{in} - w_{out})u + m c_c \dot{T} = w_{in} c_p T_{in} - w_{out} c_p T + Q \quad (2.28)$$

By utilizing that  $R = c_p - c_v$  the energy balance becomes

$$\dot{T} = \frac{RT}{pV c_v} (w_{in} c_p T_{in} - (w_{out} R + w_{in} c_v) T + Q) \quad (2.29)$$

## 2.1.6 Resulting compression system with recycle line

The resulting compressor model with a recycle line driven by a shaft can be summarized as

$$\dot{p}_1 = \frac{c_{01}^2}{V_1} (w_f - w_1 + w_r) \quad (2.30)$$

$$\dot{p}_2 = \frac{c_{01}^2}{V_2} (w_1 - w_r + w_t) \quad (2.31)$$

$$\dot{w}_1 = \frac{A}{L} (p_c(w_1, \omega) - p_2) \quad (2.32)$$

$$\dot{\omega} = \frac{1}{J} \tau_d - \tau_c \quad (2.33)$$

## 2.1.7 Model of compression system without feedback

A compression system without the feedback loop is also described from shaft dynamics, mass balance and momentum. Such a system can be seen in figure 2.3, containing a compressor, duct, plenum volume and throttle. The shaft dynamics will be the same as for the recycling compression system, since it is not directly affected by the feedback. However, the model of the compressor is somewhat easier, considering that there is now only one volume, namely the plenum.

The mass balance of the plenum volume  $V_p$  is now dependent of the sonic velocity of

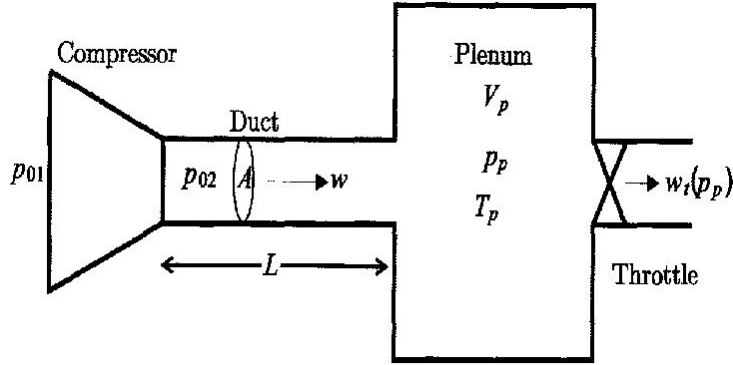


Figure 2.3: Compression system. Retrieved from Egeland & Gravdahl (2003)

the gas and plenum volume, as well as the mass flow difference between the input and output of the plenum.

$$\dot{p}_p = \frac{c_p^2}{V_p}(w - w_t(p_p)) \quad (2.34)$$

The sonic velocity  $c_p = \sqrt{\kappa RT_p}$  is also here based on the assumption that the gas is ideal and isentropic. The mass flow from the duct to the plenum is  $w$ . The mass flow through the throttle is dependent of the plenum pressure drop and throttle opening

$$w_t(p_p) = k_t \sqrt{p_p - p_{01}} \quad (2.35)$$

The pressure of the inlet to the compressor,  $p_{01}$ , is often set to the atmospheric pressure.

The momentum equation is developed in the same manner as for the control loop compression system and yields the equation

$$\dot{w} = \frac{A}{L}(p_c(w, \omega) - p_p) \quad (2.36)$$

where  $L$  is the length the gas travels from the compressor to the plenum and  $A$  is the area of the duct.

A resulting model for a compression system without gas recycling, using the names

of figure (2.3) is

$$\dot{p}_p = \frac{c_p^2}{V_p}(w - w_t) \quad (2.37)$$

$$\dot{w} = \frac{A}{L}(p_c(w, \omega) - p_p) \quad (2.38)$$

$$\dot{\omega} = \frac{1}{J}(\tau_d - \tau_c) \quad (2.39)$$

### 2.1.8 Downstream pressure measurements

When a compression system is simulated or described mathematically, a compressor map describing the characteristics is needed for the equation of mass flow. But for control- or observer-purposes a description of the compressor characteristics based on available measurements could be an option. Bøhagen (2007) presents how such an expression can be derived for a basic compression system without control feedback, and will here be presented. In figure 2.4 a basic compression system is presented, the system is the same

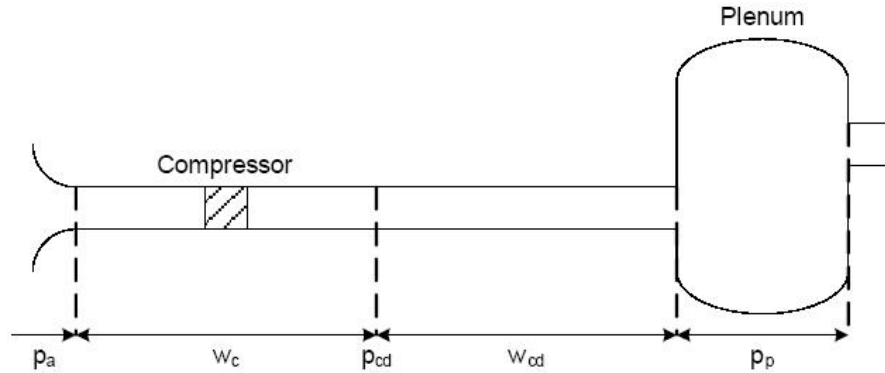


Figure 2.4: Basic compression system. From Bøhagen (2007)

as in figure 2.3 but the duct between the compressor and the plenum is split into two theoretic parts. The compressor draws air from the system surroundings. The mass flow from the compressor inlet to the plenum is divided in two parts, the mass flow through the compressor  $w_c$  and the downstream mass flow  $w_{cd}$ .

$$\dot{w}_c = \frac{A}{L_c}(p_a + F_c(w, \omega) - p_{cd}) \quad (2.40)$$

$$\dot{w}_{cd} = \frac{A}{L_{cd}}(p_{cd} - p_p) \quad (2.41)$$

The length of the duct is now divided into two parts,  $L = L_c + L_{cd}$ , by the place where downstream pressure  $p_{cd}$  is measured. It is however important to mention that the lengths are not the same as the physical duct, but rather the distance the gas travels to reach the plenum. The flow of the lower part of the duct,  $w_{cd}$  is assumed to be incompressible.

The mass flow in the duct is still assumed to be one dimensional, incompressible and constant area, so that  $w_c = w_{cd}$ , and therefore  $\dot{w}_c = \dot{w}_{cd}$ . From this an expression of the resulting force for the compressor is derived.

$$F_c(w, \omega) = \frac{1}{L_{cd}}(p_{cd} - p_p) + (p_{cd} - p_a) \quad (2.42)$$

The pressures and forcing term are in steady state related by  $p_{cd} = p_p$  and  $F_c(w_c, \omega) = p_{cd} - p_a = p_p - p_a$ . The compressor characteristic is in this set-up  $\Psi_c = \frac{p_{cd}}{p_a}$ , and in steady state  $\Psi_c = 1 + \frac{F_c(w, \omega)}{p_a}$ .

The mass flow equation (2.40) can now be written as an expression of measurable pressures and identifiable sizes. By inserting eq. (2.42) to substitute for  $p_{cd}$  in eq. (2.40) it can be shown that

$$\dot{w}_c = \frac{A}{L_c + L_{cd}}(p_a + F_c(w, \omega) - p_p) \quad (2.43)$$

Equation (2.43) describes the mass flow from the inlet of the compressor to the plenum. By using the relation in eq. (2.42) to substitute for  $F_c(w, \omega)$ , a model of the mass flow utilizing only measurable pressures and known parameters is written

$$\dot{w}_c = \frac{A}{L_c + L_{cd}} \left( \left( 1 + \frac{L_c}{L_{cd}} \right) p_{cd} - \frac{L_c}{L_{cd}} p_p - p_p \right) \quad (2.44)$$

A parallel can be drawn to that of eqs. (2.22) and (2.38), and we recognize

$$\left( 1 + \frac{L_c}{L_{cd}} \right) p_{cd} - \frac{L_c}{L_{cd}} p_p = p_c(t) = p_c(w, \omega) \quad (2.45)$$

### 2.1.9 Generic component simulation model

In Murphy et al. (1995) a generic component model for a compression system with recycling valve is presented together with the corresponding state space description. It uses mass, momentum and energy conservation laws of one-dimensional flow. The article presents a single stage compression system operating between two constant pressures, with a recycle and load throttle. The model does not say anything about defined volumes

up- and down-stream the compressor, compared to the model suggested in figure 2.1. The generic model is presented, with nomenclature in table 2.1 as

$$\frac{1}{T_{in}}\dot{p}_{in} + \frac{1}{T_{out}}\dot{p}_{out} = \frac{2\gamma R}{V_s}(w_{in} - w_{out}) \quad (2.46)$$

$$\dot{w}_{in} + \dot{w}_{out} = \frac{2A_s}{L_s}(\Psi_c(p_{in}, w_{in}, \omega) - p_{out}) \quad (2.47)$$

$$J\dot{\omega} + \beta\omega + \frac{\dot{E}_{NET}}{\omega} + T_{ext} = 0 \quad (2.48)$$

$$T_{out} = T_{in} + \frac{\dot{E}_{NET}}{C_p w_{in}} \quad (2.49)$$

$$\dot{E}_{NET} = \frac{F_{NET}(p_{in}, w_{in}, \omega)}{c_p \rho(p_{in}, T_{in}) \eta} \quad (2.50)$$

$$F_{NET} = (r(w_{in}, \omega) - 1) p_{in} \quad (2.51)$$

A state space model is then presented for the compressor system:

$$\dot{p}_{out} = \frac{2\gamma R}{V_s} T_{out} (w_{in} - w_{out}) \quad (2.52)$$

$$\dot{w}_{in} = \frac{2A_s}{L_s} (\Psi_c(w_{in}, \omega) - p_{out}) - \dot{w}_{out} \quad (2.53)$$

$$0 = p_L - p_{out} + K_L(u_L)(w_{out} - w_R)^2, \quad w_{out} - w_R \triangleq w_L \quad (2.54)$$

$$0 = p_{in} - p_{out} + K_R(u_R)w_R^2 \quad (2.55)$$

$$\dot{w}_{out} = \dot{w}_R + \dot{w}_L \quad (2.56)$$

$$= \frac{2\gamma R}{V_s} T_{out} \left( \frac{\partial \Psi_L}{\partial p_{out}} + \frac{\partial \Psi_R}{\partial p_{out}} \right) (w_{in} - w_{out}) + \frac{\partial \Psi_L}{\partial u_L} \dot{u}_L + \frac{\partial \Psi_L}{\partial u_R} \dot{u}_R \quad (2.57)$$

$$T_{out} = \xi_3 + \frac{F_{NET}(p_{in}, w_{in}, \phi)}{C_p \rho_1(p_{in}, \xi_3)} \quad (2.58)$$

The model presents a dynamical description of what is believed to be the mass flow in,  $w_{in}$  and the mass flow out of the compressor  $w_{out}$ . The inlet pressure  $p_{in}$  is assumed to be constant ambient pressure, while  $p_{out}$  is the pressure downstream of the compressor.  $p_L$  is the load exit pressure,  $w_L$  is the mass flow through the load valve. The mass flow through the recycle valve is  $w_r$ . The temperature of the gas leaving the compressor  $T_{out}$  is described in eq. (2.58). There are some uncertainties to this model due to lack of descriptions, but it is assumed that  $\xi_3 = T_{in}$  and  $\phi = \omega$ . Also, the transfer between eq. (2.50) to (2.58) is not mathematically clear, but not further described in the literature.

$A_s$	Cross sectional area	$\Psi_c$	Comp. characteristics
$c_p$	Specific heat	$\Psi_L, \Psi_R$	Load, recycle char
$L_s$	Compressor length	$K_L, K_R$	Valve loss coefficients
$V_s$	Compressor volume	$\beta$	Viscous friction
$r$	Pressure ratio	$\dot{E}_{NET}$	Net blade power
$w$	Mass flow	$\gamma$	Specific heat ratio
$p$	Pressure	$\rho$	Density
$R$	Gas constant	$\eta$	Efficiency
$T$	Temperature	$\omega$	Rotational speed
$T_{ext}$	Ext. torque	$J$	Inertia

Table 2.1: Nomenclature of generic component model (Murphy et al. 1995).

Murphy et al. (1995) uses the following characteristic descriptions

$$\Psi_c(w_{in}, \omega, p_{in}) = p_{in} r(w_{in}, \omega) \quad (2.59)$$

$$\Psi_L(p_{out}, u_L, p_L) = \pm \sqrt{\frac{(p_{out} - p_L)}{K_L(u_L)}} \quad (2.60)$$

$$\Psi_R(p_{out}, u_R, p_{in}) = \pm \sqrt{\frac{(p_{out} - p_{in})}{K_R(u_R)}} \quad (2.61)$$

### 2.1.10 The surge phenomenon

The operation of compressors is limited by flow instabilities called rotating stall and surge. Rotating stall is a local instability where the mass flow in one or more regions stagnate. The regions propagate in the same directions as the blades in the compressor with a speed somewhere between 20-70% of the rotor speed (de Jager 1995), (de Jager & Willems 1998). This leads to a change in the characteristics of the compressor by a rapid change from an unstalled to a stalled characteristic, as seen in figure 2.5. de Jager (1995) discusses the relevance of rotating stall in centrifugal compressors as well as single stage axial compressors. It is concluded that in centrifugal compressors rotating stall has little effect on the pressure rise and therefore on surge, which is a greater problem in this compressor.

Surge is characterized by fluctuations in pressure and unsteady mass flow. This is a one-dimensional instability that affects the whole pressurization system, and results in

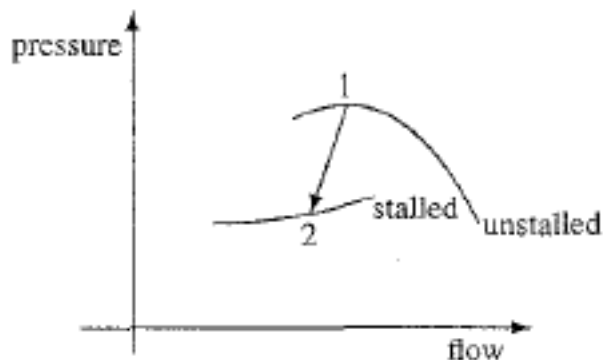


Figure 2.5: Characteristics stall. From (de Jager & Willems 1998).

a limit cycle on the compressor map (de Jager & Willems 1998). Egeland & Gravidahl (1999) separates between mild/classic and deep surge. In mild/classic surge oscillations in mass flow and pressure occur, while in deep surge the amplitudes of the mass flow becomes so large that reversal of the flow through the compressor may occur. The deep surge phenomena yields the limit cycle in the compressor map seen in figure 2.6. The cycle starts where the flow becomes unstable in (1), and then jumps to the reversed characteristics (2) before it follows this branch until approximately zero mass flow (3). It then jumps to (4) before it works its way back to (1). The cycle is repeated. Egeland & Gravidahl (1999) emphasizes that a positive compressor characteristic slope is necessary for surge to occur. In the compressor map this equals the area where the pressure rise reaches its maximum. A surge line can therefore be drawn through the highest pressure rise levels, as seen in figure 2.10. Surge can lead to severe damage of the compression system, as well as a decrease in overall efficiency for a process. It is therefore of great importance that the compressor does not go into surge.

## 2.2 Compressor Control

Rotating surge is a phenomenon that restricts the performance and efficiency of the compressor because of the pressure rise and power consumption related to this instability. This may lead to a temperature rise both in the blades of the compressor and the exit temperature from the system, which may affect the overall process result. The variations in the fluid dynamics (back flow) will add load to the compressor blades causing vibrations,

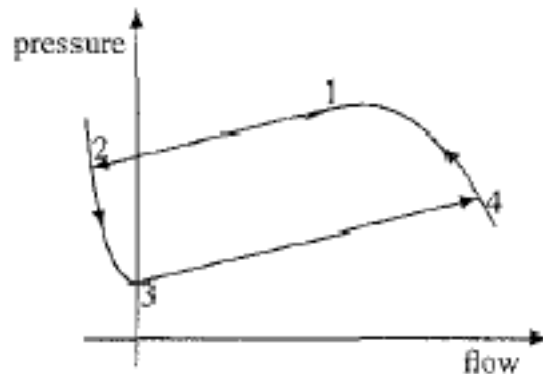


Figure 2.6: Deep surge cycle (de Jager & Willems 1998).

fatigue and in the worst case total damage (de Jager 1995). Because of the trouble related to surge it is of great importance to control the systems ensuring the phenomenon never occurs. In de Jager (1995) and Egeland & Gravidahl (1999) it is presented three measures for coping with surge.

- **Surge avoidance.** The machine is prevented from entering the area of the compressor map where surge may occur.
- **Surge detection and avoidance.** The control system detects surge, then starts acting to avoid it.
- **Active surge control.** Stabilization of flow instabilities by effectors acting upon relevant information from sensors.

Active surge control is based on trying to stabilize some of the unstable parts of the compressor map close to the surge line by using feedback (Egeland & Gravidahl 1999). This will open for more efficient and optimized use of compressor systems, being that the surge line normally is close to the optimal compressor values. Active control was introduced in 1989 and has since then been subject to extensive research. Egeland & Gravidahl (1999) presents that a lot of the research has been for axial compressor because these are used in aircraft engines, and the gas turbine industry has been the main sponsor of the research.

Surge detection and avoidance is based on monitoring variations in mass flow, pressure and temperatures as well as their derivatives and oscillation frequencies. The measurements are then compared to a threshold value for the specific compressor (Egeland

& Gravdahl 1999). If surge is detected, the control system is activated to avoid the phenomenon. Botros & Henderson (1994) emphasizes that this control principle has not grabbed hold in the industry due to several uncertain difficulties related to the detection of surge. Reliability of measurements, machine specific surge detection techniques and slow response time of mechanical components (valves) are presented as the major drawbacks of this control method.

Surge avoidance is the control principle most commonly applied in the gas industry today. It prevents the compressor from reaching the surge line by either feeding gas back from the outlet to the inlet, or blowing it off at the outlet. This way the compressor always has enough mass flow to avoid surge, and can also run at a set-point value. Botros & Henderson (1994) concludes that surge avoidance has reached a level where further research is in the perfection state. Improvements are predicted to be within better sensors and computational methods. Surge avoidance will be presented later in this chapter, emphasizing the solutions that are most commonly used in the industry. The goal is to increase the understanding of surge avoidance for later building and implementation in laboratory set-up.

### **2.2.1 Industrial compression recycling systems**

A structural sketch of a compression system with surge control feedback was presented in figure 2.1 and the resulting Greitzer model describing the dynamics of the system was derived earlier in this chapter and presented in equations (2.30) - (2.33). A compressor is normally a small part of a larger process, and it is not uncommon to have several compressors in series to increase the gas pressure to a needed level. Niesenfeld (1982) and Kurz & White (2006) both present several different combinations of compressors in series or parallel that are common in different processes. They also suggest different combinations of instrumentation. A very common set up for a single stage compressor with surge avoidance recycling is shown in figure 2.7. The main components in an industrial compression system is here seen, it consists of a recycle line, valve, cooler, knock-out pot and check valve. The temperature of the gas does increase during the compression, and a cooler is therefore placed downstream of the compressor to ensure that gas being delivered to the process has correct temperature, i.e. to avoid liquefaction. If the gas in the recycle line is not cooled, the temperature will increase more during the next compression, this means that the discharge pressure will grow higher, causing a degeneration in performance. A gas cooler is therefore necessary to keep the compressor running stable and perform well.

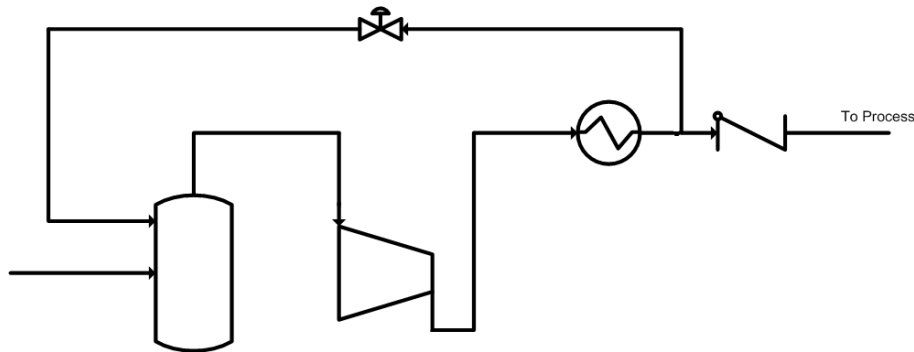


Figure 2.7: Compressor with recycle line, knock out pot, cooler and check valve.

The placement of the cooler will differ from system to system, and is dependent on type of gas compressed, but also economical aspects such as materials, size of cooler and size of recycle control valve. In some processes where the pressure and temperature increase is large during the compression it is common to place the cooler downstream of the control valve to ensure that cooling of high-pressure gases does not result in condensation.

A suction knock-out pot, sometimes referred to as a scrubber, is placed upstream of the compressor. It serves as a place to mix inlet and recycle mass flow, and to gather fluids that may have condensed in the gas before it is compressed. In equation (2.30), the dynamics of a pressure in a volume  $V_1$  is calculated, in a real system this would be the knock out pot. A check valve is situated after the recycle intersection and serves as a security installment to ensure that high level gas does not flow back into the compressor. It should be placed as close as possible to the compressor nozzle outlet, but downstream of the recycle line such that there always will be mass flow when the control valve is opened.

Kurz & White (2006) addresses the issue of choosing a correct control recycle scheme to handle both normal recycling and shutdown of compressor. For normal control a small valve with smooth throttling would be preferable, while for shutdown sequences such as an emergency shutdown a fast valve that handles rapid major changes would be better. A different approach often used is a double recycle line solution, one recycling the cold gas for surge avoidance, and one recycling uncooled gas through a rapid changing valve in a so-called hot recycle loop. A sketch of this principle is presented in figure 2.8.

Kurz & White (2006) emphasizes the necessity of choosing the right instrumentation in a surge avoidance system, and presents tips as to what type of instruments could be used as well as accuracy to be expected. Pressure and temperature is suggested to be

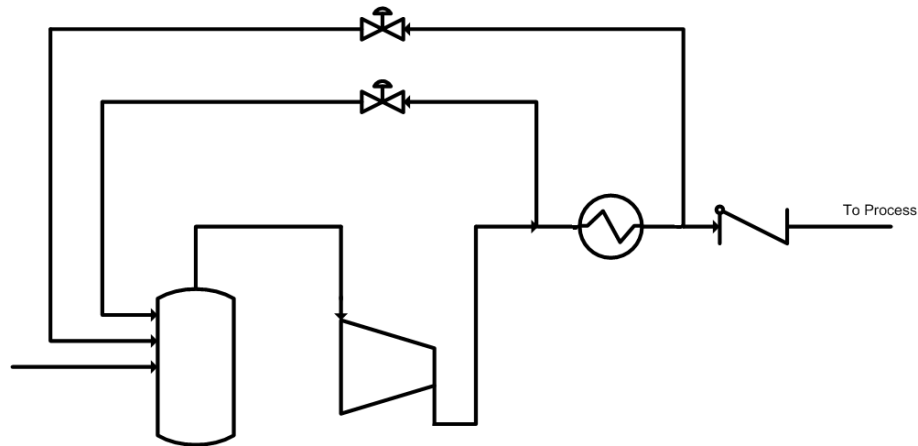


Figure 2.8: Surge avoidance using hot and cold recycle.

measured up and downstream of the compressor. In Niesenfeld (1982) it is presented that the usual way to measure the upstream pressure is in the scrubber, which matches the modeling of the upstream pressure very well. The downstream pressure measurement is somewhat more varying, but it seems that it is measured either at the recycle intersection, or right before the check valve. The instruments measuring the flow is emphasized to be the most important (Kurz & White 2006). This because when the system is getting close to surging the mass flow will change the most. It is of great importance that the mass flow transmitter is fast, at least one order of magnitude faster than the real system. This is somewhat important also for pressure and temperature measurements. Both Kurz & White (2006) and Niesenfeld (1982) suggests measuring the mass flow upstream of the compressor due to less variations in pressure, temperature and turbulence compared to a downstream measurement. A suction-to-eye method, using the inlet volute to measure mass flow, is recommended for surge avoidance by Kurz & White (2006). A surge avoidance system should be able to discriminate between single digit percentage of surge margin, and therefore the measurement instruments should be accurate to 0.1%. The placement of measurement devices are of great importance to a surge avoidance control system, and should be thoroughly analysed before implemented. Compressor Controls Corporation (CCC) is one of the worlds leading companies within compressor control, and utilizes among others a recycling solution as here discussed. Figure 2.9 shows part of a principal sketch of where the company measures their variables. Mass flow, temperature and pressure is measured directly upstream the compressor, while pressure and temperature is measured also downstream. This does differ a little from the previous discussion,

where the upstream pressure was measured in the scrubber. This emphasizes the fact that there are several different solutions to measurements and how the physical systems are installed.

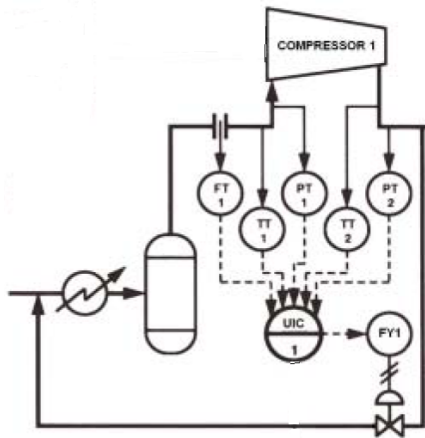


Figure 2.9: Part of surge recycle system from CCC. From Fausel (2002).

## 2.2.2 Surge avoidance control

As earlier mentioned, the surge line is in the area close to the compressors highest performance efficiency area, and it is therefore desirable to run the system as close to the surge line as possible. However, great problems may occur if the system goes into surge, and surge avoidance is implemented to ensure that this does not happen. If the complete compressor characteristics were known and there were no measurement noise, the surge line could be used as a reference for the avoidance control. This is however not the case and a security margin, a *surge avoidance line*, is defined to the right of the surge line. In figure 2.10 the principle of a surge avoidance line is shown. Egeland & Gravdahl (1999) presents that the surge margin between the two lines are fairly conservative, and de Jager & Willems (1998) presents that the surge margin needs to be set by the actuator and sensor limitations, uncertainty of exact location of surge line and disturbances. A margin of 10 - 25% is suggested (de Jager & Willems 1998), (Kurz & White 2004). A simple method for defining the surge margin is presented in Egeland & Gravdahl (1999)

$$SM_1 = \frac{PR_s - PR_{sa}}{PR_{sa}} \quad (2.62)$$

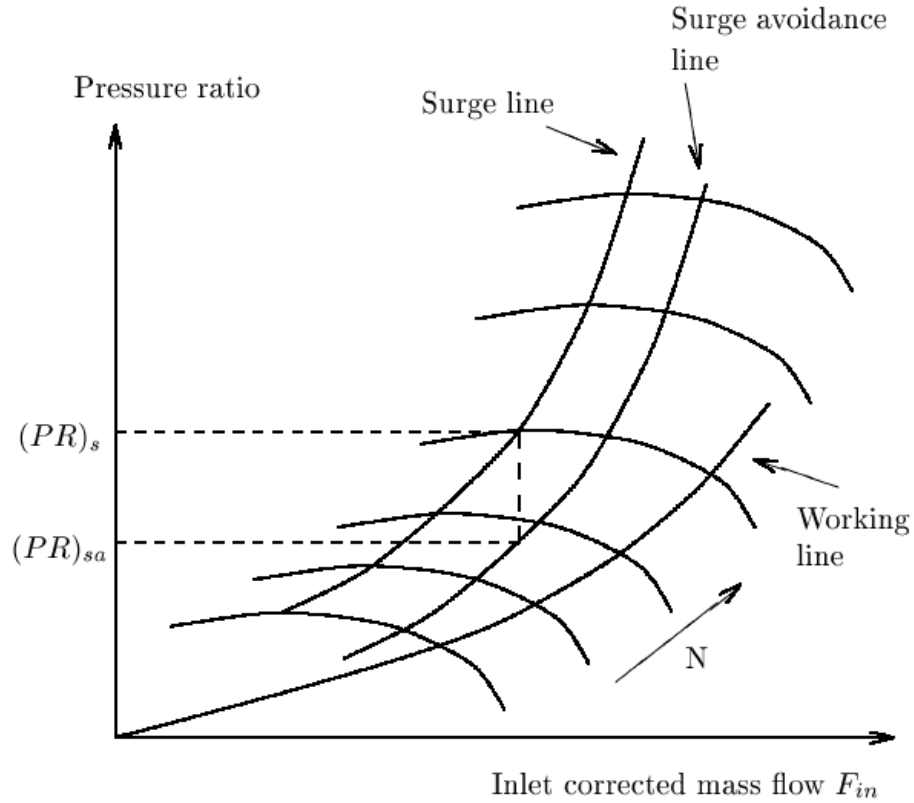


Figure 2.10: Surge margin. From Egeland & Gravdahl (1999).

$PR_{sa}$  is the pressure ratio on the surge avoidance line for a given mass flow, while  $PR_s$  is the pressure ratio for the same mass flow, this can be seen in figure 2.10. Another logical way to define the surge margin is based on the outlet mass flow, yielding a margin described as

$$SM_2 = \frac{F_{out,sa} - F_{out,s}}{F_{out,sa}} \quad (2.63)$$

$F_{out,sa}$  is the mass flow on the surge avoidance line, while  $F_{out,s}$  is the mass flow on the surge line. Defining the margin by using the corrected mass flow,  $m_{corr} = m\sqrt{\frac{T_{01}/T_{ref}}{p_{01}/p_{ref}}}$  is also suggested. This because it will give a measure of throttle change needed to take the compressor into surge.  $T_{ref}$  and  $p_{ref}$  are normally taken as sea level static.

The surge avoidance line can be defined to be a parallel to the surge line, with a slope less than the surge line or by a vertical line. The last two methods will not yield efficient control since the margin to the surge line will be uneven and the system will easier reach surge either at low pressures (less slope) or high pressures (vertical line).

When the surge line and surge margin is defined, a avoidance scheme will work by continuously comparing the working point of the compressor to the surge avoidance line. If the working point gets to close, or crosses the line, action is taken by actuation device (i.e. recycle valve), and the working point of the compressor is forced back into the correct area of the compressor map. The most common controller for surge avoidance is a PI-control scheme.

In the industry there are several avoidance schemes implemented, and these have been categorized by Botros & Henderson (1994) into 4 categories depending on measured values and definitions of surge margin. These are conventional anti-surge control, Flow/rotational speed ( $Q/N$ ) technique, microprocessor and PLC based controllers and control without flow measurements.

1. Conventional anti-surge control is also referred to as the " $Flow/\Delta P$ "-control. It defines a linear surge avoidance line based on the relation between inlet mass flow and pressure ratio

$$\Delta P_0 = k_1 \Delta P_c + k_2 \quad (2.64)$$

where  $\Delta P_c$  is the pressure ratio,  $k_1$  and  $k_2$  are constants. Mass flow is measured at the compressor inlet and results in a differential pressure  $\Delta P_0$ .

2.  $Q/N$ -technique defines a constant control point using the relation of the volumetric flow  $Q$  and rotational speed  $N$ ;  $(Q/N)_c$ . If then  $(Q/N)_{measured} < (Q/N)_c$ , control is activated.
3. Microprocessors and PLC-based control is the most common scheme used today. The compressor characteristics can be used to compare the surge line and working point. Being that the relation between mass flow and pressure ratio is nonlinear, this is a better solution. Measurements of pressures and temperature together with a compressor map are needed for a control scheme such as this.
4. Control without mass flow measurements applies the same principle as the  $Q/N$ -technique, but uses  $H/N^2$  instead, where  $H$  is the head across the compressor. The motivation for this scheme is that mass flow measurement often is corrupted by noise or simply hard to measure correctly, for example in surge. This method will only work if the compressor map is steep enough.

## 2.3 Kalman filter

In order to control a system, whether it being keeping a ship in its predefined path or having a compressor avoid surge, the states of the system needs to be available at all times. A system is normally described by several states, but all of them may not be available for measurement. Still, these are needed for control of the system and/or optimization of production. The need to estimate the non-measurable states is obvious.

The data available from the plant is normally corrupted by process and measurement noise, and this needs to be considered when using the information and estimating the missing states. Normally the available information about a system is the measurement data and the mathematical model. With the help of these the missing states can be retrieved. It is important that the states to be estimated are observable through the measurements and model.

In Henriksen (1998) different methods for estimating a missing state is presented, included minimum variance and least-squared error method. The kalman filter is also presented in this book, and is a recursive algorithm based on minimizing the mean of the squared estimation error. Kalman first introduced his method in the paper "A new approach to linear filtering and prediction problems" in 1960, and due to the rapid development in digital computing the method of kalman filtering soon grabbed hold and became subject to extensive research (Bishop & Welch 2006). The filter was initially developed for discrete time linear systems, but later both continuous kalman filters and extended filters for nonlinear systems were developed. The kalman filter is today used in many applications, either to estimate states, predict states or as a filter. In this section the discrete kalman filter for a linear system is developed. The extended filter for a nonlinear discrete system is then presented, followed by the development of the continuous kalman filter equations. In the end the equations for the extended continuous filter is presented.

### 2.3.1 Discrete kalman filter

The theory behind the discrete kalman filter is retrieved from chapter 5 in Brown & Yang (1997) unless otherwise is specified.

The random process to be estimated is assumed to have the general model

$$x_{k+1} = \phi_k x_k + v_k \quad (2.65)$$

$$z_k = H_k x_k + w_k \quad (2.66)$$

where  $x_k \in \mathcal{R}^{n \times 1}$  are the system states,  $\phi_k \in \mathcal{R}^{n \times n}$  is the relation matrix between  $x_k$  and  $x_{k+1}$ ,  $z_k \in \mathcal{R}^{m \times 1}$ ,  $m \leq n$ , are the measured values from the system and  $H_k \in \mathcal{R}^{m \times n}$  gives the ideal noiseless value of the measured states. The two vectors  $v_k$  and  $w_k$  are process noise and measurement error, both are assumed to be white sequences with known expectancy and covariance values as follows

$$E[v_k] = 0 \quad (2.67)$$

$$E[w_k] = 0 \quad (2.68)$$

$$E[v_k v_i^T] = \begin{cases} V_k, & i = k \\ 0 & otherwise \end{cases} \quad (2.69)$$

$$E[w_k w_i^T] = \begin{cases} W_k, & i = k \\ 0 & otherwise \end{cases} \quad (2.70)$$

Both  $v_k$  and  $w_k$  are uncorrelated with each other and the states of the system  $x$ , so that

$$E[v_k w_k^T] = 0 \quad (2.71)$$

$$E[v_k x_k^T] = 0 \quad (2.72)$$

$$E[w_k x_k^T] = 0 \quad (2.73)$$

An assumption is made that there is a known initial estimate  $\bar{x}_k$  of the state  $x_k$  at time  $t_k$ , based on earlier knowledge of the system. The estimation error and error covariance at that time is also known

$$\bar{e}_k = x_k - \bar{x}_k \quad (2.74)$$

$$\bar{X}_k = E[\bar{e}_k \bar{e}_k^T] = E[(x_k - \bar{x}_k)(x_k - \bar{x}_k)^T] \quad (2.75)$$

At time  $t_k$  the measurement  $z_k$  is retrieved. The goal is now to use the information from  $z_k$  to improve the estimate  $\bar{x}_k$  by implementing a linear combination of the noisy measurement and the earlier estimate

$$\hat{x}_k = \bar{x}_k + K_k [z_k - H_k \bar{x}_k] \quad (2.76)$$

The new estimate,  $\hat{x}_k$  is referred to as the a posterior estimate of the state, meaning the improved estimate after the measurement has been updated.  $K_k$  is the blending factor that is used to balance the combination between the old estimate and the new noisy measurement.

For a kalman filter,  $K_k$  is referred to as the kalman gain and is chosen to minimize

the error between the real and estimated states. First the covariance of the a posterior estimation error is developed

$$\hat{X}_k = E [(x_k - \hat{x}_k)(x_k - \hat{x}_k)^T] \quad (2.77)$$

Using equation (2.66)  $\hat{x}_k$  is rewritten to become

$$\hat{x}_k = \bar{x}_k + K_k(H_k x_k + w_k - H_k \bar{x}_k) \quad (2.78)$$

and the error covariance now becomes

$$\begin{aligned} \hat{X}_k &= E \{ [x_k - (\bar{x}_k + K_k(H_k x_k + w_k - H_k \bar{x}_k))] \\ &\quad [x_k - (\bar{x}_k + K_k(H_k x_k + w_k - H_k \bar{x}_k))]^T \} \\ &= E \left\{ [(I - K_k H_k)(x_k - \bar{x}_k) - K_k w_k] [(I - K_k H_k)(x_k - \bar{x}_k) - K_k w_k]^T \right\} \\ &= (I - K_k H_k) E [(x_k - \bar{x}_k)(x_k - \bar{x}_k)^T] (I - K_k H_k)^T \\ &\quad - (I - K_k H_k) E [(x_k - \bar{x}_k) w_k^T] K_k^T - K_k E [w_k (x_k - \bar{x}_k)^T] (I - K_k H_k)^T \\ &\quad + K_k E [w_k w_k^T] K_k^T \end{aligned}$$

The a prior estimate error  $(x_k - \bar{x}_k)$  is uncorrelated with the measurement error  $w_k$ , and the covariance between the two signals is then zero. Using the expression for the a prior error covariance in equation (2.75) and the covariance of the measurement error from (2.70) the a posterior error covariance can be written

$$\hat{X}_k = (I - K_k H_k) \bar{X}_k (I - K_k H_k)^T + K_k W_k K_k^T \quad (2.79)$$

The main goal is to find a  $K_k$  such that the estimation error becomes minimized, and using minimum-mean-square error method as a performance criterion this can be obtained. By minimizing  $\hat{X}_k$  with regards to  $K_k$ , the total square error will be minimized, and from this it is assumed that also the individual square-errors are minimized. It is the diagonal of  $\hat{X}_k$  that is of interest because it describes the error variances of the elements being estimated. Differentiating  $\hat{X}_k$  with regards to  $K_k$ , setting the expression to zero and solving for  $K_k$  yields the kalman gain update equation

$$K_k = \bar{X}_k H_k^T (H_k \bar{X}_k H_k^T + W_k)^{-1} \quad (2.80)$$

We started with an initial estimate prior to the measurement of the system,  $\bar{x}_k$  and its error

covariance  $\bar{X}_k$ . To fully use the measured values and optimize the kalman gain to achieve a better estimate, these values needs to be updated after every sample as well. The a prior estimate of the states is easy to calculate once the posterior estimate is updated

$$\bar{x}_{k+1} = \phi_k \hat{x}_k \quad (2.81)$$

There is no need to include the process noise  $v_k$  in the estimate since it is uncorrelated with prior  $v$  and  $E[v_k] = 0$ . The a prior estimation error then becomes

$$\begin{aligned} e_{k+1} &= x_{k+1} - \bar{x}_{k+1} \\ &= (\phi_k x_k + v_k) - \phi_k \hat{x}_k \\ &= \phi_k (x_k - \hat{x}_k) + v_k = \phi_k e_k + v_k \end{aligned} \quad (2.82)$$

The covariance can then be calculated

$$\begin{aligned} \bar{X}_{k+1} &= E [(\phi_k e_k + v_k)(\phi_k e_k + v_k)^T] \\ &= \phi_k E [e_k e_k^T] \phi_k^T + \phi_k E [e_k v_k^T] + \\ &E [v_k e_k^T] \phi_k + E [v_k v_k^T] \\ &= \phi_k \hat{X}_k \phi_k^T + V_k \end{aligned} \quad (2.83)$$

The kalman filter is formed by the equations (2.80), (2.76), (2.79), (2.81) and (2.83). However, to make the calculations online faster it is common to substitute eq.(2.80) into (2.76) and use the following a posterior error covariance

$$\hat{X}_k = (I - K_k H_k) \bar{X}_k \quad (2.84)$$

An alternative to rewriting the kalman gain matrix is also suggested in equation 2.71 of (Henriksen 1998)

$$K_k = \hat{X}_k H_k^T W_k^{-1} \quad (2.85)$$

A suggestion to how the kalman filter equations are implemented is shown in figure 2.11.

## Extended kalman filter

The theory of the extended discrete kalman filter is retrieved from chapter 3 of Henriksen (1998). The system to be estimated is now modeled by the nonlinear equations

$$x_{k+1} = f(x_k, u_k) + v_k \quad (2.86)$$

$$z_k = h(x_k) + w_k \quad (2.87)$$

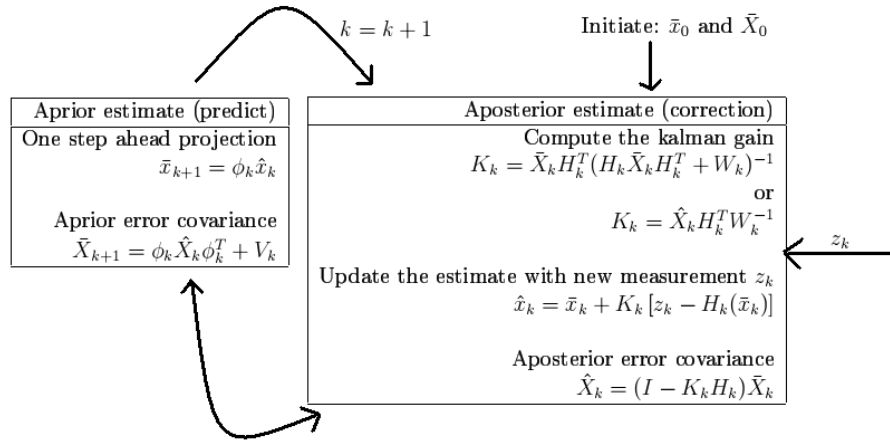


Figure 2.11: The implementation of the discrete kalman filter can be split in two parts.

$v_k$  and  $w_k$  have the same properties as in eqs. (2.67)-(2.70).  $f$  is a nonlinear mapping between  $x_{k+1}$  and  $x_k$  driven by input  $u_k$ , while  $h$  is the nonlinear measurement function. Assuming the same initial conditions as for the linear discrete filter, namely that  $\bar{x}_k$  and  $\bar{X}_k$  are both known at time  $t_k$  before the first sample is available.

A 1-order Taylor expansion gives a linearized measurement function around the aprior estimate of the states

$$z_k = h_k(\bar{x}_k) + w_k + H_k(x_k - \bar{x}_k) \quad (2.88)$$

$$H_k = \frac{\partial h_k}{\partial x_k^T}(\bar{x}_k) \quad (2.89)$$

Assuming  $\bar{x}_k$  is the expected value of the real states,  $x_k$ , based on the knowledge of all the prior measurements  $Y_{k-1}$ , an expected value of the next measurement can be derived

$$\bar{z}_k = E[z_k | Y_{k-1}] = h_k(\bar{x}_k) \quad (2.90)$$

The covariance of the measurement error between the real and linearized measurement functions,  $z_k - \bar{z}_k$  can now be calculated using eqs. (2.88) and (2.90).

$$\begin{aligned} & E[(z_k - \bar{z}_k)(z_k - \bar{z}_k)^T] \\ &= E\left\{[H_k(x_k - \bar{x}_k) + w_k][H_k(x_k - \bar{x}_k) + w_k]^T\right\} \\ &= H_k \bar{X}_k H_k^T + W_k \end{aligned} \quad (2.91)$$

The equations for aposterior update equations of the kalman filter can now be written

$$\hat{x}_k = \bar{x}_k + K_k [z_k - H_k(\bar{x}_k)] \quad (2.92)$$

$$\hat{X}_k = (I - K_k D_k) \bar{X}_k \quad (2.93)$$

$$K_k = \bar{X}_k H_k^T (H_k \bar{X}_k H_k^T + W_k)^{-1} = \hat{X}_k H_k^T W_k^{-1} \quad (2.94)$$

To be able to update the aprior estimates of the states, a linearization of  $f$  is performed around  $\hat{x}_k$ .

$$x_{k+1} = f_k(\hat{x}_k, u_k) + A_k(x_k - \hat{x}_k) + v_k \quad (2.95)$$

$$A_k = \frac{\partial f_k}{\partial x_k^T}(\hat{x}_k, u_k) \quad (2.96)$$

The aprior prediction one step ahead in the kalman filter becomes

$$\bar{x}_{k+1} = f(\hat{x}_k, u_k) \quad (2.97)$$

The estimation error and its covariance is now calculated

$$\bar{e}_{k+1} = x_{k+1} - \bar{x}_{k+1} = A_k(x_k - \bar{x}_k) + v_k \quad (2.98)$$

$$E [\bar{e}_{k+1} \bar{e}_{k+1}^T] = A_k \bar{X}_k A_k^T + V_k \quad (2.99)$$

### 2.3.2 Continuous kalman filter

The theory in this section is based on Brown & Yang (1997), chapter 7.

The kalman filter was initially developed for discrete systems, and the presentation of the continuous filter will take its base in the discrete filter. The process to be estimated and its measurement model is now on the form

$$\dot{x} = Fx + Cv \quad (2.100)$$

$$y = Hx + w \quad (2.101)$$

where matrices  $F$ ,  $G$  and  $H$  can be time varying. The state vector is  $x$ , while  $y$  is the noisy measurement.  $v$  and  $w$  are both white noise processes with expectancy and covariance values as follows

$$E [v(t)] = 0 \quad (2.102)$$

$$E [w(t)] = 0 \quad (2.103)$$

$$E [v(t)v^T(\tau)] = V\delta(t - \tau) \quad (2.104)$$

$$E [w(t)w^T(\tau)] = W\delta(t - \tau) \quad (2.105)$$

The system sampling time is  $\Delta t$ , and is assumed to be small. To be able to make the transition from a discrete to a continuous system, we need the relation between the discrete and continuous covariance matrices for the process and measurement noise. When a continuous signal is sampled at times  $t_0, t_1, \dots, t_k, t_{k+1}$ , a difference equation can be developed to relate the samples of  $x$

$$x(t_{k+1}) = \phi(t_{k+1}, t_k)x(t_k) + \int_{t_k}^{t_{k+1}} \phi(t_{k+1}, \tau)C(\tau)v(\tau)d\tau = \phi_k x_k + v_k \quad (2.106)$$

$\phi_k$  is the state transition matrix for the step from  $t_k$  to  $t_{k+1}$ , and  $v_k$  is the response at time  $t_{k+1}$  due to the white noise input. The discrete representation of the continuous process noise covariance can now be developed when  $t_{k+1} - t_k = \Delta t$

$$\begin{aligned} V_k &= E [v_k v_k^T] \\ &= E \left\{ \left[ \int_{\Delta t} \phi(t_{k+1}, \xi)C(\xi)v(\xi)d\xi \right] \left[ \int_{\Delta t} \phi(t_{k+1}, \eta)C(\eta)v(\eta)d\eta \right]^T \right\} \\ &= \iint_{\Delta t} \phi(t_{k+1}, \xi)C(\xi)E [v(\xi)v^T(\eta)] C^T(\eta)\phi^T(t_{k+1}, \eta)d\xi d\eta \end{aligned} \quad (2.107)$$

When  $\Delta t \rightarrow 0$  the state transition matrix  $\phi \approx I$  and the discrete representation of the continuous process noise covariance matrix becomes

$$\begin{aligned} V_k &= \iint_{\Delta t} C(\xi)E [v(\xi)v^T(\eta)] C^T(\eta)d\xi d\eta \\ &= CVC^T \Delta t \end{aligned} \quad (2.108)$$

To derive the relation between  $W_k$  and  $W$ , eq. (2.101) is transformed to a discrete representation

$$\begin{aligned} y_k &= \frac{1}{\Delta t} \int_{t_{k-1}}^{t_k} y(t)d(t) = \frac{1}{\Delta t} \int_{t_{k-1}}^{t_k} Hx(t) + w(t)dt \\ &\approx Hx_k + \frac{1}{\Delta t} \int_{t_{k-1}}^{t_k} w(t)dt = Hx_k + w_k \end{aligned} \quad (2.109)$$

The discrete representation of the continuous measurement noise covariance matrix now becomes

$$\begin{aligned}
W_k &= E [w_k w_k^T] \\
&= \frac{1}{\Delta t^2} \iint_{\Delta t} E [w(\xi) w^T(\eta)] d\xi d\eta \\
&= \frac{W}{\Delta t}
\end{aligned} \tag{2.110}$$

When the sampling rate becomes very small the a priori error covariance matrix will become the same as the a posterior covariance matrix,  $\bar{X}_{k+1} \rightarrow \hat{X}_k$  when  $\Delta t \rightarrow 0$ . Because of this there is no need to separate between a prior and a posterior estimates in the continuous kalman filter. The kalman gain matrix for the discrete filter is  $K_k = \bar{X}_k H_k^T (H_k \bar{X}_k H_k^T + W_k)^{-1}$ , and using eq. (2.110) it is seen that  $\frac{W}{\Delta t} \gg H_k \bar{X}_k H_k^T$ , this leads to

$$K_k = \bar{X}_k H_k^T W^{-1} \Delta t \tag{2.111}$$

Dropping all subscripts, and defining  $\bar{X}_k = X$  the continuous kalman gain can be defined as the coefficient of  $\Delta t$

$$K \triangleq X H^T W^{-1} \tag{2.112}$$

The a priori error covariance in the discrete case can be written as

$$\begin{aligned}
\bar{X}_{k+1} &= \phi_k \hat{X}_k \phi_k^T + V_k = \phi_k (I - K_k H_k) \bar{X}_k \phi_k^T + V_k \\
&= \phi_k \bar{X}_k \phi_k^T - \phi_k K_k H_k \bar{X}_k \phi_k^T + V_k
\end{aligned} \tag{2.113}$$

Approximation  $\phi_k \approx I + F \Delta t$  is made, and substituted into the expression of  $\bar{X}_k$ . Keeping in mind that  $K_k$  is of order  $\Delta t$  and ignoring higher order terms in  $\Delta t$ , the following description is developed

$$\begin{aligned}
\bar{X}_{k+1} &= \bar{X}_k + F \bar{X}_k \Delta t + \bar{X}_k F^T \Delta t - K_k H_k \bar{X}_k + V_k \\
\frac{\bar{X}_{k+1} - \bar{X}_k}{\Delta t} &= F \bar{X}_k + \bar{X}_k F^T - \bar{X} H^T W^{-1} H_k \bar{X}_k + C V C^T
\end{aligned} \tag{2.114}$$

Now letting  $\Delta t \rightarrow 0$  the continuous representation of the error covariance is obtained

$$\begin{aligned}\dot{X} &= FX + XF^T - XH^TW^{-1}HX + CVC^T \\ X(0) &= X_0\end{aligned}\tag{2.115}$$

Lastly, an update expression for the state estimate is needed. By inserting  $\bar{x}_k = \phi_{k-1}\hat{x}_{k-1}$  in the discrete state estimate the following representation is obtained

$$\hat{x}_k = \bar{x}_k + K_k(y_k - H_k\bar{x}_k)\tag{2.116}$$

$$= \phi_{k-1}\hat{x}_{k-1} + K_k(y_k - H_k\phi_{k-1}\hat{x}_{k-1})\tag{2.117}$$

Again the approximation  $\phi_k \approx I + F\Delta t$  is made, together with  $K_k = K\Delta t$ . Ignoring higher order terms in  $\Delta t$ , and lastly letting  $\Delta t \rightarrow 0$  the continuous state estimate becomes

$$\begin{aligned}\frac{\hat{x}_k - \hat{x}_{k-1}}{\Delta t} &= F\hat{x}_{k-1} + K(y_k - H\hat{x}_{k-1}), \quad \Delta t \rightarrow 0 \\ \dot{\hat{x}} &= F\hat{x} + K(y - H\hat{x})\end{aligned}\tag{2.118}$$

Together the eqs.(2.112), (2.115) and (2.118) form the continuous linear kalman filter, and a suggestion to its implementation can be seen in figure 2.12.

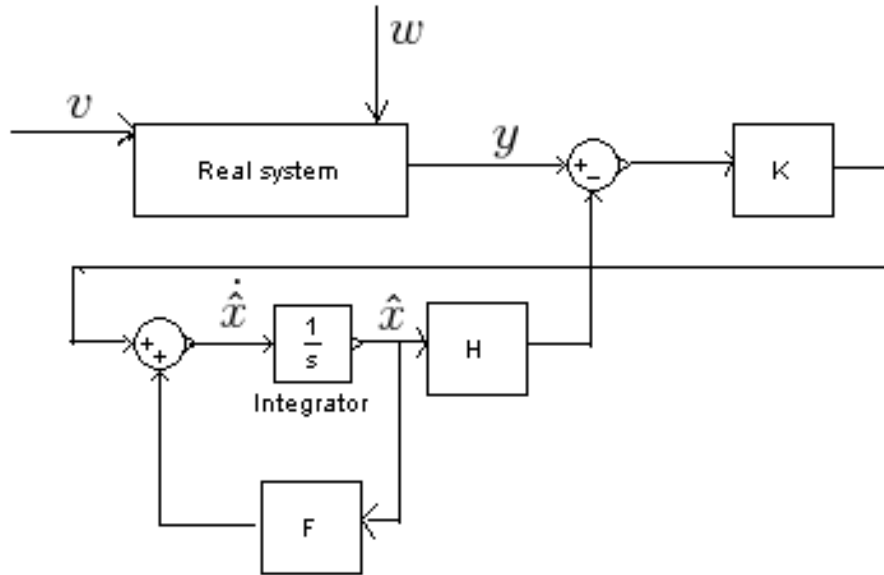


Figure 2.12: Linear continuous kalman filter

## Extended kalman filter

The development of the continuous extended kalman filter is very similar to that of the discrete case, and will therefore not be repeated here. The nonlinear system is modeled

$$\dot{x} = f(x(t), u(t), t) + C(t)v(t) \quad (2.119)$$

$$y(t) = g(x(t), t) + w(t) \quad (2.120)$$

with the process and measurement noise being white noise sequences with known covariances. The equations describing the extended kalman filter are presented in chapter 2.6 of Henriksen (1998) and will be summarized here.

$$\dot{\hat{x}}(t) = f(\hat{x}(t), u(t), t) + K(t) [y(t) - g(\hat{x}(t), t)] \quad (2.121)$$

$$\dot{X}(t) = A(t)X(t) + X(t)A^T(t) + C(t)V(t)C^T(t) - K(t)W(t)K^T(t) \quad (2.122)$$

$$K(t) = X(t)D^T(t)W^{-1}(t) \quad (2.123)$$

where

$$A(t) = \frac{\partial f}{\partial x^T}(\hat{x}(t), u(t), t) \quad (2.124)$$

$$D(t) = \frac{\partial g}{\partial x^T}(\hat{x}(t), t) \quad (2.125)$$

# Chapter 3

## Development, simulations and implementation

In this chapter the development of kalman filters, compression models and surge avoidance schemes is presented. All models have been fitted to the laboratory compressor system available at NTNU. Matlab and simulink have been used for all simulations, and all the models developed are found on the cd added to this report. A presentation and simulation of the existing compression system is first presented, before four kalman filters are developed, tuned and lastly implemented on the compressor. Then three models for simulation of surge avoidance recycling were developed and simulated. Lastly a surge avoidance simulation model was built.

### 3.1 Presentation of compressor model and lab set-up.

Due to many of the uncertainties in the model of the compressor shaft dynamics in equation (2.39) we choose to ignore the dynamic description when developing the kalman filters. Instead the measurement of the impeller speed  $\omega$ , from now on noted  $N$ , is used as input to the mass flow description. The resulting system that has been used is then described by equations (2.37) and (2.38). The inlet pressure is set to ambient pressure  $p_{01} = p_a$ , while the plenum pressure is renamed  $p_p = p$  for the compression system with no recycling. The system that has been worked with is now described by

$$\dot{p} = \frac{c_p^2}{V_p}(w - k'_t \sqrt{p - p_a}) \quad (3.1)$$

$$\dot{w} = \frac{A}{L_c + L_{cd}}(p_c(w, N) - p) \quad (3.2)$$

We use notations  $\frac{c_p^2}{V_p} = k_1$  and  $\frac{A}{L_c + L_{cd}} = k_2$  for convenience, but note however that  $k_2$  will vary in some cases, these will be thoroughly noted. The throttle gain  $k'_t$  is for the system modeled by the square of the throttle opening and a gain factor,  $k'_t = k_t u^2$ , where the gain

is identified to be  $k_t = 1.9259 * 10^{-7}$ . The throttle opening  $u$  is noted in percent. The other various constants of the compression lab system have been identified to be

$$A = 0.003848$$

$$L_c = 180 * 10^{-2}$$

$$L_{cd} = 270 * 10^{-2}$$

$$V_p = 0.1$$

$$R = \frac{8.314 * 10^3}{28.97}$$

$$\kappa_p = 1.4$$

$R$  and  $\kappa_p$  are used to calculate the sonic velocity in the plenum,  $c_p = \sqrt{\kappa_p R T_p}$ . The plenum temperature  $T_p$  will be taken as an average of measurements. It usually lies between 315 and 335 K. All the units presented are SI.

If the compressor goes into surge, it may occur that  $p_a > p$  in eq (3.1), and  $p$  will become an imaginary number. For implementational reasons the throttle mass flow is therefore slightly altered, and using the new notations the compressor model becomes

$$\dot{p} = k_1(w - k_t u^2 \text{sign}(p - p_a) \sqrt{|p - p_a|}) \quad (3.3)$$

$$\dot{w} = k_2(p_c(w, N) - p) \quad (3.4)$$

A compressor map has been derived for the lab set-up compression system, and is seen in figure 3.1. The x-axis is the mass flow, while the y-axis describes the pressure ratio. The characteristics are plotted for different levels of the impeller speed  $N$ . On each characteristic curve in the map different values of the throttle opening  $u$  is indicated. The throttle is fully open at the indications far right in the map. For implementation of the compressor the relation  $p_c(w, N) = F_c(w, N) + p_a$  will be used, where  $F_c(w, N)$  is the compressor characteristics seen in the compressor map. These are available through calculations in a matlab file.

The lab set-up of the compressor with duct and plenum has been built by Bjørnar Bøhagen. He is also responsible for identifying physical sizes, mathematical model and compressor map. A principal sketch of the compressor laboratory set-up with measurement points relevant to this thesis is seen in figure 3.2. It consists of a centrifugal compressor, duct and plenum. The compressor is driven by a motor, and takes air as inlet gas, setting the inlet pressure to be the ambient pressure. A closer description of the indicated measured values is seen in table 3.1. The values of the downstream and plenum pressures are both averaged before further use in implementations.

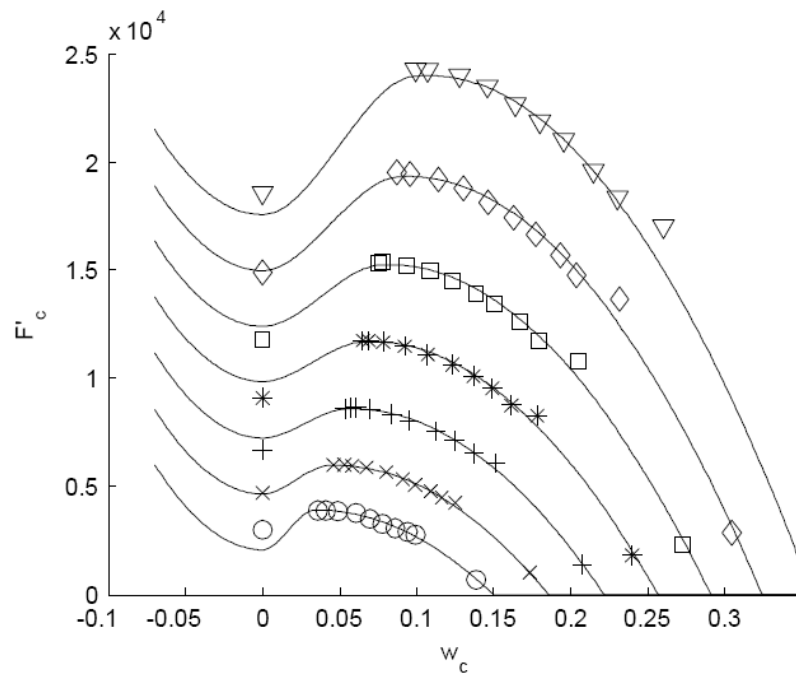


Figure 3.1: Compressor map. From Bøhagen (2007).

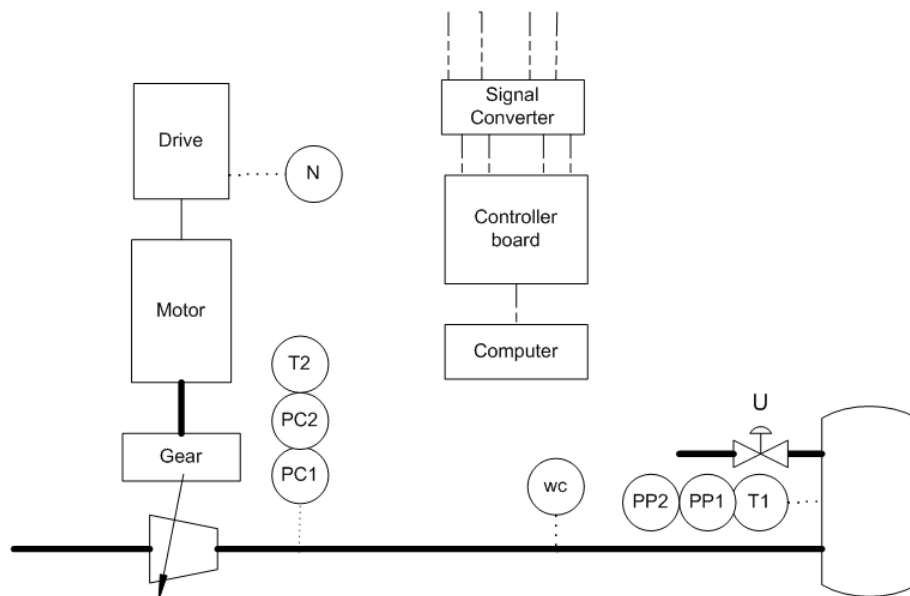


Figure 3.2: Lab set-up of compression system.

Name	Description
PC1	Downstream pressure, $p_{cd1}$
PC2	Downstream pressure, $p_{cd2}$
PP1	Plenum pressure, $p_1$
PP2	Plenum pressure, $p_2$
T1	Temperature plenum, $T_p$
T2	Downstream temperature, $T_a$
N	Impeller speed, $N$
WC	Mass flow, $w$
u	throttle opening, $u$

Table 3.1: Measured signals in lab set-up

## 3.2 Matlab model of compression system

A simulation model of the compressor system was implemented and tested using simulink. Taking the impeller speed and throttle opening as input, the model was compared to measured surge data of the plenum pressure. Unfortunately there are no measurements available to evaluate the transient behavior of the mass flow, but due to the high correlation between the two dynamic equations we assume that the model describing mass flow will be correct to an acceptable level. The simulink implementation of the compressor is presented in figures 3.3 and 3.4.

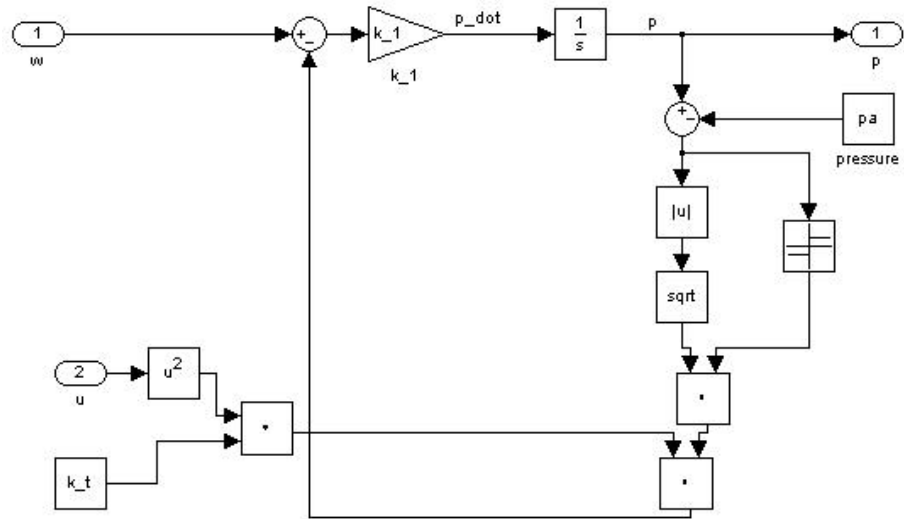


Figure 3.3: Implementation of compressor. Pressure.

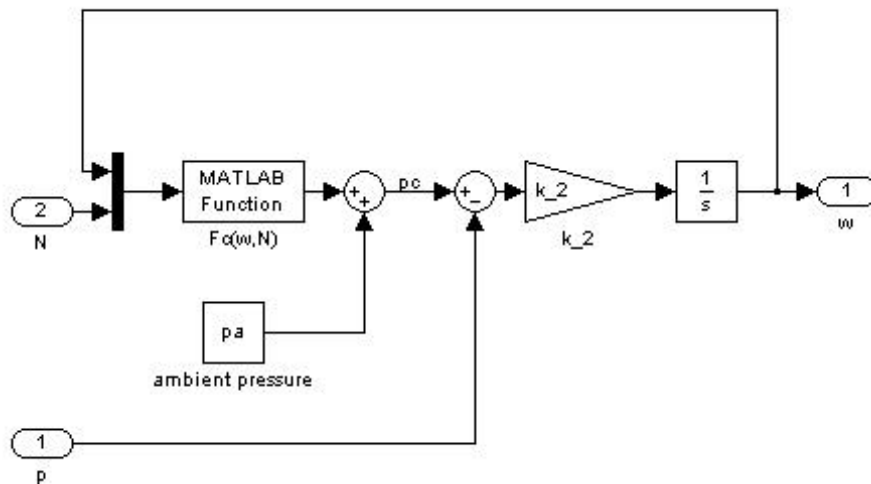


Figure 3.4: Implementation of compressor. Mass flow.

### 3.3 Kalman filters

Based on available measurements of plenum pressure  $p$ , downstream pressure  $p_{cd}$ , impeller speed  $N$  and throttle opening  $u$  a kalman filter to estimate mass flow and plenum pressure was seeked. Mass flow is measurable in steady state, but in surge the measured values becomes useless. An estimation of the mass flow will therefore prove itself useful to continuously control system behavior. To filter noise from the measured pressure we

simultaneously estimate the plenum pressure. Four different kalman filters were developed and tested differing in what signals they measure and what states they estimate. One filter was also developed without using the compressor map, this meaning that the estimated mass flow was calculated based directly on the measurement of  $p_{cd}$  using a slightly different compressor model. At an early stage of the assignment a discrete time extended kalman filter was developed, but due to high sampling rates compared to compressor dynamics a continuous extended kalman filter was chosen and implemented. The reader is referred to chapter 2.3 for a development of the extended kalman filter. The four different cases are here shortly summarized.

1. Estimate plenum pressure  $p$  and mass flow  $w$  without compressor map. Measured value is  $p$ . The downstream pressure  $p_{cd}$  is also measured, but used as system input, and not as a correctional term.
2. Estimate  $w$  using compressor map. Measured value is  $p_{cd}$
3. Estimate  $p$  and  $w$  using compressor map. Measured value is  $p$ .
4. Estimate  $p$  and  $w$  using compressor map. Measured values are  $p$  and  $p_{cd}$

All filters were simulated and implemented using Matlab Simulink, and the overall test bench can be seen in figure 3.5. During development and simulation period the input to the filters were taken from files with earlier measurement data. During implementation the input to the filters were connected to the I/O-ports in the lab set-up. There were two PT-cells sampling each of the pressures  $p$  and  $p_{cd}$ , these were averaged before use in observers. The downstream pressure is used to calculate  $p_c(w, N)$  using equation (2.45). Kalman filter 1 takes the average downstream pressure as input. All data was gathered and plotted in the subsystems to the far right in figure 3.5.

All four filters were simulated and tuned with surge data from compressor, with impeller speed around 25000 rpm and throttle opening at about 54 %. No filtering of data was performed prior to use. When tuning the plenum pressure estimate the measured value was used together with the innovation process to determine a good estimate. The mass flow is not measurable in surge, and the innovation process and comparison to simulated values were here used to determine a good estimate. There were no unfiltered steady



### 3.3.1 Kalmanfilter 1

Considering the system

$$\dot{p} = k_1(w - k_t u^2 \sqrt{p - p_a}) + v_1 \quad (3.5)$$

$$\dot{w} = k_2(p_c(w, N) - p) + v_2 \quad (3.6)$$

$$y = p + w \quad (3.7)$$

where  $v_1$ ,  $v_2$  and  $w$  are system noise with the same assumptions as presented in the development of Kalman filters in chapter 2, namely uncorrelated white noise sequences. Process noise covariance is a  $2 \times 2$ -matrix  $V$ , while measurement noise covariance is a scalar  $W$ . Both states were here to be estimated using  $p$  as measured value, and the implemented kalman estimates becomes

$$\begin{aligned} \dot{\hat{p}} &= k_1(\hat{w} - k_t u^2 \text{sign}(\hat{p} - p_a) \sqrt{|\hat{p} - p_a|}) + K_1(p - \hat{p}) \\ \dot{\hat{w}} &= k_2(p_{cd} - \hat{p}) + K_2(p - \hat{p}) \end{aligned} \quad (3.8)$$

In this filter the compressor map is not used to estimate the states, but rather the downstream pressure directly. To be able to do this a model of the compression system developed from the downstream measuring point and to the plenum is used rather than the complete model. The alteration is done by modeling the mass flow with only length  $L_{cd}$ , so we get constant factor

$$k_2 = \frac{A}{L_{cd}} \quad (3.9)$$

The kalman gains  $K_1$  and  $K_2$  are calculated from the equations

$$K = D^T X W^{-1} \quad (3.10)$$

$$\dot{X} = F X + X F^T + C V C^T - K W K^T \quad (3.11)$$

$$F = \begin{bmatrix} \frac{-k_1 k_t u^2}{2 \text{sign}(\hat{p} - p) \sqrt{|\hat{p} - p_a| + \delta}} & k_1 \\ -k_2 & 0 \end{bmatrix} \quad (3.12)$$

$$D = \begin{bmatrix} 1 & 0 \end{bmatrix} \quad (3.13)$$

A small value  $\delta = 10^{-4}$  is added to the denominator of the first element of the  $F$ -matrix. This to ensure that no problems with zero-division occurs in the case if  $\hat{p} = p_a$ .

The structure of the simulink implementation of the kalman filters is seen in figure 3.7, where the estimates from equation (3.8) are calculated. The subsystem "f(\*)" implements

the compressor model with estimated values, while subsystem "K" is the correctional terms. In figure 3.7 the implementation of the correctional term built by equations (3.10) and (3.11) are seen together with the linearization of the compressor model, variable F in equation (3.11). For the full simulink implementation of all kalman filters, as seen in figure 3.5, the reader is referred to the added cd.

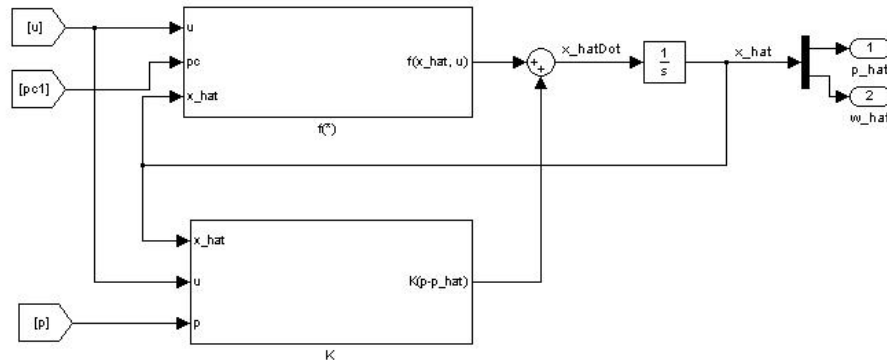


Figure 3.6: Kalman filter

Initially the tuning values were  $V = eye(1)$  and  $W = 1$ , it became obvious however, that a decrease in  $V$  would filter out some of the measurement noise experienced. An increase in  $W$  also gave better results when comparing the measured pressure and the amplitudes of the simulated mass flow. The filter was implemented with covariance matrices

$$V = \begin{bmatrix} 0.000001 & 0 \\ 0 & 0.00001 \end{bmatrix} \quad (3.14)$$

$$W = 2 \quad (3.15)$$

these values were held throughout the four cases the implementation test was run.

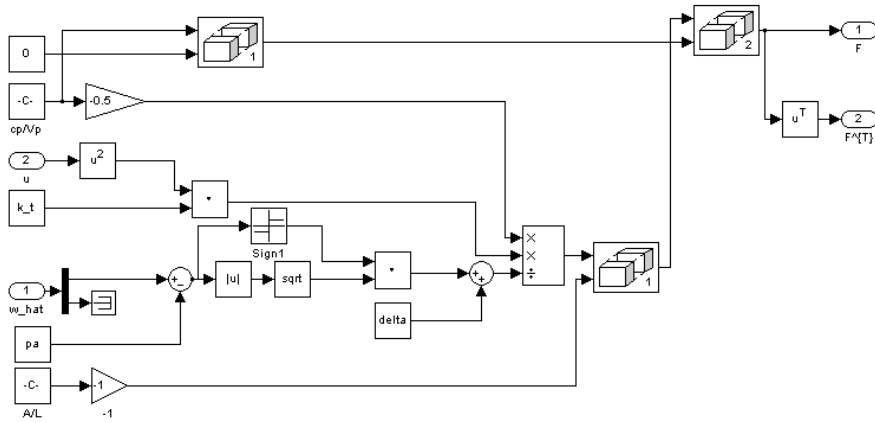
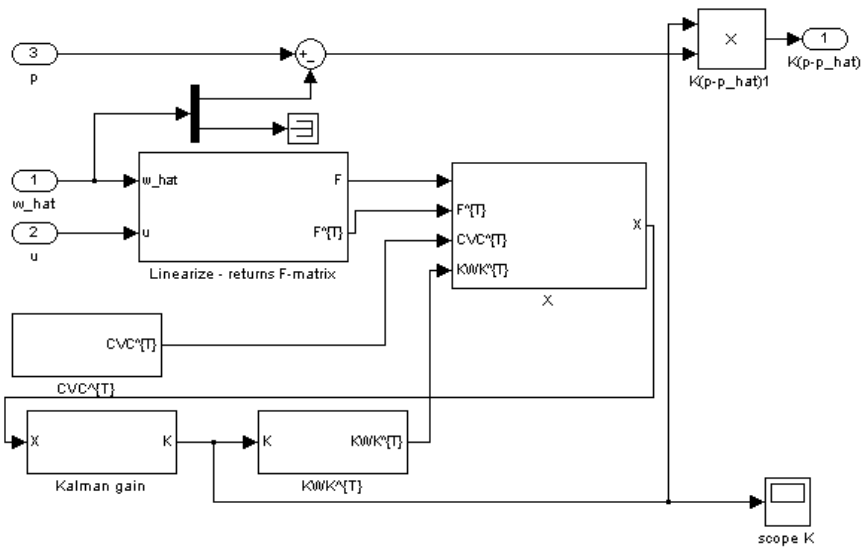


Figure 3.7: Subsystem "K" from fig. 3.6 (top). Linearization of F (bottom).

### 3.3.2 Kalmanfilter 2

An estimate of the mass flow based on the measurement of the downstream pressure was sought. The system model will be the same as in eqs. (3.5) and (3.6), but the input to the observer will be

$$y = p_c(w, N) + w \quad (3.16)$$

The kalman estimate will therefore become

$$\dot{\hat{w}} = k_2(p_c(\hat{w}, N) - p) + K_2(p_c(w, N) - p_c(\hat{w}, N)) \quad (3.17)$$

In this filter the compressor map was implemented and used in the observer. The length of the duct therefore needs to take into account also the length the gas travels through the compressor, and the mass flow constant therefore becomes

$$k_2 = \frac{A}{L_c + L_{cd}} \quad (3.18)$$

The remaining three filters will operate with the compressor map, and  $k_2$  will therefore have the same value for the three remaining observers. The kalman gain is calculated in the same manner as in eqs. (3.10) and (3.11). The linearized values around the estimated value,  $A$  and  $D$ , will now both become expressions containing the derivative of  $p_c(w, N)$  in which no mathematical description is available since  $p_c(w, N) = F_c(w, N) + p_a$ , where  $F_c(w, N)$  is implemented as a matlab file. We therefore use the following approximation for deriving the gradient of  $p_c(w, N)$

$$\frac{\partial(p_c(w, N))}{\partial w} \approx k_2 \frac{p_c(w + dt, N) - p_c(w - dt, N)}{2dt} \quad (3.19)$$

The linearized mass flow function and measurement now becomes

$$F = k_2 \frac{p_c(\hat{w} + dt, N) - p_c(\hat{w} - dt, N)}{2dt} \quad (3.20)$$

$$D = \frac{p_c(\hat{w} + dt, N) - p_c(\hat{w} - dt, N)}{2dt} \quad (3.21)$$

$dt = 10^{-3}$  and is a small alteration in the mass flow The implementation was performed with the same structure as for the first kalman filter. In figure 3.8 the implementation of  $F$  is seen. It is important to emphasize that after all implementations were finished, an error made at an early stage of the development became clear. In the implementation of this filter,  $D = F$ , while it should have been  $D = \frac{1}{k_2}F$ . The result of this is that the calculation

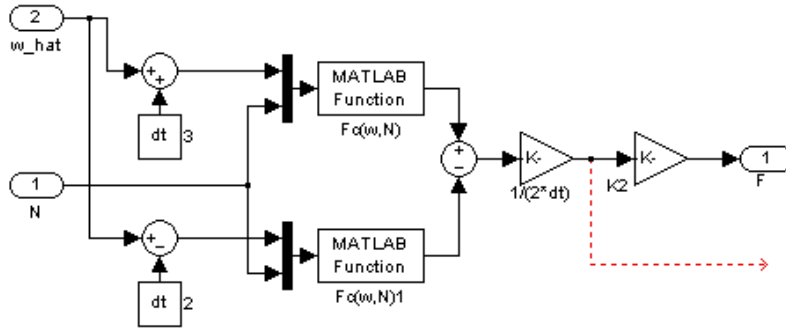


Figure 3.8: Implementation of  $F$ . Kalman filter 2

of kalman gain  $K = D^T X W^{-1}$  will yield a smaller gain. The error was unfortunately not discovered until after all tuning and implementations were finished. In figure 3.8 the dotted line shows where the  $D$ -value should have been taken from. The tuning of the process and measurement noise covariance  $V$  and  $W$ , now both scalar values, proved itself to be very difficult. The estimate was generally noisy and did become unstable fairly quickly. Main focus was on minimizing the innovation process  $p_c(w, N) - p_c(\hat{w}, N)$ . The tuning was terminated on the values

$$V = 1 \tag{3.22}$$

$$W = 1000 \tag{3.23}$$

giving great weights to the model, and almost none to the residual containing the value of  $K$ . This makes sense considering the error that was noted earlier. Post implementation the error was corrected, and the filter was tested toward the implementation data.

### 3.3.3 Kalmanfilter 3

This filter estimates both mass flow and pressure, using the plenum pressure  $p$  as input. The system equations will therefore be the same as in eqs. (3.5) - (3.7). The compressor map is used in the kalman filter, and the estimates becomes

$$\begin{aligned} \dot{\hat{p}} &= k_1(\hat{w} - k_t u^2 \text{sign}(\hat{p} - p_a) \sqrt{|\hat{p} - p_a|}) + K_1(p - \hat{p}) \\ \dot{\hat{w}} &= k_2(p_c(\hat{w}, N) - \hat{p}) + K_2(p - \hat{p}) \end{aligned} \tag{3.24}$$

The kalman gain is calculated from equations (3.10) and (3.11) with  $F$  and  $D$ -matrices

$$F = \begin{bmatrix} -\frac{k_1 k_t u^2}{2 \text{sign}(\hat{p} - p_a) \sqrt{|\hat{p} - p_a| + \delta}} & k_1 \\ -k_2 & \frac{k_2 (p_c(\hat{w} + dt, N) - p_c(\hat{w} - dt, N))}{2dt} \end{bmatrix} \quad (3.25)$$

$$D = \begin{bmatrix} 1 & 0 \end{bmatrix} \quad (3.26)$$

The filter was implemented in the same manner as the earlier shown observers, and the reader is referred to the appended cd for simulink diagrams. The tuning gave the following process and measurement noise covariance values

$$V = \begin{bmatrix} 0.01 & 0 \\ 0 & 0.0001 \end{bmatrix} \quad (3.27)$$

$$W = 35 \quad (3.28)$$

### 3.3.4 Kalmanfilter 4

The filter estimates both plenum pressure and mass flow based on the measurements of plenum and downstream pressure. The compression system equations are the same as in eqs. (3.5) and (3.6), however the measurement matrix now becomes

$$y = \begin{bmatrix} p + w_1 \\ p_c(w, N) + w_2 \end{bmatrix} \quad (3.29)$$

and the measurement noise covariance matrix has the structure  $W = \begin{bmatrix} W_1 & 0 \\ 0 & W_2 \end{bmatrix}$ . The kalman estimates both have two correctional terms, yielding  $K$  to be a 2-by-2 matrix

$$\begin{aligned} \dot{\hat{p}} &= k_1(\hat{w} - k_t u^2 \text{sign}(\hat{p} - p_a) \sqrt{|\hat{p} - p_a|} + \delta) \\ &\quad + K_{11}(p - \hat{p}) + K_{12}(p_c(w, N) - p_c(\hat{w}, N)) \end{aligned} \quad (3.30)$$

$$\dot{\hat{w}} = k_2(p_c(\hat{w}, N) - \hat{p}) + K_{21}(p - \hat{p}) + K_{22}(p_c(w, N) - p_c(\hat{w}, N)) \quad (3.31)$$

The kalman gains are calculated by equations (3.10) and (3.11), with matrices  $F$  and  $D$  given by

$$F = \begin{bmatrix} -\frac{k_1 k_t u^2}{2 \text{sign}(\hat{p} - p_a) \sqrt{|\hat{p} - p_a| + \delta}} & k_1 \\ -k_2 & \frac{k_2 (p_c(\hat{w} + dt, N) - p_c(\hat{w} - dt, N))}{2dt} \end{bmatrix} \quad (3.32)$$

$$D = \begin{bmatrix} 1 & 0 \\ 0 & \frac{p_c(\hat{w} + dt, N) - p_c(\hat{w} - dt, N)}{2dt} \end{bmatrix} \quad (3.33)$$

The observer was implemented using the same structure as the other filters and is found on the cd. The reader is referred to appendix A for the simulink diagram. The tuning matrices used in the implementation of the filter was

$$V = \begin{bmatrix} 0.01 & 0 \\ 0 & 0.0001 \end{bmatrix} \quad (3.34)$$

$$W = \begin{bmatrix} 3 & 0 \\ 0 & 100 \end{bmatrix} \quad (3.35)$$

### 3.4 Recycle system modeling

In order to build a recycle loop on the laboratory compression system, different solutions were investigated by simulation models taking its basis in the knowledge already available from the set-up. A simulation model capturing the dynamics of the compressor as well as describing the pressures also possible to measure was sought. Basis was taken in the studies of industrial surge recycle solutions and practical aspects of the compressor set-up available. A hot recycle scheme is assumed to be the most likely recycle solution due to physical space next to the compressor. Another aspect is that this will show the principle of surge avoidance in a good way without interrupting the plenum volume in any way. Still solutions taking the recycle gas from the plenum were also investigated. The temperature has been held constant through all the simulations in this report. From studies of available temperature data from the implementation of kalman filters it is observed that the change in temperature for a 60 second run was between 3 and 11 Kelvin. The longest simulation that was performed with surge recycle was 20 seconds, but most test were under 10 seconds. It was therefore assumed that the temperature would not change greatly during the simulation period, and it was therefore held constant.

#### 3.4.1 Recycle directly downstream

The goal was here to develop a simulation model of the compressor after the recycle part is added, but also to investigate how different descriptions and parameter sizes would effect the system, especially the pipe lengths to be used. The model of a compressor feedback system was presented in chapter 2.1, and it models the compressor with a volume up- and down-stream. This description is also chosen here, even though the real system does not have defined volumes on each side of the compressor. A figure of the lab-setup the

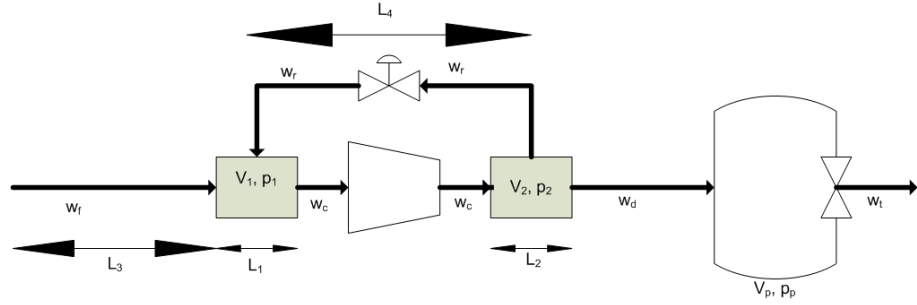


Figure 3.9: Principal sketch of compression system with recycling , duct and plenum.

way it has been modeled for simulation is seen in figure 3.9. Basis is therefore taken in equations (2.30)-(2.32), considering that we also in this model choose to ignore the speed dynamics and use measurement of the impeller speed as input instead. In addition to the two mass balances describing the volumes of the model in chapter 2.1, the mass balance for the plenum will still be needed. The three pressures are therefore described by

$$\dot{p}_1 = \frac{c^2}{V_1}(w_f + w_r - w_c) \quad (3.36)$$

$$\dot{p}_2 = \frac{c^2}{V_2}(w_c - w_r - w_d) \quad (3.37)$$

$$\dot{p}_p = \frac{c^2}{V_p}(w_d - w_t) \quad (3.38)$$

The two modeled volumes  $V_1$  and  $V_2$  are calculated based on the two lengths  $L_1$  and  $L_2$  in figure 3.9, and will be varied through simulations. The mass flow through the compressor  $w_c$  is assumed to have the same structure as it did in the lab-setup, and the same compressor characteristics are used. However the pressure difference will now be between the two imaginary volumes

$$\dot{w}_c = \frac{A}{L_c}(p_1 + F_c(w_c, N) - p_2) \quad (3.39)$$

where  $L_c = 270$  cm. The mass flow through the plenum throttle  $w_t$  is the same as it was earlier

$$w_t = k_t u_t^2 \text{sign}(p_p - p_a) \sqrt{|p_p - p_a|} \quad (3.40)$$

The mass flow downstream  $w_d$  is described by the momentum balance between  $V_2$  and the plenum. It is assumed that the length of the duct from the second volume and till the

plenum is the same as what was referred to as the duct length in the lab-model, namely  $L_{cd} = 180$  cm. Downstream mass flow is then modeled

$$\dot{w}_d = \frac{A}{L_{cd}}(p_2 - p_p) \quad (3.41)$$

The inlet mass flow  $w_f$  and recycle mass flow  $w_r$  were both modeled with one static and one dynamic representation. The motivation was to see how the system would behave using the different models. The pressure difference over the inlet duct in steady state is described as

$$p_1 - p_a = F_{cu}(w_f) \quad (3.42)$$

where  $F_{cu}(w_f)$  is a forcing term describing the pipe friction, flow profile and unmodeled dynamics. The same characteristics that were developed for the compressor without recycling is used with the hope that mass flow in this part of the system does not change greatly when adding the recycling. In Bøhagen (2007) the characteristics for inlet flow was developed for the compression system, and can be seen in figure 3.10. It is obvious that the pressure difference upstream is completely dependent on the mass flow alone, since all the characteristics for the different impeller speeds and throttle openings collapse to the same line. From the characteristics a function for the forcing term is derived,

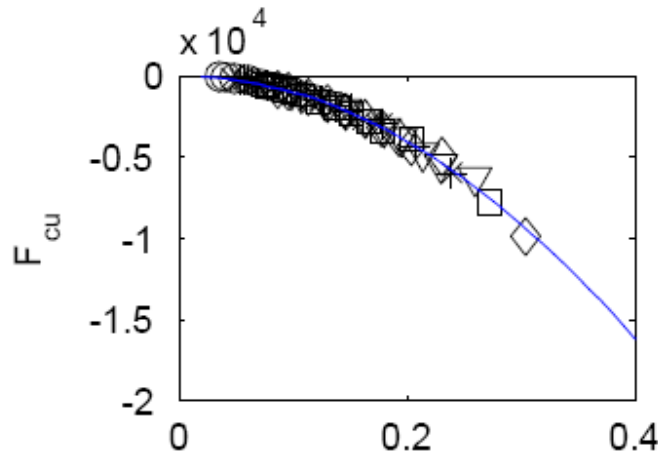


Figure 3.10: Forcing term  $F_{cu}$  in steady state. From (Bøhagen 2007).

$F_{cu}(w_f) = -k_f w_f^2$ , where  $k_f = 1.0109 \times 10^5$ . The pressure difference over the inlet duct

now becomes

$$\begin{aligned} p_1 - p_a &= -k_f w_f^2, & w_f > 0 \\ p_1 - p_a &= k_f w_f^2, & w_f < 0 \end{aligned} \quad (3.43)$$

and an expression for static mass flow can be written

$$w_f = \text{sign}(p_a - p_1) \sqrt{\frac{1}{k_f} |p_a - p_1|} \quad (3.44)$$

The dynamic representation of the inlet mass flow is modeled from the momentum equation and yields

$$\dot{w}_f = \frac{A}{L_3} (p_a - p_1) \quad (3.45)$$

where  $L_3$  is the length of the duct as shown in figure 3.9.

The mass flow over the recycle valve  $w_r$  was also described by a static and dynamic description. Knowing that the valve used in the recycle line will be the same as the plenum valve, the same pressure difference description was chosen for the recycle mass flow as for mass flow from plenum  $w_t$ .

$$w_r = k_r u_r^2 \text{sign}(p_2 - p_1) \sqrt{|p_2 - p_1|} \quad (3.46)$$

This is also the same description as suggested by Egeland & Gravdahl (2003) in equation (2.10). Being that it is the same type of valve as used in the plenum it is assumed that  $k_r = k_t$ . The recycle valve opening is here described by  $u_r$  and is noted in percent.

A dynamic description of the recycle flow was also modeled based on the momentum balance

$$\dot{w}_r = \frac{A}{L_4} (p_2 - p_1 - F_r) \quad (3.47)$$

where  $L_4$  is the length of the recycle duct and  $F_r$  is a force term describing the forces working on the mass from the duct and valve. In steady state we have  $\dot{w}_r = 0$  and

$$F_r = p_2 - p_1$$

Solving 3.46 for  $(p_2 - p_1)$  yields a term describing the forces and the dynamic mass flow becomes

$$\dot{w}_r = \frac{A}{L_4} \left( p_2 - p_1 - \text{sign}(p_2 - p_1) \frac{w_r^2}{k_r^2 u_r^4} \right) \quad (3.48)$$

An analysis of the system behavior using different combinations of inlet and recycle mass flow, as well as different parameter values on the duct lengths  $L_1-L_4$ , was performed. The main motivation was to search for trends in dynamics and behavior when the different combinations and lengths were applied. All simulations were run with impeller speed at 12500 rpm and followed the same scheme.

1. Plenum throttle  $u_t = 100\%$  and recycle valve  $u_r = 0\%$  for one second. Compression system in steady state
2. Plenum throttle  $u_t = 40\%$  and recycle valve  $u_r = 0\%$  for one second. System enters surge.
3. Plenum throttle  $u_t = 40\%$  and recycle valve  $u_r = 50\%$  for one second. System restabilizes.

No dynamics or time delays were modeled on the valves at this point, so all valve changes were immediate. The test plan presenting the different throttle lengths are presented in appendix D, while the simulink simulation model is added to the appended cd. The simulation step size was set to  $10^{-6}$  due to trouble with numerical calculations initially.

### 3.4.2 Recycling from plenum

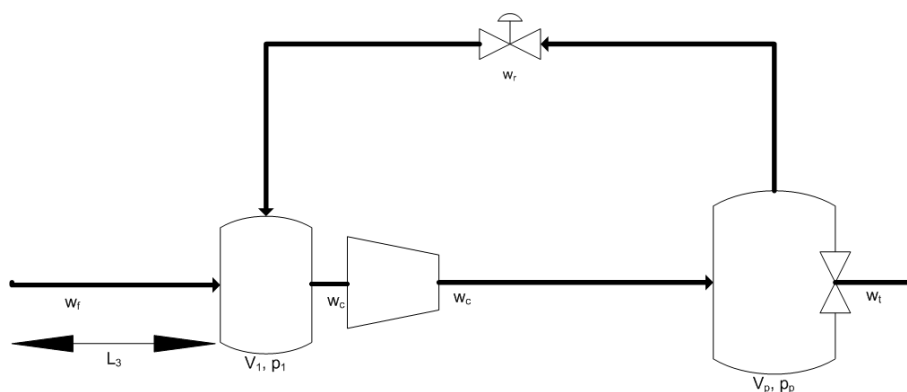


Figure 3.11: Recycling from plenum.

As presented in chapter 2 it is common to have a knock-out pot, or scrubber, situated upstream of the compressor. Mathematical models also presents a volume downstream. A simulation model of the compressor taking its recycle gas from the plenum volume and

with a scrubber upstream was created. A sketch of the system is seen in figure 3.11. The equations describing the system are similar to the ones describing the recycle system in chapter 3.4.1, though with one less pressure state. The model build is therefore described by

$$\dot{p}_1 = \frac{c^2}{V_p}(w_f + w_r - w_c) \quad (3.49)$$

$$\dot{p}_p = \frac{c^2}{V_1}(w_c - w_r - w_t) \quad (3.50)$$

$$\dot{w}_c = \frac{A}{L_c + L_{cd}}(p_1 + F_c(w_c, N) - p_p) \quad (3.51)$$

$$\dot{w}_f = \frac{A}{L_3}(p_a - p_1) \quad (3.52)$$

$$w_t = k_t u_t^2 \sqrt{p_p - p_a} \quad (3.53)$$

$$w_r = k_r u_r^2 \sqrt{p_p - p_1} \quad (3.54)$$

where  $V_1 = 0.08 \text{ m}^3$  is the volume of the imagined knock-out pot in front of the compressor. The length  $L_3$  is set to 50 cm. Both the mass flow from the plenum and the recycle mass flow are modeled statically. All other parameters are kept with the same size as in previous simulations. A simulink model of the compression system is found on the added disc. One simulation similar to the scheme used in chapter 3.4.1 was run, but prolonging each of the intervals from one to three seconds. The goal was to see if the system behaved similar, and how the relatively large volume in front of the compressor would effect the system.

### 3.4.3 Simulation of generic component model

Since the laboratory set-up does not have defined volumes directly up- and down-stream of the compressor, attention was drawn to the model suggested by Murphy et al. (1995), and presented in equations (2.52) to (2.58). An extensive theoretical study of the model was tried, but finding it hard to achieve any theory explaining and backing up the suggested system, basis was taken in the article by Murphy et al. (1995) alone. To model the system between two constant pressures the recycling was taken from the plenum, yielding a model as sketched in figure 3.12. The model was fitted to the real compression system, using the same compressor map and valve characteristics as for the other two recycle models. The temperature was initially held constant mainly due to the uncertainties related to the description in eq. (2.58), but also since I do not see how the

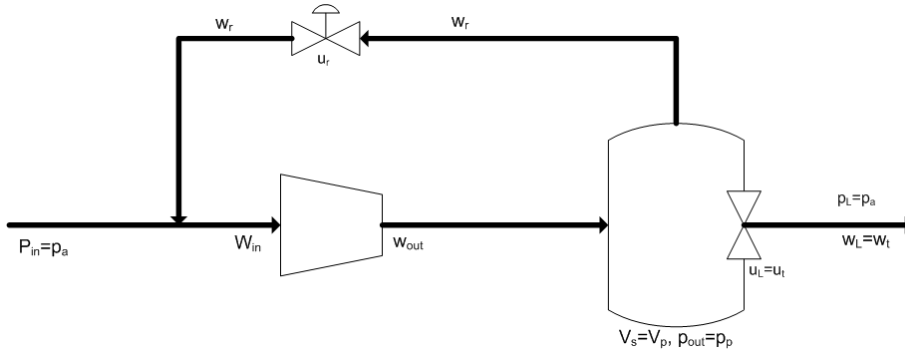


Figure 3.12: Recycle from plenum using model suggested by Murphy et al. (1995).

mathematical transfer from the generic component description in eq. (2.50) to the state space description in (2.58) is achieved. It was planned to add the temperature description after the rest of the system was implemented. Using our compressor measurements the model implemented becomes

$$\dot{p}_p = \frac{2c_p^2}{V_p}(w_{in} - w_{out}) \quad (3.55)$$

$$\dot{w}_{in} = \frac{2A}{L_c + L_{cd}}(p_c(w_{in}, N) - p_p) - \dot{w}_{out} \quad (3.56)$$

$$w_t = k_t u_t^2 \text{sign}(p_p - p_L) \sqrt{|p_p - p_L|} \quad (3.57)$$

$$w_r = k_r u_r^2 \text{sign}(p_p - p_{in}) \sqrt{|p_p - p_{in}|} \quad (3.58)$$

$$\begin{aligned} \dot{w}_{out} &= \dot{w}_t + \dot{w}_r \\ &= \left( \frac{\partial w_r}{\partial p_p} + \frac{\partial w_t}{\partial p_p} \right) \dot{p}_p + \frac{\partial w_r}{\partial u_r} \dot{u}_r + \frac{\partial w_t}{\partial u_t} \dot{u}_t \\ &= \left( \frac{k_r u_r^2 \text{sign}(p_p - p_{in})}{2\sqrt{|p_p - p_{in}|}} + \frac{k_t u_t^2 \text{sign}(p_p - p_L)}{2\sqrt{|p_p - p_L|}} \right) \dot{p}_p \\ &\quad + \left( 2k_r u_r \text{sign}(p_p - p_{in}) \sqrt{|p_p - p_{in}|} \right) \dot{u}_r \\ &\quad + \left( 2k_t u_t \text{sign}(p_p - p_L) \sqrt{|p_p - p_L|} \right) \dot{u}_t \end{aligned} \quad (3.59)$$

The simulink model is added to the appended cd. Both  $V_p$  and  $L_c + L_{cd}$  were altered during the simulation of the system to see if there was opportunity of gaining the same behavior from this system as seen in previous simulation schemes.

### 3.5 Implementation and simulations surge avoidance.

A surge avoidance scheme was built and simulated using the compression recycle scheme presented in chapter 3.4.1, with dynamic inlet mass flow,  $\dot{w}_f$  and static recycle mass flow,  $w_r$ . The recycle mass flow was chosen statically being that this was presented in the theory and because the simulation results yielded no large impact on the system by choosing this representation. The length of the inlet pipe from eq. (3.45) was set to  $L_3 = 40$  cm, and the two imaginary volumes up and downstream the compressor in eqs. (3.36) and (3.37) were both calculated with  $L_1 = L_2 = 10$  cm. The gas temperature was held constant throughout all simulations.

Both the throttle valve of the plenum and the recycle valve will in the physical system be the same type of valves with the same dynamics. Because the change of a set point in any of the valves will not occur instantly, it became of interest to investigate the behavior of the valves and develop a transfer function describing the step response of the valves. Several different steps were applied to the valve, gathering measurements of the valve behavior. The tests performed are presented in appendix E, and all measurements gathered are added on disc. An average of the step responses from the valve test was taken and yielded the following valve dynamics used in the implementation and testing of surge avoidance controller

$$H(s) = \frac{1}{0.6s + 1} e^{-0.65s} \quad (3.60)$$

The surge line seen in figure 3.13 was identified by Bøhagen (2007) to be

$$p_c = 21.85 * 10^5 (w_c^2) + 52.18 * 10^3 (w_c) - 175.6 \quad (3.61)$$

Taken its basis in theory presented about surge avoidance control, the avoidance line was placed approximately 10% to the right of the surge line. At one stage the surge line was moved even further to the right for test of a specific case.

A linear PI-controller was used to control the recycle valve, based on measurements of either mass flow, downstream pressure or a combination of both

$$u_r = K_p \left( e + \frac{1}{T_i} \int e(\tau) d\tau \right) \quad (3.62)$$

The variable  $e$  gives a measurement of how far away from the surge avoidance line the system is in the compressor map. The controller gain  $K_p$  and integration time  $T_i$  was tuned roughly using a Ziegler-Nichols method. Not much effort was put into fine tuning

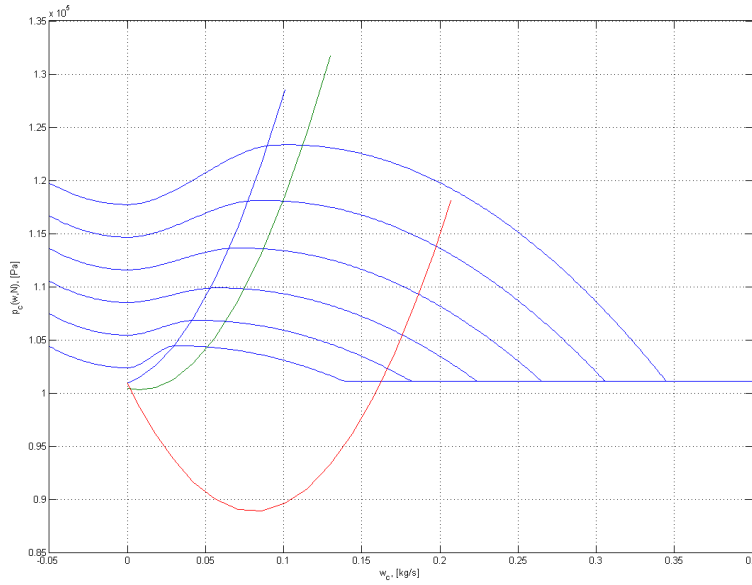


Figure 3.13: Compressor map with surge line (blue), avoidance lines.

of the system, being that this is both very compressor specific and tedious. It was decided to let the controller be a little aggressive, being that  $u_r$  would open more than strictly necessary, in this way the concept of surge avoidance would still be clear.

Three different schemes were simulated, using different measured values in the compressor map.

1.  $e_1 = w_c - w_{avoidline}$ ,  $K_p = 500$  and  $T_i = 0.17$
2.  $e_2 = p_{avoidline} - p_c$ ,  $K_p = 0.02$  and  $T_i = 0.17$
3.  $e_3 = e_1 + e_2$ ,  $K_p = 0.01$  and  $T_i = 0.17$

The opening of the control valve to avoid surge was activated by the PI-controller when  $e \leq 0$ . The control valve did not fully close again until there was assurance that the compressor was working in the steady state area of the map, in this case there were set points of  $e$  and the throttle valve that needed to be fulfilled for the recycle valve to close completely. The simulink diagrams of the three different controllers are added on the appended disc.

Different tests were performed to see how well the avoidance scheme performed in different scenarios with the compressor. Set point changes in both throttle opening  $u_t$  and speed  $N$  were tested. In the first test  $u_t$  was completely open, and then choked down drastically to values around 30%. The motivation behind this was to see how the system behaved under a great change, such as an emergency shut down sequence. The surge avoidance line was then moved to the right in the compressor map until surge was avoided. In the second test performance around the surge avoidance line was tested by letting  $u_t = 65\%$  initially and then being choked down to values around 50%. The most efficient area in the compressor map is around the surge line, and it was therefore interesting to see if the compressor could operate in this area without surging. All tests so far were performed with a constant speed  $N = 17500$  rpm.

Changes in set points for the speed were also tested, letting  $N$  be a sinus with increasing amplitude and frequency,  $N = A\sin\omega t + b$ , about a bias of  $b = 14500$ . Initially the throttle valve was completely opened, then choked down to  $u_t = 60\%$ . Lastly  $u_t$  was kept at 65% while an increasing step in speed was tested. The drive unit was not modeled with any dynamics, and any change in speed  $N$  was therefore instantaneous.



# Chapter 4

## Results and observations

### 4.1 Results simulation of compression system.

The compressor was simulated and compared to real measured plenum pressure. The result is seen in figure 4.1. There are smaller differences both in phase and amplitude of the oscillations. The algebraic model used to describe the compression system is fairly simple compared to the real physical compressor, and therefore it can not be expected that the simulations would be dead on. However, the phase of the oscillations is in the same size area, and the dynamic behavior is similar when comparing the measured and simulated pressure.

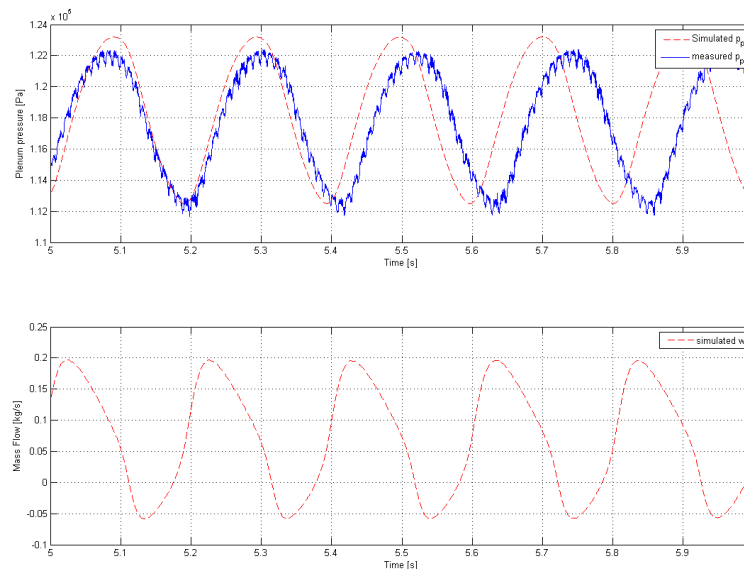


Figure 4.1: Simluated and measured compressor values.

## 4.2 Results simulations of kalman filters with no recycle feedback.

The tuning of the filters was performed prior to any laboratory implementations, and the results were compared to measurements of pressure, innovation process for the respective filter and simulations of mass flow.

### 4.2.1 Kalman filter 1

The first filter estimated pressure and mass flow using the model without compressor map. The estimates of  $p$  and  $w$  are plotted in figure 4.2 together with the measured values of the plenum pressure. The filter uses approximately 0.15 seconds to achieve a steady estimate initially. The mass flow behaves in the same pattern and with almost the same amplitudes as was seen in the simulations in figure 4.1. The innovation process  $p - \hat{p}$  is seen in figure (4.3) and has a maximum variation between approximately 700 and -800 for the whole period. The gains for the respective estimates are seen in figure 4.4. The pressure gain varies around 53.6 while the mass flow gain swings around 0.0012

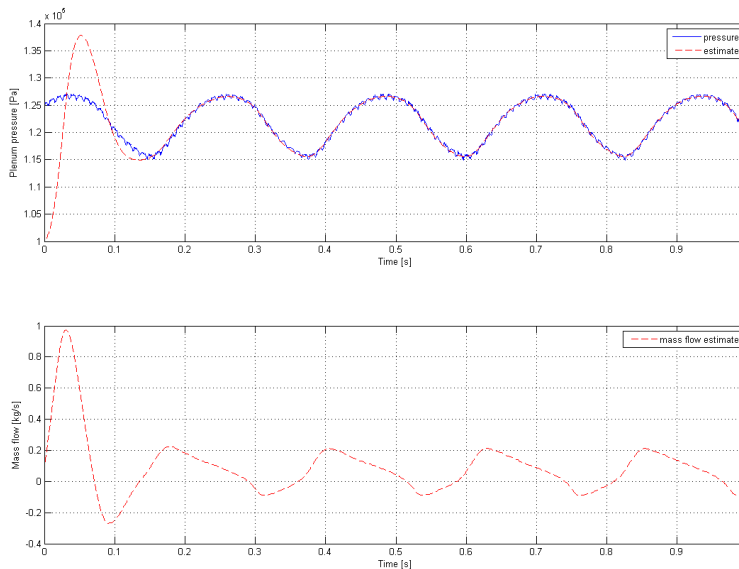


Figure 4.2: Estimated vs measured pressure, estimated mass flow.

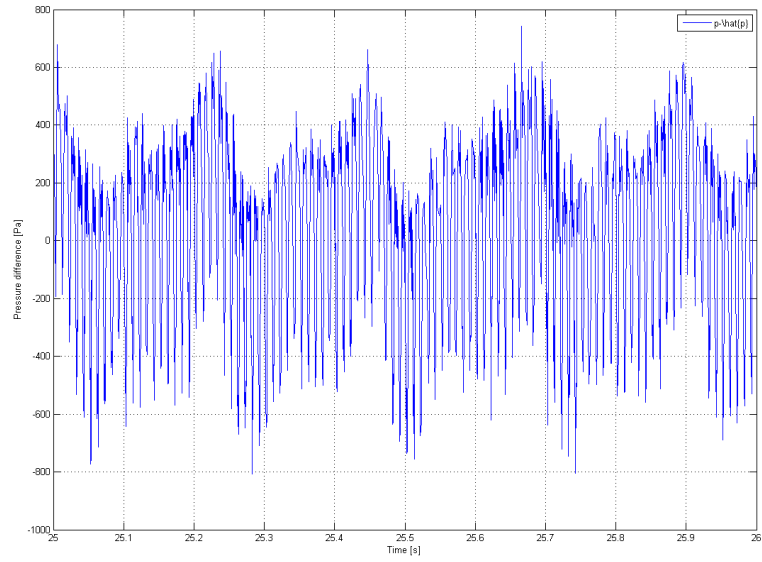


Figure 4.3: Innovation process

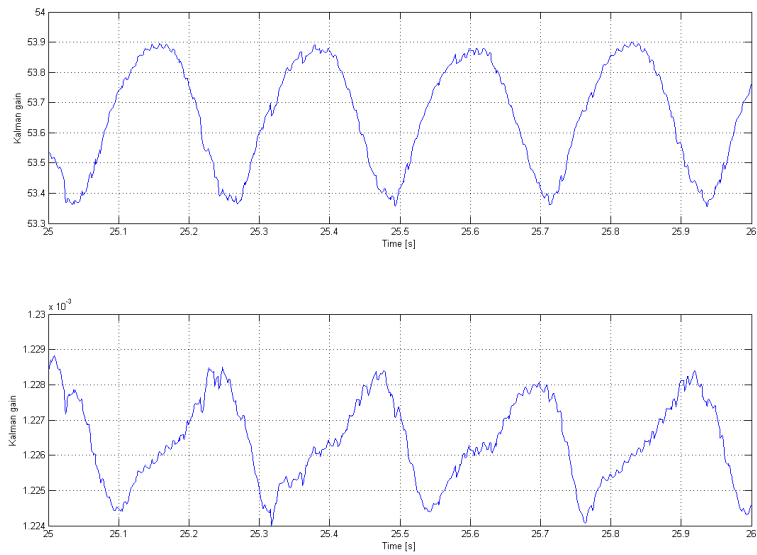


Figure 4.4: Kalman gains, plenum pressure (top) and mass flow (bottom).

## 4.2.2 Kalman filter 2

The second observer estimated mass flow only. The tuning was performed based on the innovation process in figure 4.6 and comparison to the simulations of the compressor. This filter proved to be the hardest to tune, and several tuning values tested made the estimate become unstable. The innovation process varies over a quite large area, and because of this the gain also has larger values than the first kalman filter.

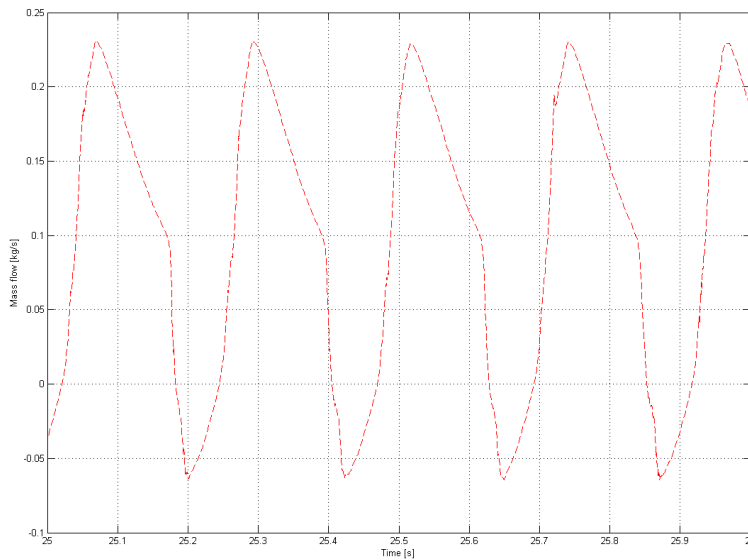


Figure 4.5: Estimated mass flow

It is important to emphasize that there was an error in the implementation of the kalman filter, and this has contributed to the difficulties of tuning the filter and keeping it stable. We will how ever later in this chapter see that there are also another, and more severe, problem associated with this filter.

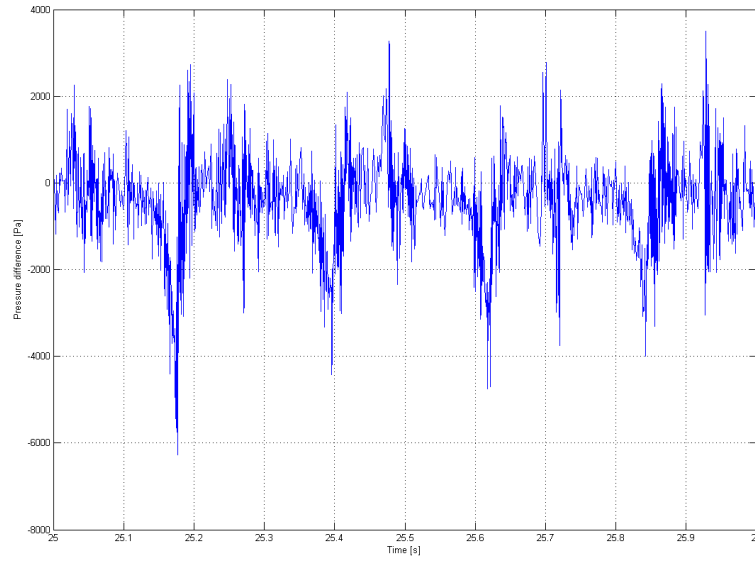


Figure 4.6: Innovation process,  $p_c(w, N) - p_c(\hat{w}, N)$

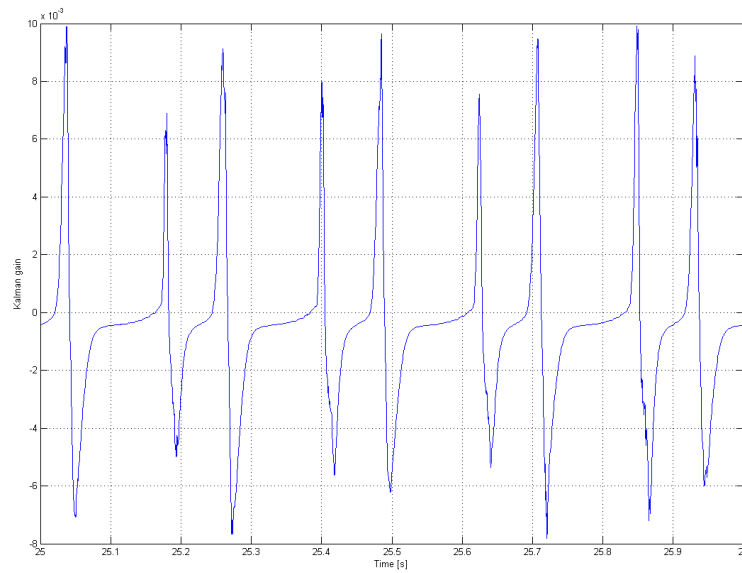


Figure 4.7: Kalman gain

### 4.2.3 Kalman filter 3

This filter is a parallel to the first kalman filter, but here the compressor map was used in the model of mass flow. The estimates are seen in figure 4.10, while the innovation process is presented in 4.9. It should be noted that it does vary over a slightly larger area than the first filter. The kalman gains in figure 4.10 are markable larger than in the first filter, and varies also over greater values. In the tuning, the measurement and process noise covariance  $W$  and  $V$  were generally given larger values than in the first filter.

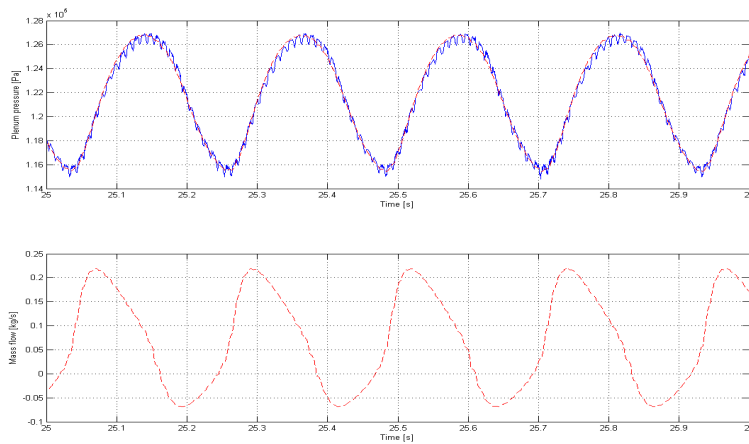


Figure 4.8: Estimated vs measured pressure (top), estimated mass flow (bottom).

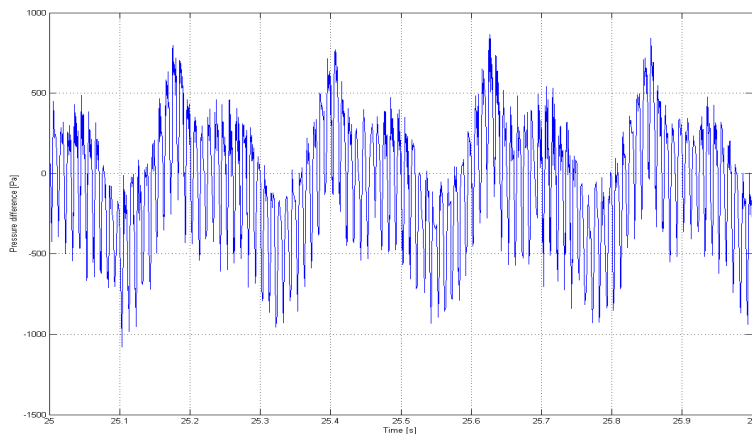


Figure 4.9: Innovation process  $p - \hat{p}$

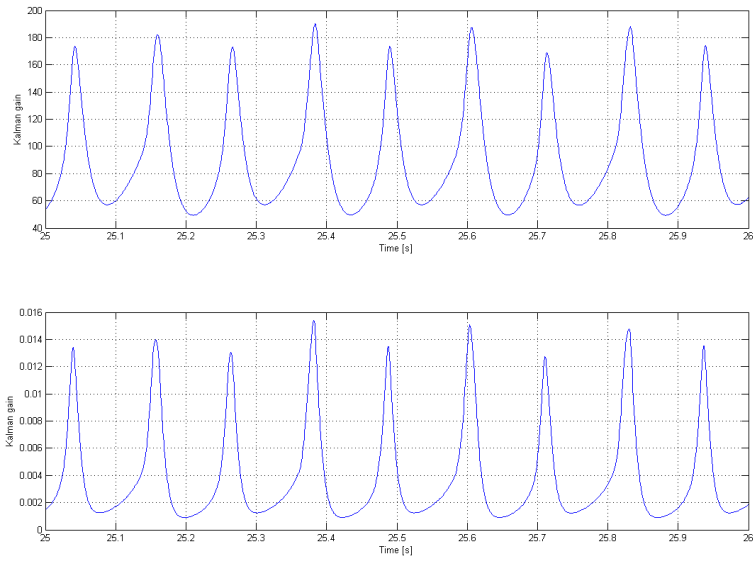


Figure 4.10: Kalman gain plenum pressure (top) and mass flow (bottom).

#### 4.2.4 Kalman filter 4

In this filter both the plenum pressure and the downstream pressure were used to correct the estimate of the two states. The results are seen in figures 4.11 to 4.13. It is clear from figure 4.13 that the filter does emphasize the plenum pressure difference more than the downstream pressure difference ( $K_{11}$  and  $K_{21}$ ).

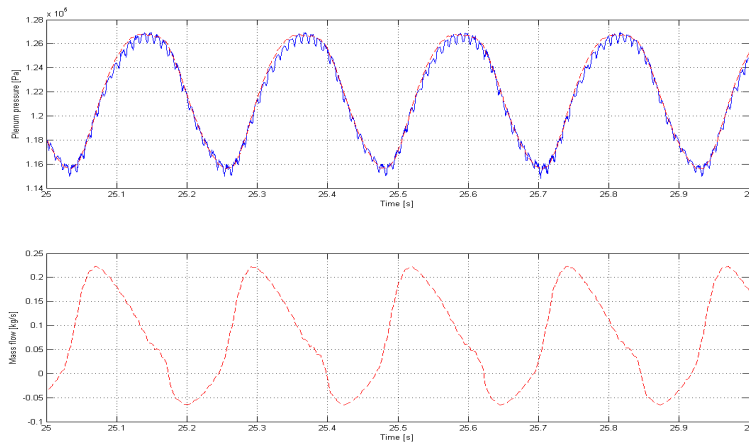


Figure 4.11: Estimated vs measured pressure (top), estimated mass flow (bottom).

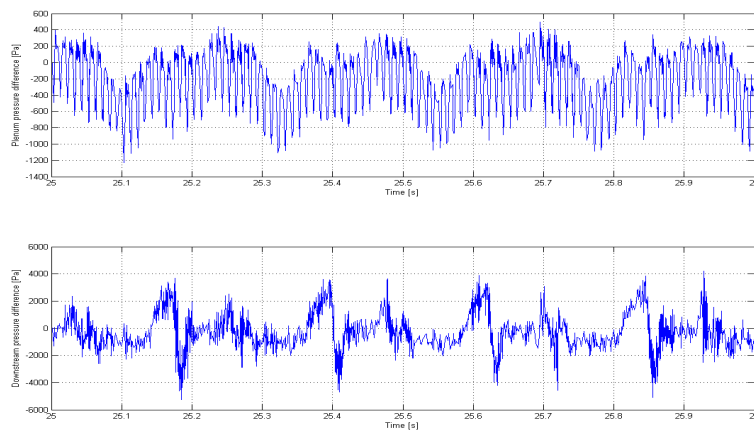


Figure 4.12: Innovation process  $p - \hat{p}$  (top) and  $p_c(w, N) - p_c(\hat{w}, N)$  (bottom).

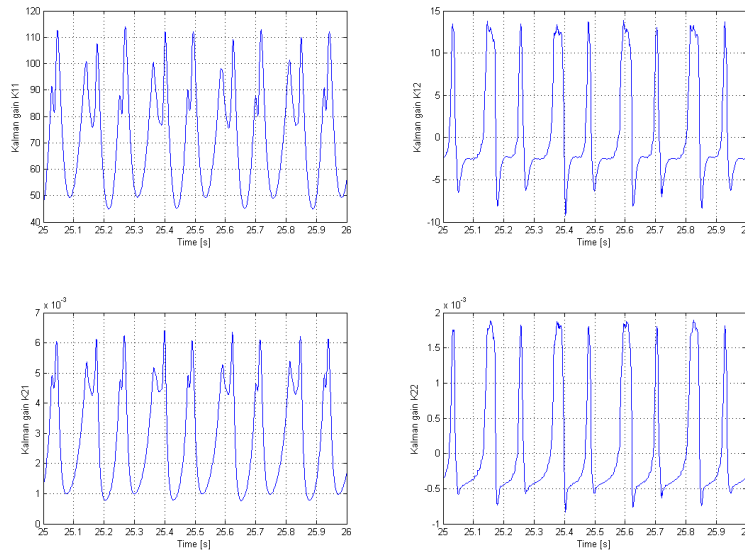


Figure 4.13: Kalman gains

### 4.3 Results implementation of kalman filters on compression system.

The system was tested for four different cases as presented in chapter 3.5 to cover the greatest parts of the steady state compressor map. The first case, where the speed is increased from 12500 rpm to 22500 rpm with full throttle opening, is here presented with plots. The plots from the other three cases are presented in appendices A-C.

#### 4.3.1 Kalman filter 1

In figure 4.14 the measured pressure and mass flow are seen plotted together with the estimated states. The filter has removed a lot of the noise in the pressure estimate, however the mass flow estimate is corrupted by noise. The mass flow estimate is calculated from the innovation process ( $p - \hat{p}$ ) seen in figure 4.15, which has a variation of approximately 1000, this is a great number compared to the mass flow size. The mass flow estimate is also generally a little higher than the real mass flow. This can be a result from the fact that the pressure estimate also lays in the top range of the measured pressure. The divergence between the median of the measured and estimated pressure is approximately 0.35%,

while for the mass flow the error comes to about 10.8% before the step occurs after 20 seconds. It is of course natural that the error will be higher for the mass flow considering the pressure is actually measured. The transient period of the mass flow estimate is faster than the real mass flow, due to the almost immediate pressure rise that occurs when the speed is increased. The kalman gains of the first filter are in the same size-range as they were during tuning of the filter, and are presented in figure 4.16.

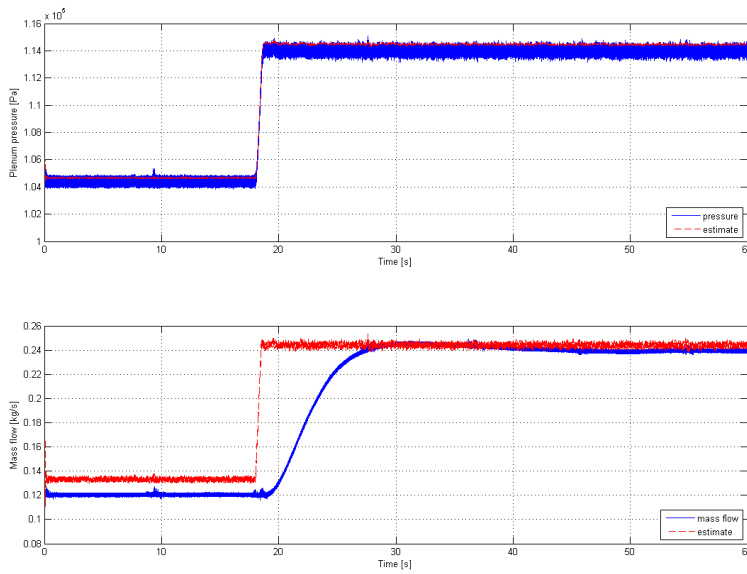


Figure 4.14: Measured and estimated pressure and mass flow

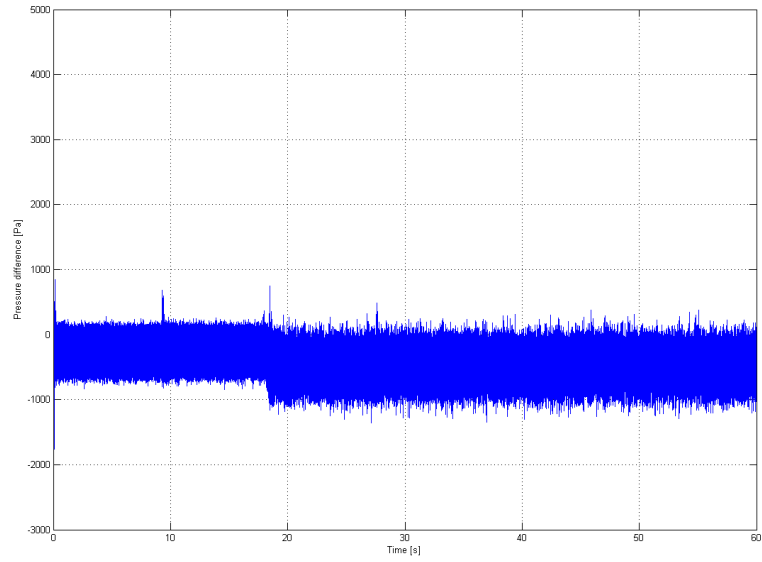


Figure 4.15: Innovation process  $p - \hat{p}$ .

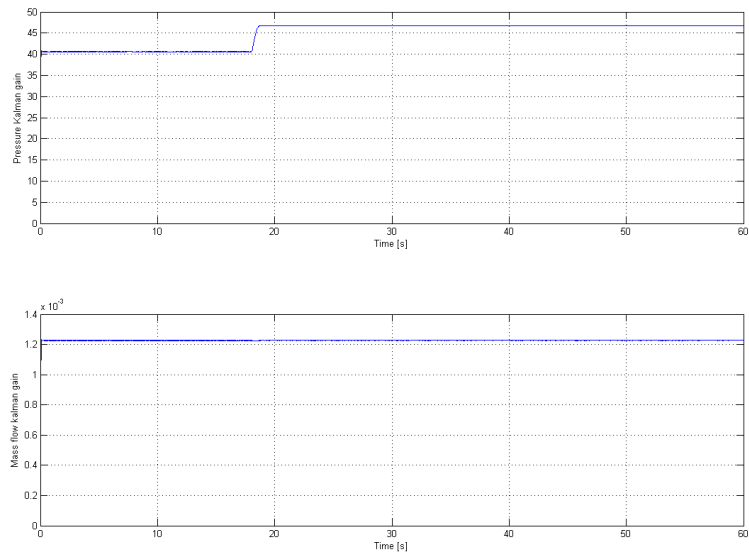


Figure 4.16: Kalman gains, pressure at top and mass flow at bottom.

### 4.3.2 Kalman filter 2

As presented in chapter 3.3, there was an implementational error in the kalman filter estimating only the mass flow. It was also emphasized that the filter easily became unstable during tuning, something also experienced during implementation as seen in figure 4.17. The filter is able to estimate the mass flow with approximately 4% error until the step in speed occurs after 19 seconds. The estimate then becomes unstable but does decrease towards a smaller value over the next 10 seconds. However, a disturbance does occur after 29 seconds, and the estimate stabilizes at  $4.2 * 10^7$ . The innovation process  $p_c(w, N) - p_c(\hat{w}, N)$  in figure 4.18 has initially a variation of  $\pm 1000$  around zero. After step in speed the variation increases to about  $\pm 2000$  and the variation is around  $1.5 * 10^4$  instead of zero. In the implementation we have  $p_c(\hat{w}, N) = F_c(\hat{w}, N) + p_a$ . When the mass flow estimate becomes too high,  $F_c(\hat{w}, N)$  is not able to calculate the correct value and returns zero. This way we get  $p_c(\hat{w}, N) = p_a$ , which is the reason for the set point change in the innovation process. The kalman gain reacts when the step and disturbance occurs but becomes zero, implying that all trust is put in the model of the system.

When the kalman model was corrected, tuned and tested toward the data from the implementation, an estimation of the mass flow did change to the better, as seen in figure 4.20. The steady state estimate is very good before the step occurs, and does not become unstable like it did earlier, but estimates the mass flow with an error of approximately 11.7 % also after the set point is changed. However there is a great change in the value of the estimate during the transient period. This change in mass flow did not alter the value of  $p_c(\hat{w}, N)$  at all. When the same filter was tested toward data from the second test, with impeller speed  $N = 22500$  rpm and the throttle choked from 100 to 60 %, the filter did become unstable after 44 seconds, as seen in figure 4.21.

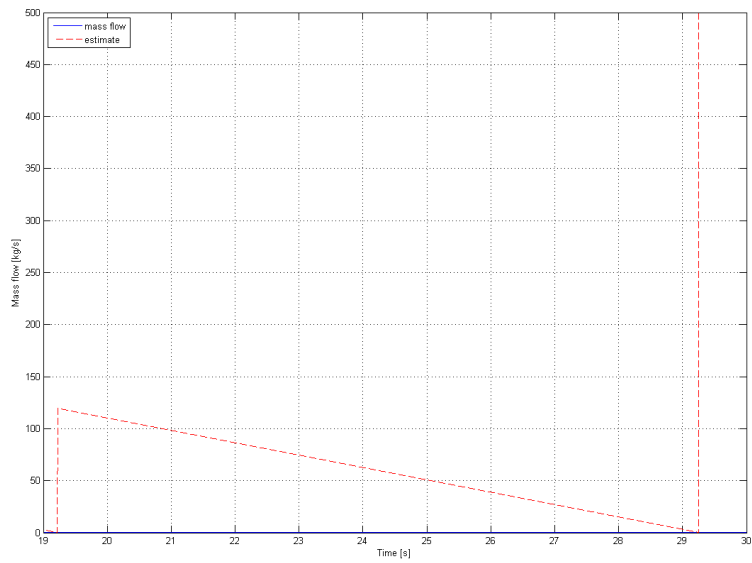
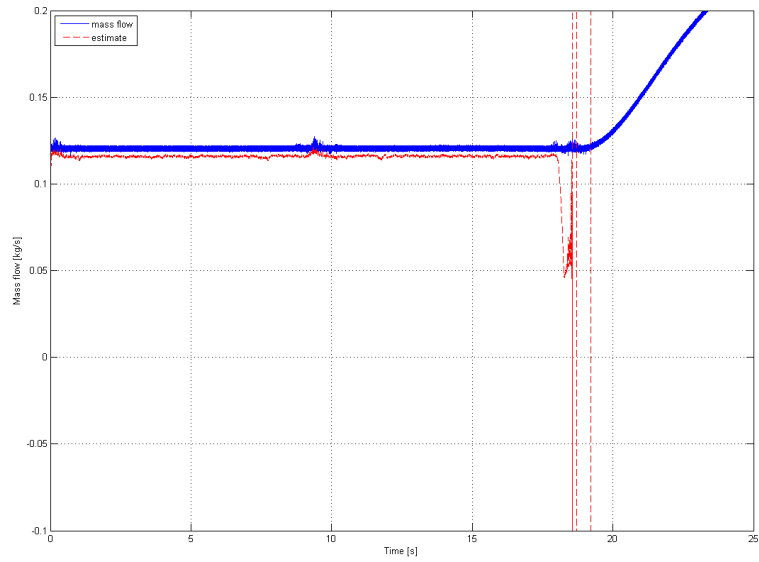


Figure 4.17: Measured and estimated mass flow, different time scales top and bottom.

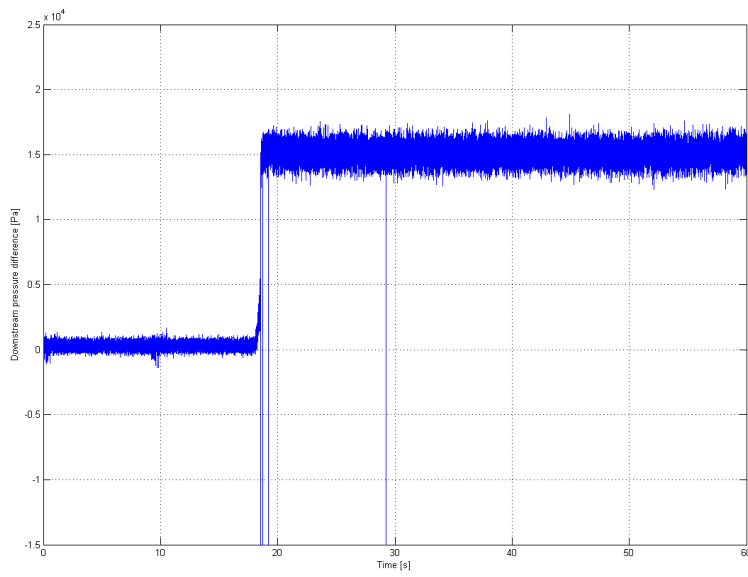


Figure 4.18: Innovation process  $p_c(w, N) - p_c(\hat{w}, N)$ .

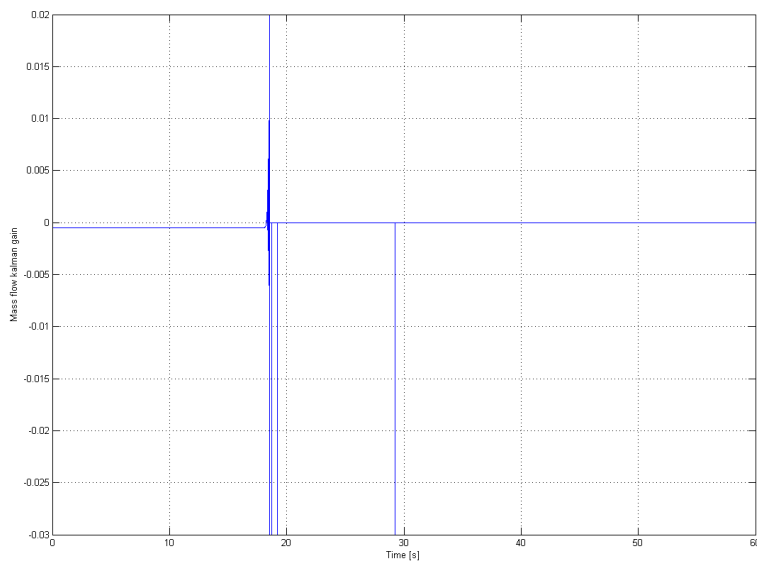


Figure 4.19: Kalman gain

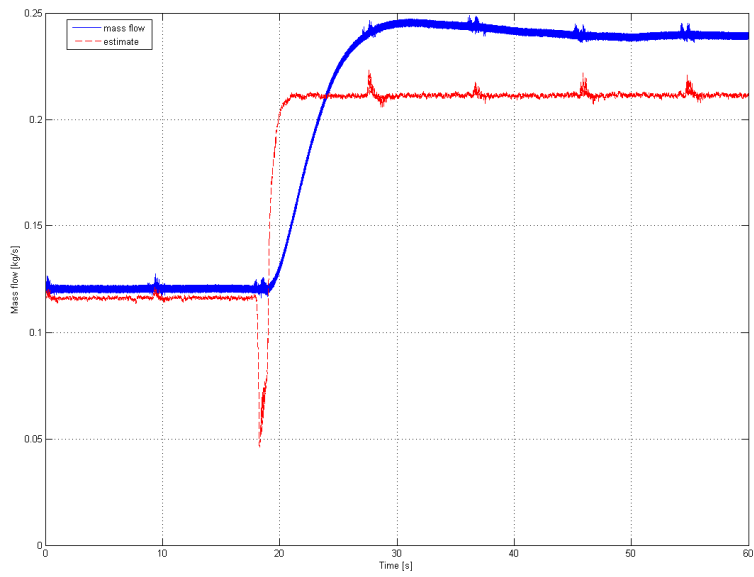


Figure 4.20: Mass flow, corrected filter

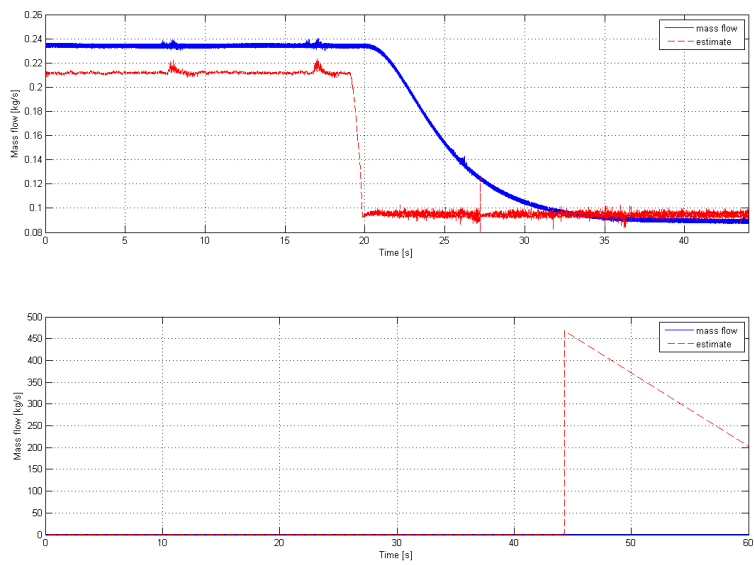


Figure 4.21: Mass flow is able to estimate until it becomes unstable at 44 s.

### 4.3.3 Kalman filter 3

The estimated pressure and mass flow plotted together with the measured values are seen in figure 4.22. The pressure is well filtered and estimated, while the estimate of the mass flow has a steady state difference after the step in speed. Before the increase in speed the mass flow estimate is slightly higher than the real value, with an error of approximately 2.1%. After the step occurs the estimate becomes smaller than the real value, and the error increases to 9%. The innovation process also increases after the step, and it can be observed from figure 4.24 that the kalman gains does become smaller after the increase in speed giving less weight to the innovation process. This works well for the pressure since the estimate still is correct, but the mass flow does suffer from being too small.

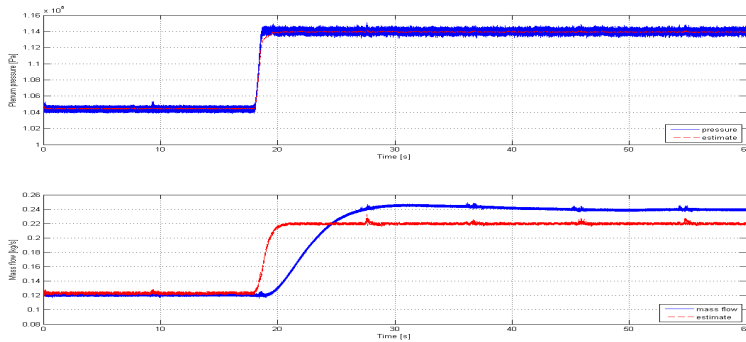


Figure 4.22: Measured vs estimated values.

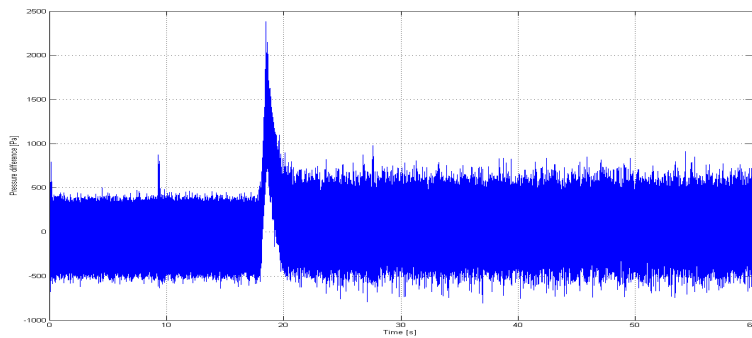


Figure 4.23: Innovation process  $p - \hat{p}$ .

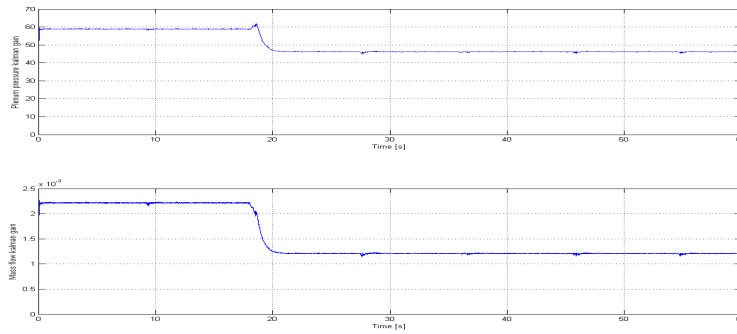


Figure 4.24: Kalman gains. Pressure on top and mass flow at the bottom.

### 4.3.4 Kalman filter 4

The last filter used both downstream and plenum pressure as correctional terms. The estimates and measured values are seen in figure 4.25. Again the mass flow has the same error as in the third kalman filter, namely a steady state difference after the change in speed. The pressure estimate also becomes a little low after the step, but the error is approximately 0.2%. For the mass flow the error is about 1.77% before the step and 10.4% after the step occurs. Again it can be seen that the innovation processes does become larger after the step, and the kalman gains decreases. From the gains in figure 4.27 it is observed that greater weight is put on the plenum pressure difference (gains  $K_{11}$  and  $K_{21}$ ) than the downstream pressure difference.

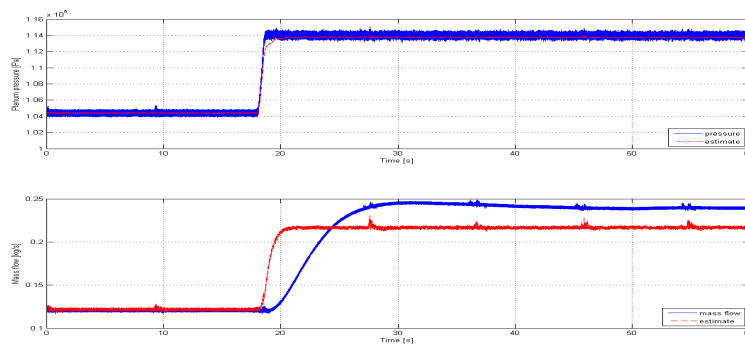


Figure 4.25: Estimated and measured pressure

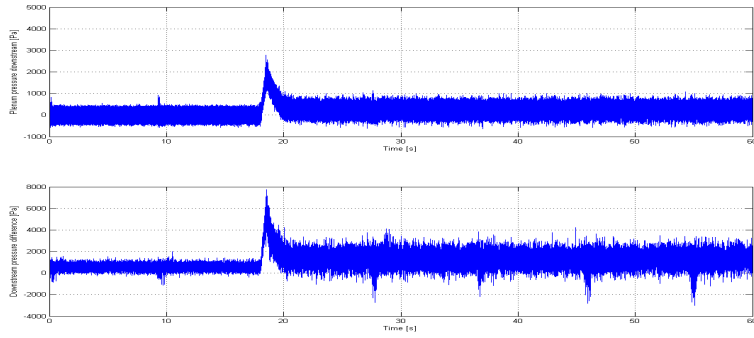


Figure 4.26: Innovation processes  $p - \hat{p}$  (top) and  $p_c(w, N) - p_c(\hat{w}, N)$  (bottom).

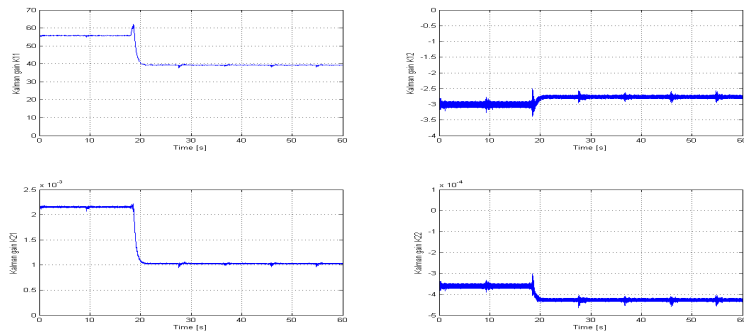


Figure 4.27: Kalman gains.

## 4.4 Simulations recycling directly downstream

Both  $w_f$  and  $w_r$  were modeled as static by eqs. (3.44) and (3.46) during the first test, and the only parameters to alter were  $L_1$  and  $L_2$ , determining the sizes of the two imaginary volumes on each side of the compressor in figure 3.9. The lengths were started at 10 cm and increased to 40 cm, yielding the same steady-state and surge values as well as surge phase as seen in the simulations of the compressor without recycle line. It was however observed that the pressures  $p_1$  and  $p_2$  did have oscillation and increasing transient period between surge and steady state as the volumes on each side of the compressor increased. The two pressures are shown in figure 4.28 for lengths 20 cm and 40 cm. Some numerical errors are here shown since the simulations were run before the step size was set to  $10^{-6}$ . No specific trends were observed for the mass flows.

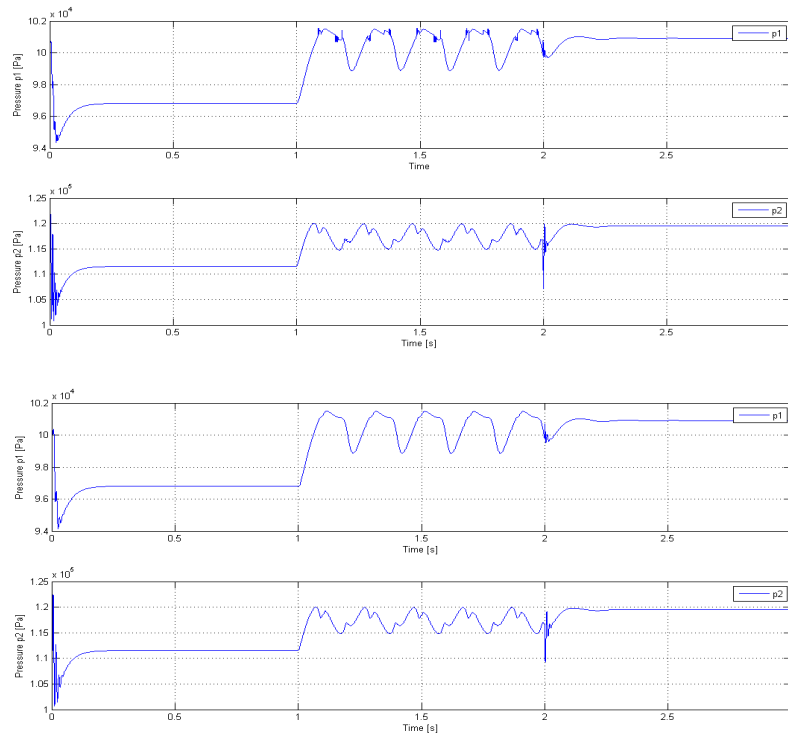


Figure 4.28: Pressures. Top:  $L_1 = L_2 = 20$  cm. Bottom:  $L_1 = L_2 = 40$  cm.

In the second test the inlet mass flow  $w_f$  was modeled dynamically by eq. (3.45) while the recycle flow was still modeled static.  $L_1$  and  $L_2$  were held at 20 cm, while the length of the inlet pipe,  $L_3$  was increased from 50 - 150 cm. The transient periods both to reach steady state initially and after surge were clearly dependent of the inlet pipe length.

In figure 4.29 the pressures of volumes  $V_1$  and  $V_2$  are shown for pipe lengths 50 and 150 cm, and it is obvious that oscillations die slower the longer the inlet pipe becomes. The plenum volume did not show any of the oscillations seen in the other two pressures. The

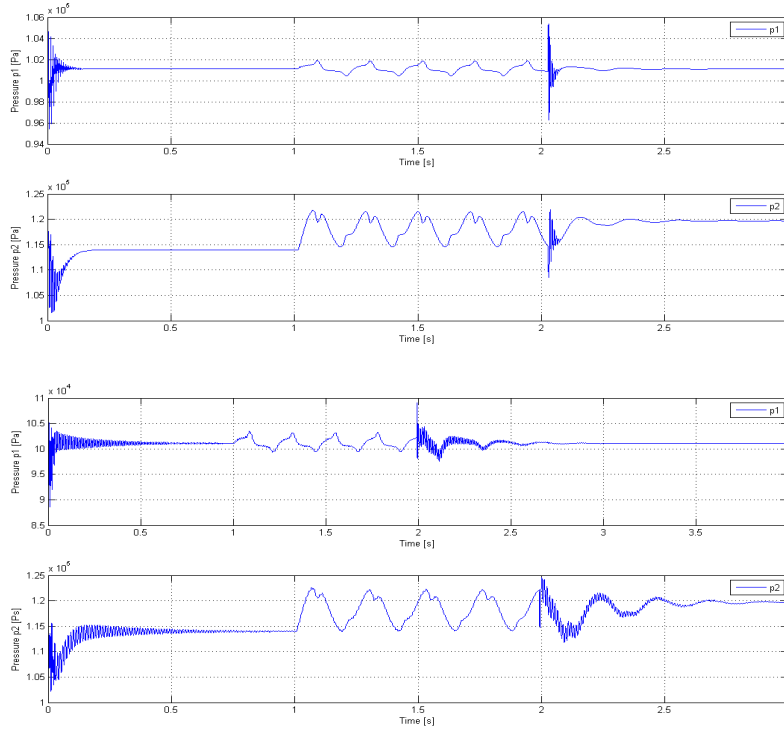


Figure 4.29: Pressures  $p_1$  and  $p_2$  with  $L_3 = 50$  cm (top) and  $L_3 = 150$  cm (bottom).

mass flow  $w_f$  does also show small oscillations that lasts longer as the inlet pipe length increases. This is especially obvious in the initial transient period as seen in figure 4.30.

The third simulation test used the static representation of  $w_f$  while recycle mass flow  $w_r$  was described dynamically by eq. (3.48).  $L_1$  and  $L_2$  were still held at 20 cm while the length of the recycle pipe was gradually increased from 80 - 160 cm. The only pressure showing any oscillation at all in the transient area was  $p_2$ , and there was hardly any increase in the oscillation time. The mass flows showed no oscillations or trends.

In the last combination of different modeling schemes both inlet and recycle mass flow were dynamical. Different combinations of pipe lengths were tested. Again the length of  $L_1$  and  $L_2$  were held at 20 cm for most cases. It was also assumed that a change in the transients would not be all that much affected by a change of these lengths, since  $L_3$  made such a large impact in the second simulation compared to what  $L_1$  and  $L_2$  did

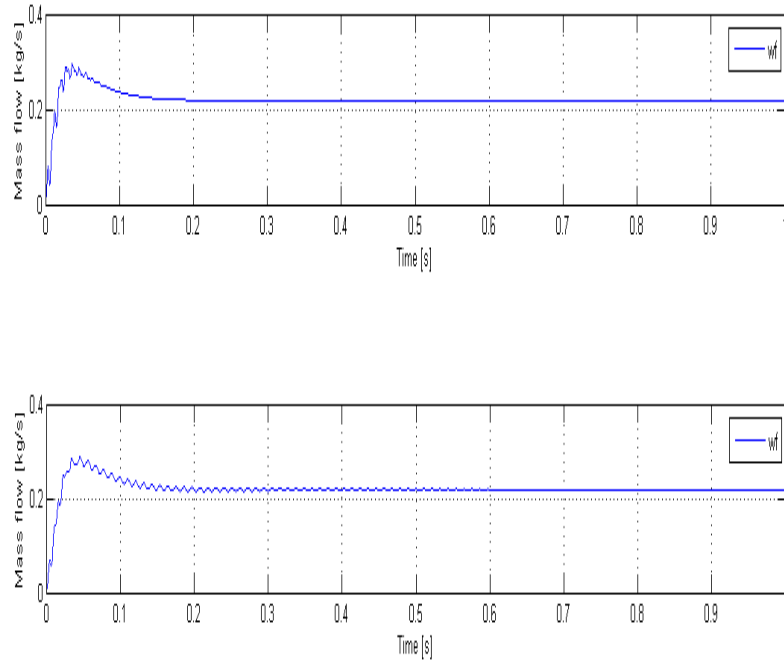


Figure 4.30: Inlet mass flow  $w_f$  with  $L_3 = 50$  cm (top) and  $L_3 = 150$  cm (bottom).

in the first. This assumption confirmed itself through the simulations, the parameter that made impact on the transients was  $L_3$ , with the same behavior that was seen in the second simulation.

## 4.5 Simulations recycling from plenum

In figures 4.31 and 4.32 the results from simulating a compression system with feedback taken from the plenum and a knock-out pot placed upstream the compressor are presented. Initially the throttle valve is completely open, and the system is stable. After three seconds the plenum valve chokes down and surge occurs, before the recycle valve opens after 6 seconds. When comparing these results to the ones obtained in chapter 4.1 and 4.4 it is observed that the steady state pressure values of  $p_1$  and  $p_p$  are lower than those seen in figure 4.29, the same goes for the mass flows. When the system surges, the phase is 0.15 seconds, compared to 0.2 seen in the earlier simulations and measured in the compressor. The shape of the oscillations are somewhat different to those observed in the compressor,

this becomes especially clear in  $p_1$  and  $w_c$ . The length of the inlet duct,  $L_3$ , still makes an impact in the transient periods.

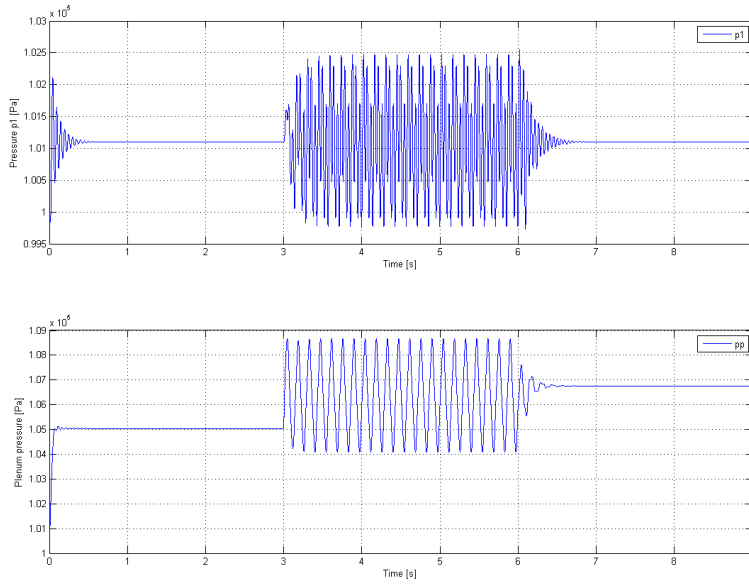


Figure 4.31: Pressures  $p_1$  and  $p_p$ .

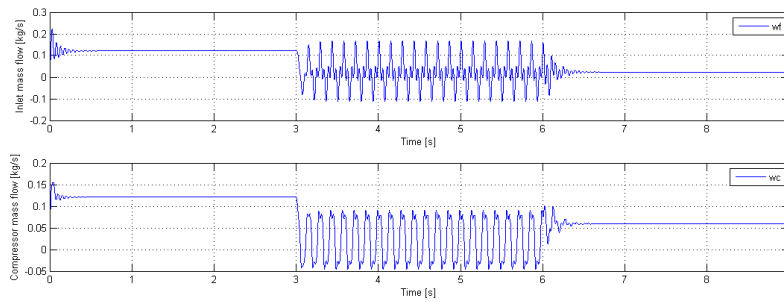


Figure 4.32: Mass flows when recycling from plenum.

## 4.6 Simulations of generic component model.

The simulations of the generic component model did not yield any results explaining the physics behind the suggested model. Termination due to infinite values of  $\dot{w}_{out}$  in eq. (3.59) became a large problem, and the simulation was very sensitive to any changes in set-points or parameters. The values obtained for  $w_{in}$  and  $w_{out}$  were negative for the few cases where the model was able to run. It was not possible to provoke surge in the actual running simulations, even though the plenum throttle  $u_t$  was closed completely. The pressure did rise, but no oscillations of any kind occurred.

## 4.7 Simulations surge avoidance schemes

When changing the set point of the throttle valve from 100 to 30% the compressor went into surge for approximately two seconds independently of what reference used to activate the controller. Figure 4.33 shows that the mass flow crosses the surge line when  $u_t$  is choked down, but leaves surge again shortly after the recycle valve in figure 4.34 starts to open. After 15 seconds  $u_t$  is reopened, and the control valve closes as the working point is back in the steady state area of the compressor map. Since there is nothing to do about the valve dynamics, a movement of the surge avoidance line was tested to see how far to the right in the map one would have to be to avoid surge at such a drastic set point change. The compressor did not avoid surge until the avoidance line was moved drastically into the steady state area as seen from the red line of figure 3.13.

When the compressor is worked toward maximum utilization around the surge line, and the set point changes are smaller the system avoids surge by activating the recycle feedback. Also here the behavior of all three controllers yielded the same results. In figure 4.35 and 4.36 the result of running the system with  $u_t = 65\%$  and choking it to 55% is seen. It becomes obvious that the controller is able to avoid surge, being that the mass flow never crosses the surge line. No oscillations are detected in the states either. Running this scheme with  $u_r$  closed will set the system into surge.

Also changes in speed reference were simulated by applying  $N$  as a sine wave to the system. Altering the frequency did not set the system into surge, and the amplitude of the sine wave could also be increased up to almost the same size as the bias without reaching surge. However, if the plenum throttle is choked the avoidance system will react by opening  $u_r$  greatly. When  $u_t$  was choked from fully open to 60% after 6 seconds, the system does touch surge when the mass flow swings at its lowest, as seen in figure 4.37,

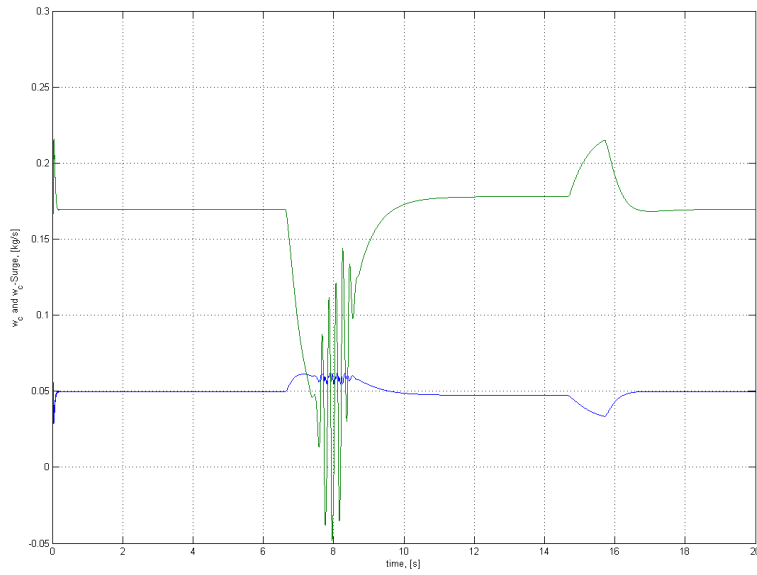


Figure 4.33: Top: Mass flow (green) and corresponding surge line value (blue).

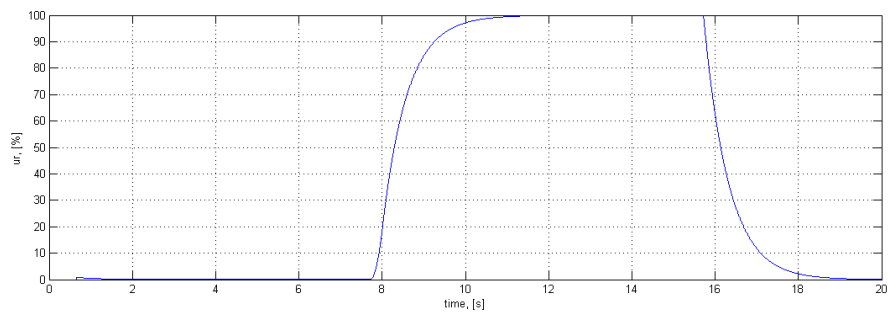


Figure 4.34: Recycle valve

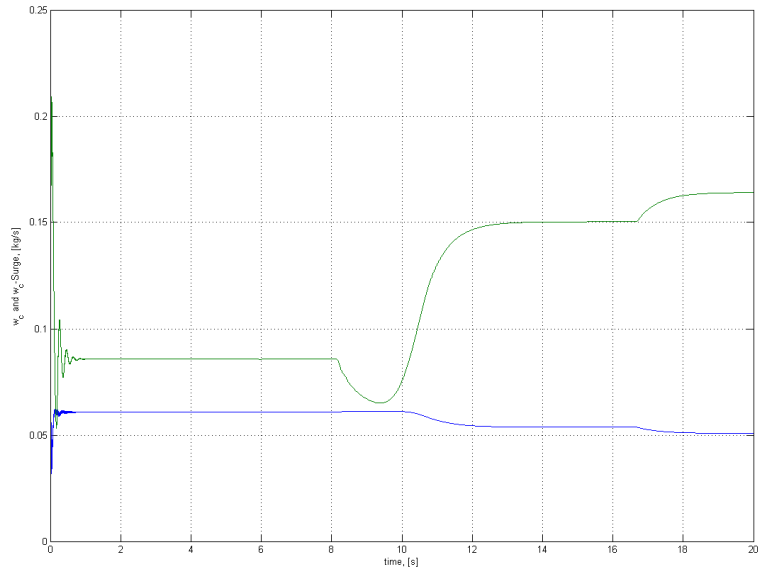


Figure 4.35: Top: Mass flow (green) and corresponding surge line value (blue).

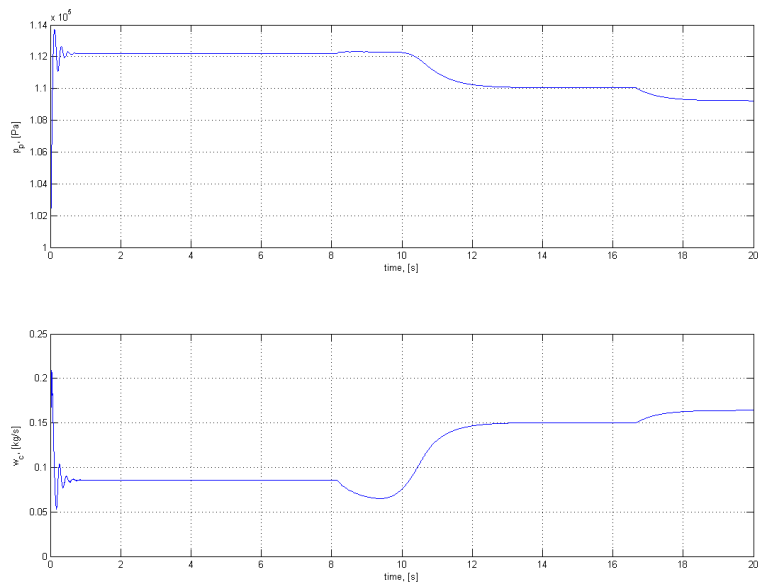


Figure 4.36: Plenum pressure and mass flow

where the speed is  $N = 12000 \sin t + 14500$ . When the throttle is re-opened at 15 seconds, the pressure amplitude does decrease and the mass flow increases, but still touches into surge at the lowest part of the oscillations.

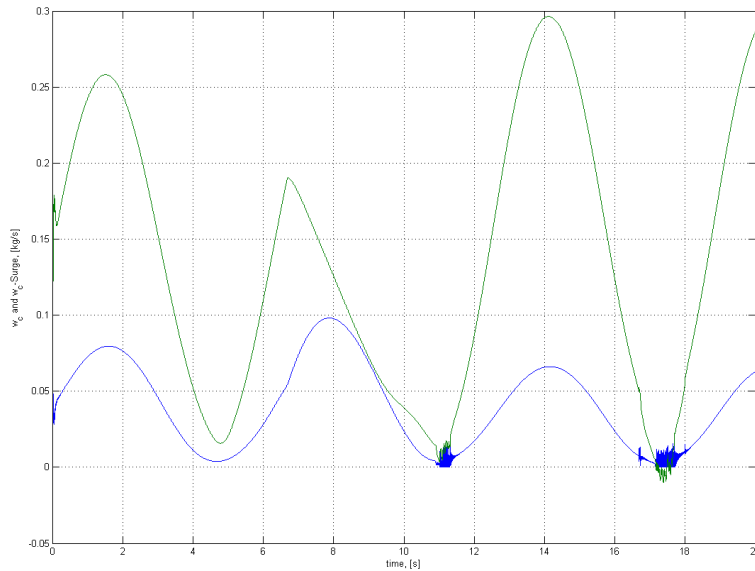


Figure 4.37: Top: Mass flow (green) and corresponding surge line value (blue).

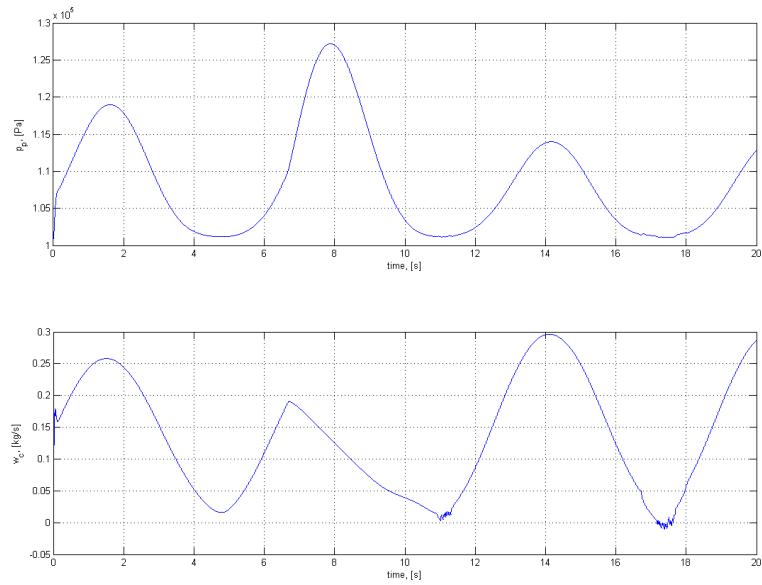


Figure 4.38: Plenum pressure and mass flow.

The last challenge given to the compression system was steps in  $N$ , while  $u_t$  was held at 65%. In figure 4.39 the speed was changed from 12500 - 25500 rpm, and did not send the system into surge. The control valve opens to approximately 15%.

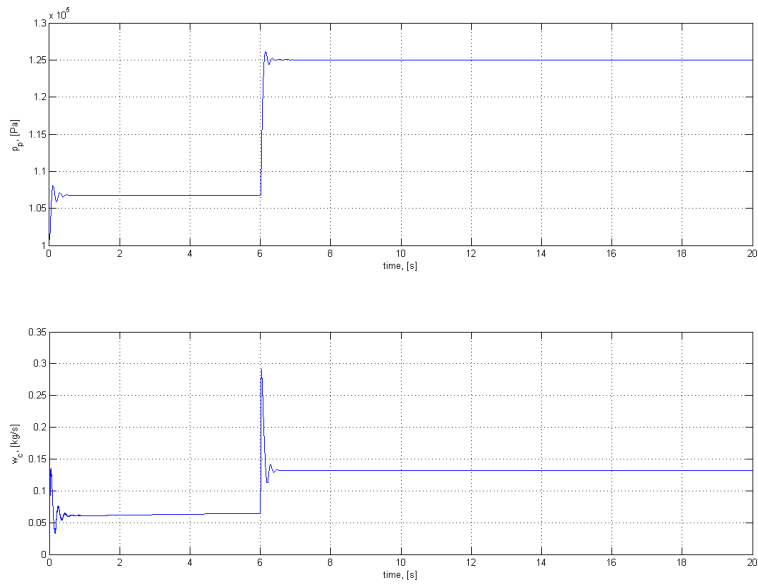


Figure 4.39: Plenum pressure and mass flow with step in speed.

# Chapter 5

## Discussion, conclusions and future work

### 5.1 Discussion results of kalman filters

Four kalman filters were developed, tuned and implemented. Filters 1,3 and 4 showed over all good results. They filter the plenum pressure well, yielding better information to a processing system than if the pure measurement was to be used. The mass flow estimates does have a steady state error of sometimes up to 10%, but given that these are purly estimated by the observer this can be considered fairly good. All the estimated steps in mass flow are faster than those measured, this is due to the faster change in the measured pressures.

The first kalman filter results in an estimate of the pressure that is in the higher range of the measurement, but if tuned differently it becomes more sensible to noise. The mass flow also has a steady-state difference before the step occurs, but estimates the mass flow very well after the change in speed. This observer was made based on the compressor model using the direct measurement of the downstream pressure  $p_{cd}$ , instead of the compressor map. The model describes the behavior of the mass flow very well even though it is a fairly easy description focusing only on the behavior in the duct downstream of the compressor.

Filters 3 and 4 also filters the pressure measurement well and yields good results in estimating the mass flow. However the difference between measured and estimated mass flow is somewhat larger in these two cases than in the first. Both observers uses the compressor map  $p_c(w, N)$  to describe the mass flow. This description is more complex than the one used in the first filter, but still a fairly easy model describing a complex system. It is natural that there will be some modeling error, as seen in the simulations of the compressor in chapter 4.1. When model errors occur, the kalman filter is likely to get a steady state difference because it believes it is estimating the states correctly, and does nothing to correct the error. In the third filter the plenum pressure was used as measurement, and the filtering result was very good, as seen in figure 4.22. The correctional term then believes that the estimate is also correct and does not apply any action to correct the steady state

difference in the mass flow.

The second kalman filter was wrongly implemented and because of this easily became unstable during implementation, even though the tuning results became fairly good using the surge data. When the kalman filter was corrected it was able to estimate the mass flow that during implementation became unstable. However, when tested on a different set of data it did again become unstable. This leads me to believe that we are perhaps not able to guarantee stability for this specific filter. During the simulation that did not become unstable it was observed that a change in the mass flow estimate occurred in the transient, but did not have any impact on  $p_c(\hat{w}, N)$  at all. This draws attention to the compressor map seen in figure 5.1. In the simulation scheme studied the speed was initially 12500 rpm and  $p_c(w, N) \approx p_c(\hat{w}, N) = 1.05 * 10^5$  Pa. When the step in speed to 22500 rpm occurred,  $p_c(w, N)$  became approximately  $1.15 * 10^5$  Pa and the measured mass flow value was 0.24 kg/s. These values in the compressor map is indicated by the blue circle in figure 5.1. The estimate does not immediately start an increase, but falls significantly, and reaches a value of 0.5 kg/s. The lowest mass flow is indicated by the red circle in the compressor map. The estimate simply went to the wrong mass flow in the compressor map initially. The set point in speed was changed and new values of  $p_c(\hat{w}, N)$  was calculated, but during the transient period until  $p_c(w, N)$  reached its correct value, the estimate did not have enough information to know what mass flow value was the correct one for the new pressure. This will be a general problem using this kalman filter, there is no way to determine what direction in the compressor map the mass flow is headed during transients, and the filter can only guess based on knowledge of pressure level. This problem makes the kalman filter useless in an online situation and emphasizes the need of enough information from the system to uniquely estimate a state.

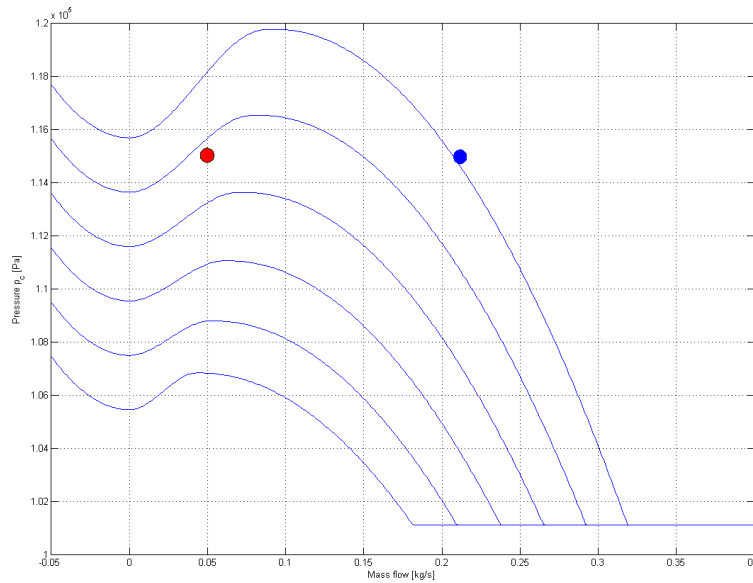


Figure 5.1: Compressor map

## 5.2 Discussion recycle models

Three simulation models for a compressor with recycle loop were adjusted to the known compressor and simulated. The first model recycled air almost directly downstream the compressor while the other two retrieved recycle gas from plenum.

### 5.2.1 Model recycling directly downstream.

Through the tests performed on the model in figure 3.9 it does become clear that the parameter yielding the most impact on the transients in the system is the inlet duct length  $L_3$ . This should be kept in mind when building the physical system. It is not likely that the inlet duct will have a length of 150 cm considering the size of the room, but the pipe length will still make an impact on the system even though the lengths are shorter. I doubt that inlet mass flow can be modeled static in a simulation model, because there will be dynamics in the real mass flow, as the compressor sets the air into rotation long before it hits the impeller.

The two volumes  $V_1$  and  $V_2$  does not exist in reality, and are only introduced for modeling purposes. The diameter of the ducts used in the lab are 70 mm, yielding  $L_1 =$

$L_2 = 10$  cm to perhaps be the best parameter guess of the simulations tested. The reason this was not chosen during most simulations was trouble with numerical calculations during the first test before step size was decreased. Still, it was not the up-and down-stream volumes that had the most impact on the simulations, so the results would not be different using a smaller length. One of the problems that may occur with the physical system is that the flow picture in the volumes, especially  $V_1$ , will be greatly disturbed when the recycle valve is opened. This needs to be considered when choosing the length of the inlet pipe  $L_3$  as well as the placement of PT-cells for measuring pressure.

### 5.2.2 Recycling from plenum

The motivation behind building a system with defined volumes up- and down-stream the compressor was that this would match the mathematical descriptions more closely, as well as be closer to the industrial systems described. The simulation model was build to see if there would be any prominent differences from the previous system simulated. The pressures were lower than observed when simulating the system recycling directly downstream, this is mainly due to the relatively large volume situated upstream of the compressor. When  $p_1$  becomes smaller, so does  $p_p$ . The dynamics of the system does change when using this model, especially the surging mass flow,  $w_c$ , shows deviation from that observed in the previous simulations. This is mainly due to the fact that we have a new description of the plenum pressure  $p_p$ , where it is dependent also on the recycle mass flow. When the dynamic description of a system changes it can also be expected that the dynamic behavior will change, and this is what we see through a smaller phase and amplitude of the surge oscillations.

### 5.2.3 Generic component model

There were many uncertainties related to the generic component model suggested in eqs. (2.52) - (2.58). First and foremost was the description of the mass flow in equation (2.53), where  $\dot{w}_{out}$  is subtracted from the more familiar description of compressor mass flow. I am having a hard time understanding the physics and reason for this description, and after extensive search for literature explaining and backing this model failed, it was decided to still try and implement the model to see if further understanding could be achieved. The implementation of the model fitted to the compressor did fail, and since there were no literature to help find errors, it was hard to determine if variables were placed in the

wrong part of the compressor or if I needed another form of characteristics, using throttle opening between 0 – 1 instead of 0 – 100%. I do not recommend using the model suggested by Murphy et al. (1995) for modeling a surge avoidance system, unless more theory and a better understanding can be achieved of the model. It was decided to not spend any more time with this model, and focus on the more familiar descriptions instead.

### **5.3 Discussion surge avoidance simulations**

Three PI-controller schemes were built and simulated for different possible situations the compressor may meet. The controllers differed in what measurement they used as reference. There were no prominent differences detected in the resulting reaction from the controller based on what measurement was used. All in all the controllers does work well for some settings, but the scheme definitely shows shortcomings for certain cases. As earlier mentioned I decided not to put too much effort into tuning, and chose a fairly aggressive tuning strategy that was adequate for the purpose of avoiding surge. I do however understand that tuning of controllers is a very important aspect of surge avoidance control, and that financially a lot of money can be earned by having a optimal surge avoidance scheme, both in energy savings and production rate. An improvement of the PI-controller could be using gain scheduling, where the controller gain is determined from the speed of the motor or the change of rate in mass flow. This way the compressor can work closer to its optimal values independent of what pressure and speed level in the compressor map the working point is at.

The surge avoidance line was initially situated approximately 10% to the right of the surge line, being that this was mentioned as a normal set-point for industrial compressors. For control of small changes in set-points and speed close to the avoidance line this worked fairly well and surge was avoided. However, for large changes in set points, being for example an emergency shutdown or some other problem changing the system greatly, the avoidance line was too close to the surge line. Running the simulation the compressor did leave surge again as the recycle valve opened, but it may be that in reality surge can not be afforded at all. A compressor is normally not set as a single stage isolated system, and if one part becomes unstable this may effect production and safety of more than only the compressor. The avoidance line had to be moved radically to the right in the compressor map to avoid surging when large set-point changes in the throttle valve occurred. For the pure purpose of keeping the system stable this is ok, but the problem

with such a solution is the extreme conservatism concerning the control valve during normal production. Moving the avoidance line far away from the surge line will result in a more aggressive control, and much energy will be lost controlling the recycle valve. Also the production rate will fall drastically, which may not be an option in some industries. This leads us into a discussion of choosing control valves as well as reconsidering the avoidance scheme initially chosen. In chapter 2 it was mentioned that there is different demands to control valves being if they are for normal control or handling great changes in a system. This is exactly what we see in the controller simulations performed. The control valve that is available is subject to a transport delay as well as first order dynamics, meaning that it will not be able to open the instant a set point is changed, but it will reach a requested set point fairly exactly after some time. When there is great risk of the system surging we need a valve that reacts fast and fully opens very quickly. This is the main reason why many companies chooses to run a double recycle scheme with different valves, one ensuring normal control by recycling cooled gas, and one hot-recycle emergency valve. There is only one recycle valve available for the laboratory compression system, and being placed in the room it is now, I do not see that a double recycle loop is an option. A decision then needs to be made either to replace the recycle valve with a faster one, or to develop a different control algorithm ensuring the system does not surge even though great set-point changes occur. One could start by moving the avoidance line approximately 25% to the right of the surge line, which is the other end of the suggested area of 10 – 25% gap between the two lines. However, this would not be enough to ensure stable results for all set-points, so a control algorithm implemented on the system should be able to handle the great changes as special cases. In the controller scheme simulated attention was not brought to the start-up sequence a compressor goes through, when this also is a case different from normal control, as well as dependant of surrounding systems.

## **5.4 Discussion practical aspects of building and modeling the recycle loop.**

The compressor with measurements as is today was presented in figure 3.2. For the purpose of keeping the system as unchanged as possible we want to keep the measurement points that are already there today such that observers and control systems already built will continue to function also after the recycle loop is added. This way both active surge and surge avoidance schemes can be implemented and tested on the system. The model

that recycles air directly downstream of the compressor is suggested as a basis for building the feedback. The intersection downstream should then be placed after the measurement of  $p_{cd}$ . Upstream it was earlier suggested to keep the intersection as close to the inlet as possible to create a uniform flow picture toward the compressor.

To be able to verify simulation models, observers and control schemes, we will need measurements of the two pressures  $p_1$  and  $p_2$ . I am not sure what way is the most correct to measure the pressures in the intersection where the flow picture will be far from one dimensional. One suggestion is to measure the pressure directly underneath the intersection, another is to use one pt-cell on each side of T-section, see figure 5.2. Hopefully the

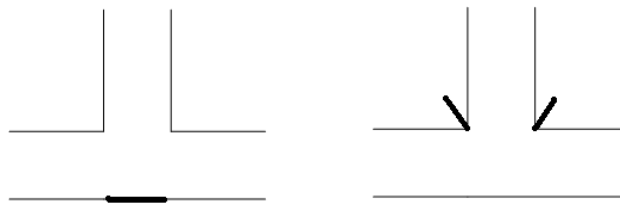


Figure 5.2: T-sections with suggestions to pressure measurement.

two modeled volumes where we measure  $p_1$  and  $p_2$  can be set to values of the same size as the real volumes in the intersection of the recycle pipe, being approximately  $0.00013m^3$ . This equals a length of  $L_1 = L_2 = 7cm$  which is the same as the pipe diameter, but this is not certain and one needs to be aware that these volumes may be very different in the resulting simulation model since they strictly are imaginary.

Also, the inlet mass flow  $w_f$  should be investigated thoroughly when the system is build. Observing that the inlet mass flow did make such an impact on the system, it could be an idea to either measure the inlet flow directly or study it through the measurements of  $p_1$ .

When the recycle valve is open we do not have a measurement of the mass flow through the compressor,  $w_c$ , but rather the flow that is not recycled  $w_d$  in the model today. It is not likely that the measurement point of mass flow should be moved, and the need for an estimate of  $w_c$  is therefore prominent. Initially the hope was that the kalman filter estimating mass flow based on downstream measurement, kalman filter 1 in chapter 3.3.1, could be used. This may be the case when the system is built and the model fully identified, however I suspect that a different filter will yield better results. The model of the compressor that was used in the first kalman filter was based on the difference between

the downstream pressure  $p_{cd}$  and plenum pressure  $p_p$ . The length between the two was fairly long, and we were able to measure the two pressures distinctively. The model of  $w_c$  when we add the recycle loop, will then calculate the difference between two pressures physically close to each other, namely  $p_{cd}$  and  $p_2$ . I am concerned if this in reality will yield two distinct measurements, being so close to each other, and that verification of the estimate may become hard. I would suggest using the observer that uses both  $p_p$  and  $p_{cd}$  as correctional terms, kalman filter 4 in chapter 3.3.4, mainly due to the fact that it did yield good results and that it utilizes more available information than the other observers. The dependency of a good simulation model is obvious, and the compressor characteristics should also take temperature change into account.

## 5.5 Conclusions

A continuous extended kalman filter can be used to estimate pressure and mass flow in a centrifugal compression system with duct, plenum and throttle. The observer will work properly given that there is enough information retrieved from the system through measurements to uniquely estimate all states. Using a kalman filter online to estimate states for the purpose of system control, such as active surge control or surge avoidance, will work as long as the observer works. However one needs to be aware that there may occur small steady state errors in the estimates if the model is not completely correct.

When modeling a compression recycle system where a T-section is placed downstream of the compressor and no physical up- and down-stream volumes are available, a static description of the recycle mass flow can be used for simulation purposes. The inlet mass flow will however differ greatly depending on what description is used, and the inlet pipe length will make an impact on the transient behavior, especially of the pressure up-stream the compressor. Concluding from the simulations performed on the system it is recommended to keep the length of the inlet pipe,  $L_3$  in figure 3.9, as short as possible before it connects with the recycle mass flow. The hope is then that the flow picture seen from the compressor is more one-dimensional as assumed when modeling a compression system. When modeling two imaginary volumes on each side of the compressor one needs to carefully consider the placement of the pressure measurement instruments so that measured values reflects the simulated pressures  $p_1$  and  $p_2$ . Even though there are no real volumes available it is concluded that this is a starting point to model the laboratory compressor, mainly because it is a model used in the industry and presented thoroughly

in theory.

Due to the physical space in the laboratory it is concluded that building a recycle loop from the plenum is not an option, even though compared to models of industrial recycle systems this realization would probably be more realistic with regards to the physical volumes. An important aspect to keep in mind when the model is build physically is that the solution chosen will have effects on todays system. This became very obvious when building a model recycling from plenum, and emphasizes the importance of a pre-study before building the model. We want to keep the system as close to the model it has today because of the research that is already put into it with active surge control.

## **5.6 Suggestions to future work**

I have now performed a pre-study on a system that is to be built for later educational purposes. A goal is to ensure that the resulting plant is able to show both active surge control and surge avoidance. The compressor was initially build for active surge control, so we want to avoid interfering too much with this system. The idea is then that the compressor should work in the same way as without a recycle line when the recycle valve is closed. There is a lot of work remaining before the compression system is at this stage, and I therefore suggest the following as a continuation to this thesis.

- Build recycle loop on laboratory set-up.
- Decide how to measure needed variables, perform system identification to obtain correct dynamics and parameter sizes, and develop a simulation model for the system. This should also contain energy balances describing the temperature changes.
- Implement kalman filter and improved surge avoidance scheme for the recycle model.

# Bibliography

- Bøhagen, B. (2007), Active surge control of centrifugal compressions systems, PhD thesis, NTNU, Trondheim, Norway.
- Bishop, G. & Welch, G. (2006), An introduction to the kalman filter, Technical report, Departement of computer science, University of North Carolina at Chapel Hill, Chapel Hill, NC 27599-3175.
- Botros, K. K. & Henderson, J. F. (1994), 'Developments in centrifugal compressor surge control - a technology assessment', *Journey of Turbomachinery* **116**, 240–249.
- Brown, R. G. & Yang, P. Y. (1997), *Introduction to random signals and applied kalman filtering*, John Wiley & Sons, Inc, New York, USA.
- de Jager, B. (1995), Rotating stall and surge control: A survey, in 'Proceedings of the 34th Conference on Decision & Control, New Orleans, LA'.
- de Jager, B. & Willems, F. (1998), Modeling and control of rotating stall and surge: An overview, in 'Proceedings of the 1998 IEEE International Conference on Control Applications, Trieste, Italy'.
- Egeland, O. & Gravdahl, J. T. (1999), *Compressor Surge and Rotating Stall: Modeling and Control*, Springer Verlag.
- Egeland, O. & Gravdahl, J. T. (2003), *Modeling and Simulation for Automatic Control*, 2 edn, Tapir Trykkeri, Trondheim, Norway.
- Fausel, R. (2002), Turbomachinery control system design objectives, Technical report, Compressor Controls Corporation, <http://www.cccglobal.com/studies.asp#P13>. Last accessed date: 05.25.07.
- Gravdahl, J. (1998), Modelling and control of surge and rotating stall in compressors, PhD thesis, NTNU, Trondheim, Norway.
- Henriksen, R. (1998), *Stokastiske systemer. Analyse, estimering og regulering*, Institute of engineering cybernetics, Trondheim, Norway.

- Kurz, R. & White, R. (2004), 'Surge avoidance in gas compression systems', *Journal of Turbomachinery* **126**, 501–506.
- Kurz, R. & White, R. (2006), Surge avoidance for compressor systems, in 'Proceedings of the thirty-fifth turbomachinery symposium'.
- Murphy, K. M., Kalata, P., Fischl, R. & Marchio, D. (1995), On modeling surge avoidance controllers (sac) in compressors: Design procedure, in 'Proceedings of the American Control Conference, Seattle, Washington'.
- Niesenfeld, A. E. (1982), *Centrifugal Compressors: principles of operation and control*, Instrument Society of America.



# Appendix A

## Results implementation, Case 2

This is a presentation of the results from the implementation of kalman filters for compressor without surge control feedback when the speed is at  $N = 22500$  rpm and the throttle  $u_t$  is chocked from 100 - 60 %. Being that the second kalman filter was wrongly implemented and will not ensure unique estimate, the results are discarded.

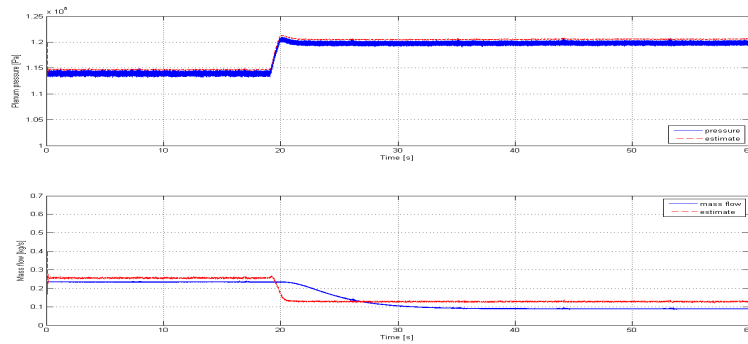


Figure A.1: Kalman filter 1: Estimated and measured states

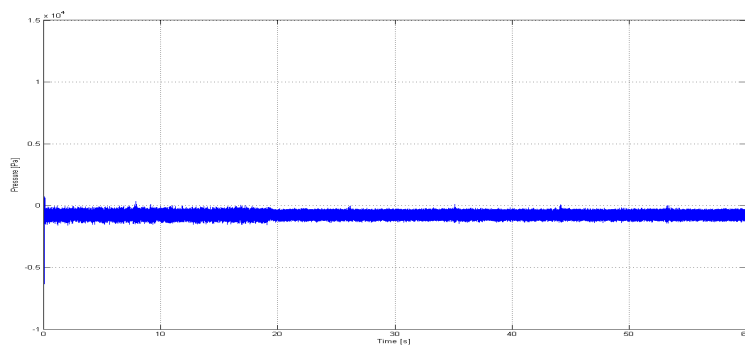


Figure A.2: Kalman filter 1: Innovation process  $p - \hat{p}$ .

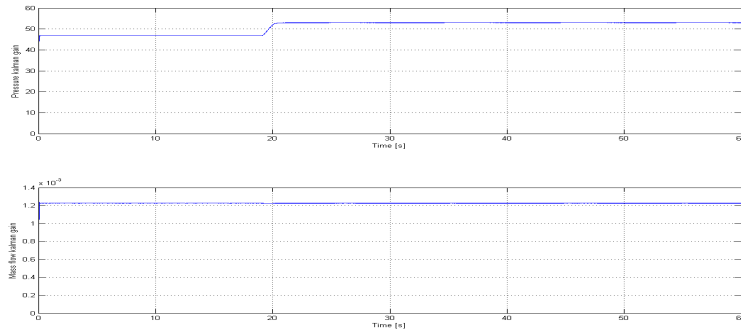


Figure A.3: Kalman filter 1: Kalman gains, pressure at top and mass flow at bottom.

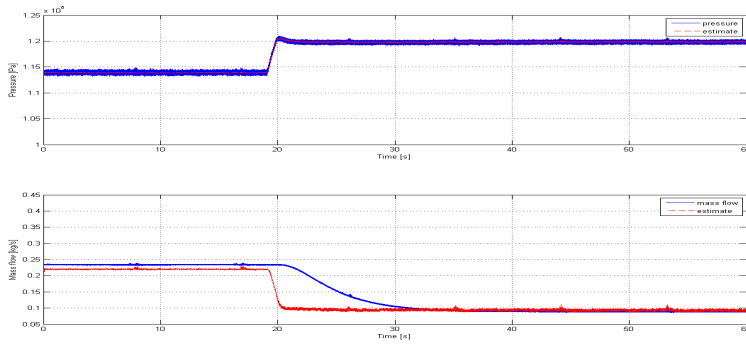


Figure A.4: Kalman filter 3: Estimated and measured states.

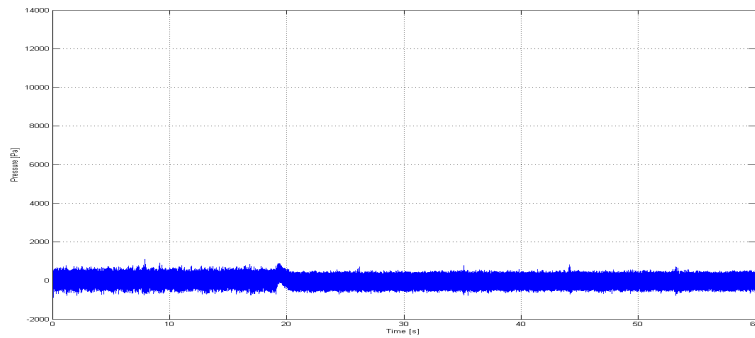


Figure A.5: Kalman filter 3: Innovation process  $p - \hat{p}$ .

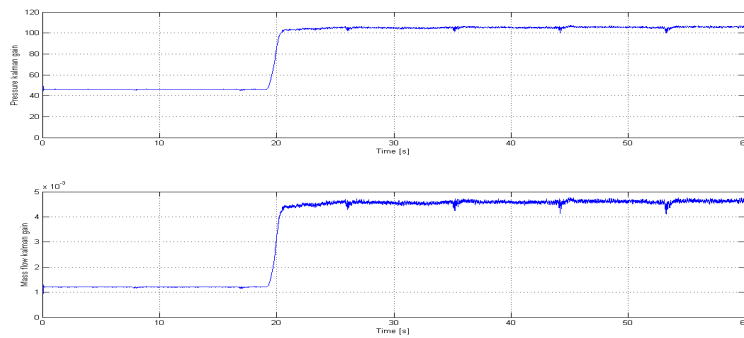


Figure A.6: Kalman filter 3: Kalman gains, pressure at top and mass flow at bottom.

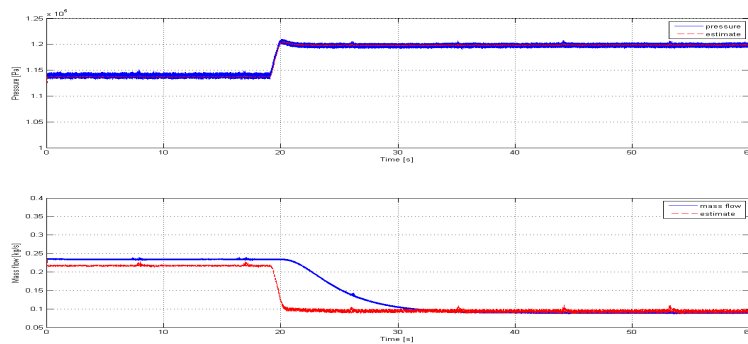


Figure A.7: Kalman filter 4: Estimated and measured states.

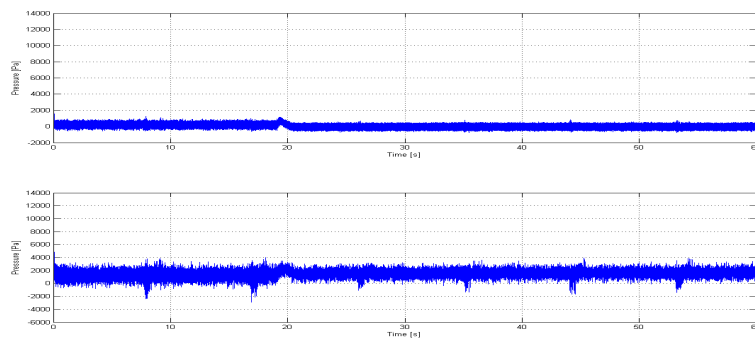


Figure A.8: Kalman filter 4: Innovation processes  $p - \hat{p}$  (top) and  $p_c(w, N) - p_c(\hat{w}, N)$  (bottom).

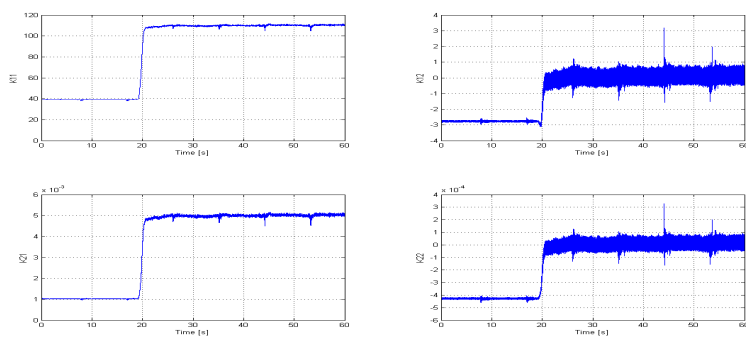


Figure A.9: Kalman filter 4: Kalman gains.

# Appendix B

## Results implementation, Case 3

This is a presentation of the results from the implementation of kalman filters for compressor without surge control feedback when the throttle opening is being held at 60% and the speed  $N$  is decreased from 25500 - 12500 rpm. The compressor did go shortly into surge during the deceleration. Being that the second kalman filter was wrongly implemented and will not ensure unique estimate, the results are discarded.

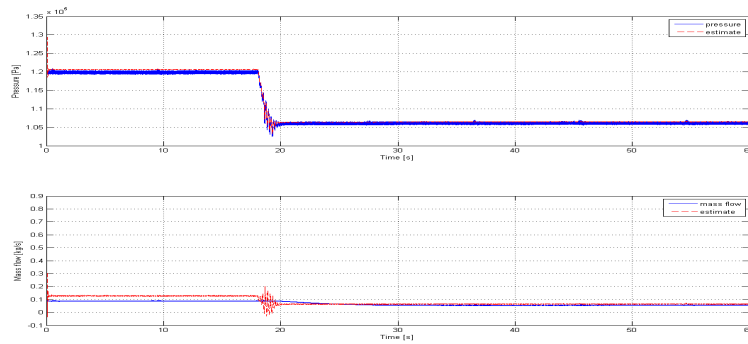


Figure B.1: Kalman filter 1: Estimated and measured states

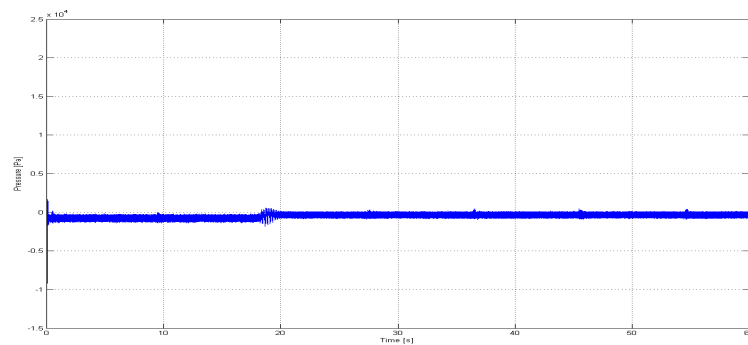


Figure B.2: Kalman filter 1: Innovation process  $p - \hat{p}$ .

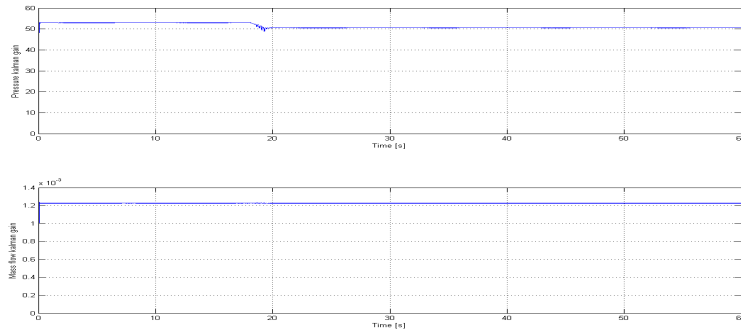


Figure B.3: Kalman filter 1: Kalman gains, pressure at top and mass flow at bottom.

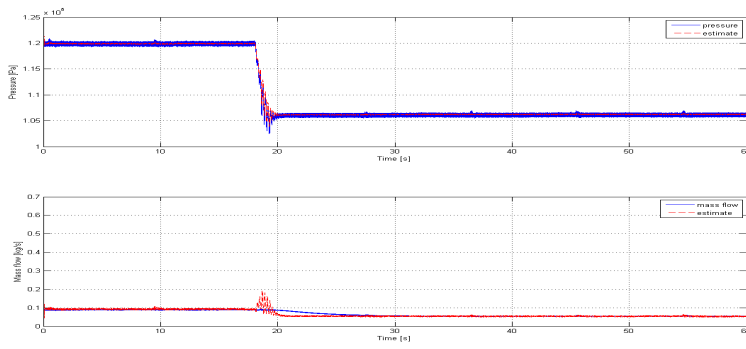


Figure B.4: Kalman filter 3: Estimated and measured states.

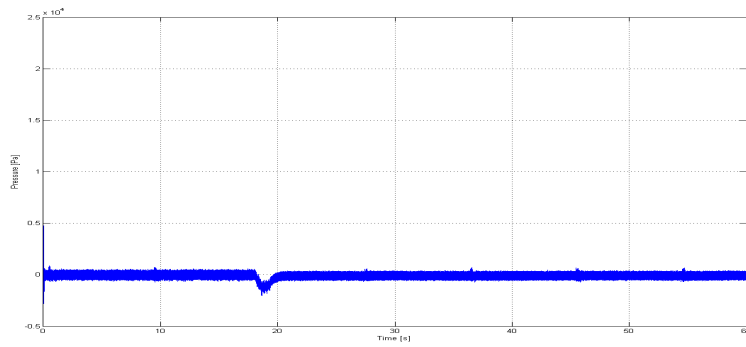


Figure B.5: Kalman filter 3: Innovation process  $p - \hat{p}$ .

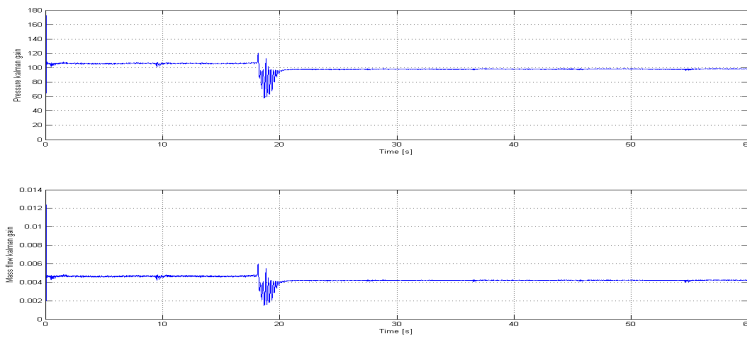


Figure B.6: Kalman filter 3: Kalman gains, pressure at top and mass flow at bottom.

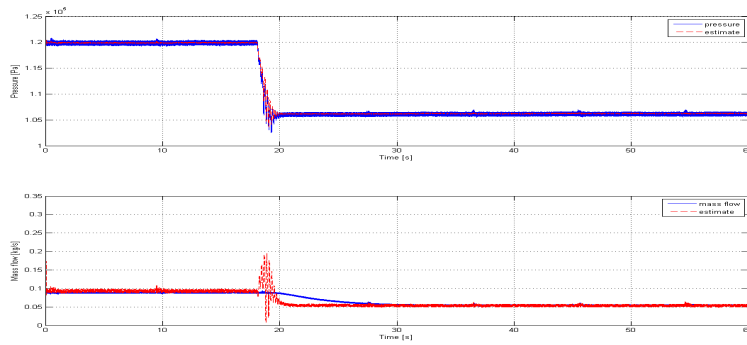


Figure B.7: Kalman filter 4: Estimated and measured states.

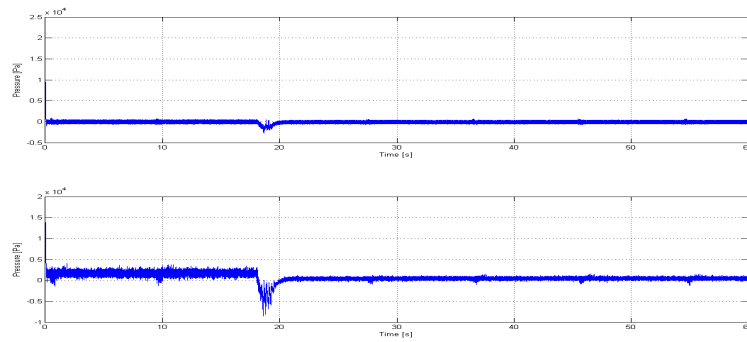


Figure B.8: Kalman filter 4: Innovation processes  $p - \hat{p}$  (top) and  $p_c(w, N) - p_c(\hat{w}, N)$  (bottom).

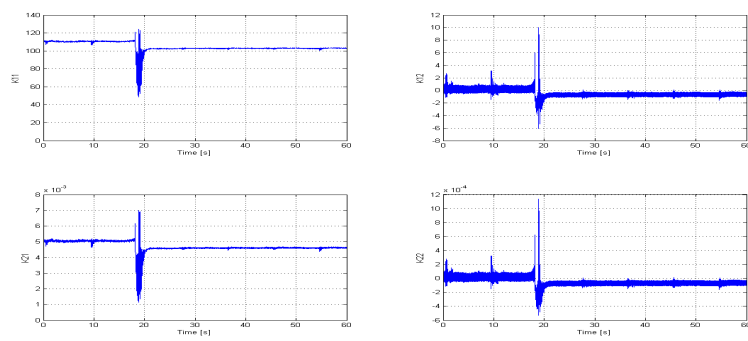


Figure B.9: Kalman filter 4: Kalman gains.

# Appendix C

## Results implementation, Case 4

This is a presentation of the results from the implementation of kalman filters for compressor without surge control feedback when the speed is at  $N = 12500$  rpm and the throttle  $u_t$  is opened from 60 to 100 %. Being that the second kalman filter was wrongly implemented and will not ensure unique estimate, the results are discarded.

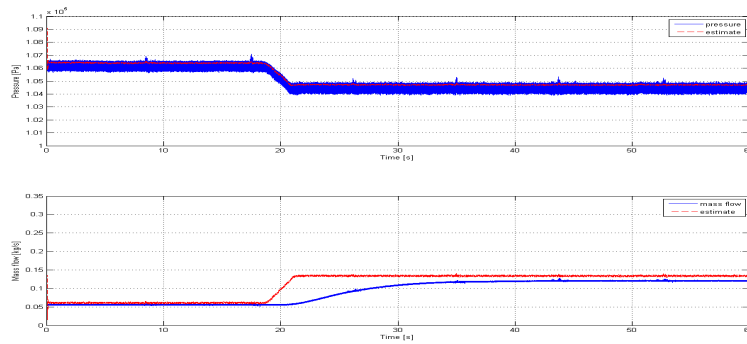


Figure C.1: Kalman filter 1: Estimated and measured states

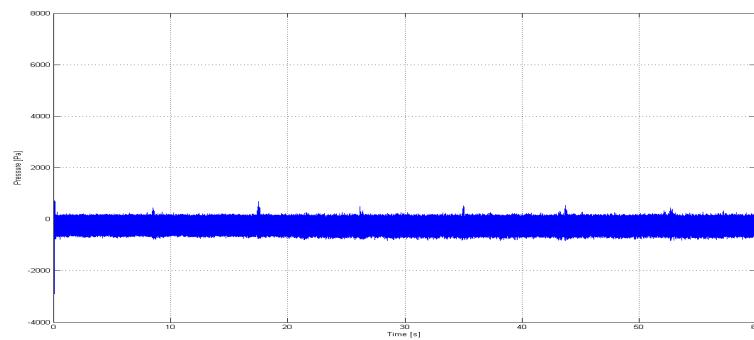


Figure C.2: Kalman filter 1: Innovation process  $p - \hat{p}$ .

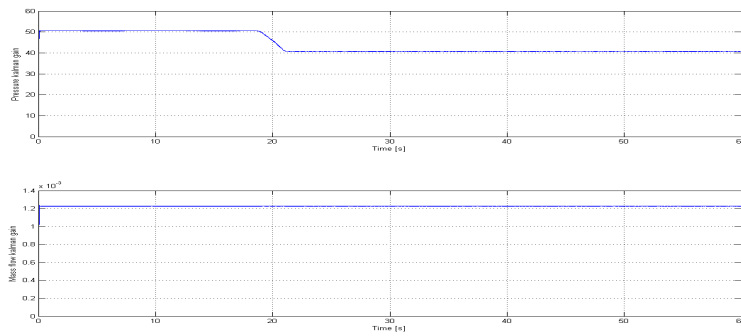


Figure C.3: Kalman filter 1: Kalman gains, pressure at top and mass flow at bottom.

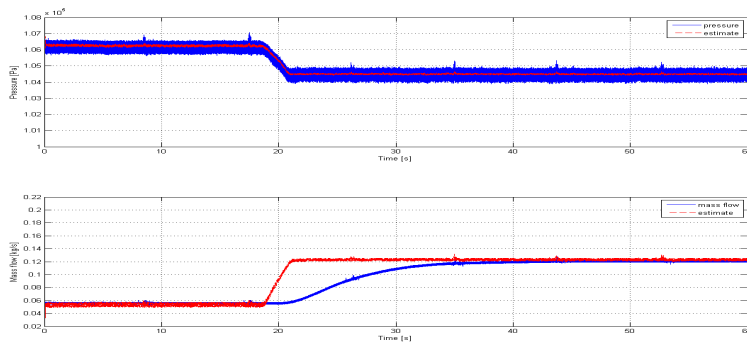


Figure C.4: Kalman filter 3: Estimated and measured states.

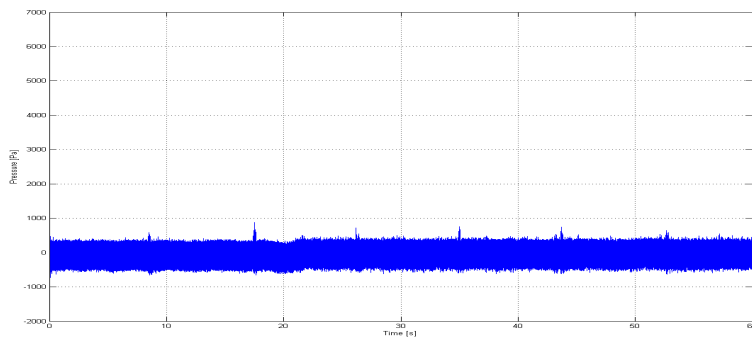


Figure C.5: Kalman filter 3: Innovation process  $p - \hat{p}$ .

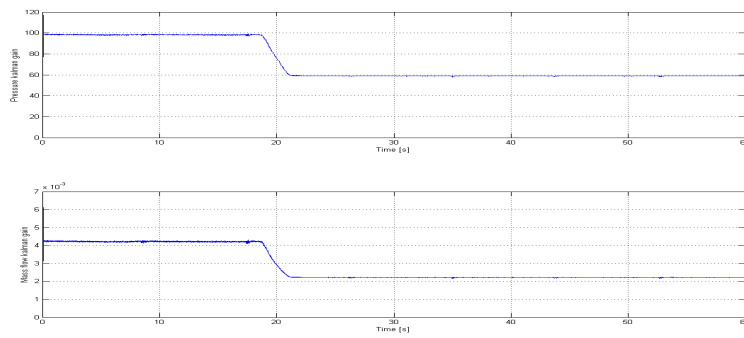


Figure C.6: Kalman filter 3: Kalman gains, pressure at top and mass flow at bottom.

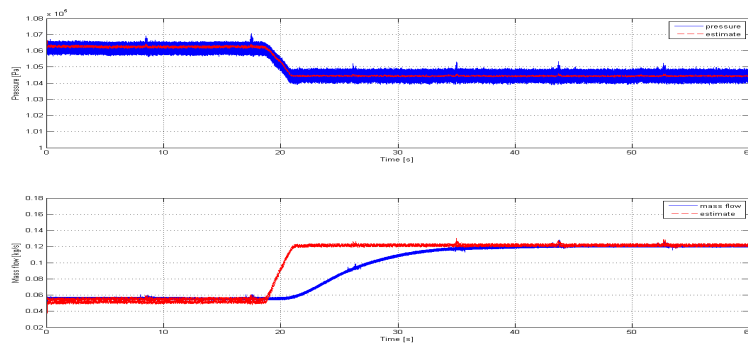


Figure C.7: Kalman filter 4: Estimated and measured states.

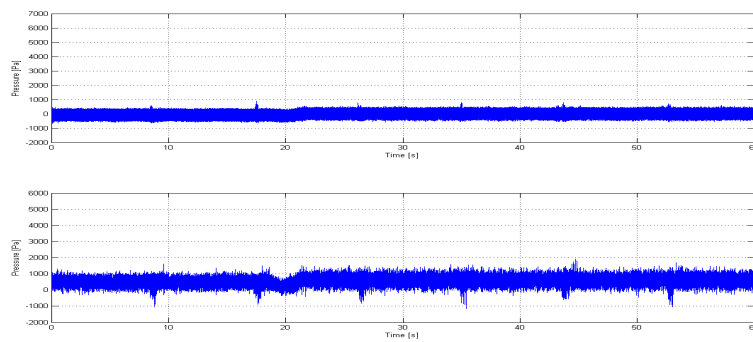


Figure C.8: Kalman filter 4: Innovation processes  $p - \hat{p}$  (top) and  $p_c(w, N) - p_c(\hat{w}, N)$  (bottom).

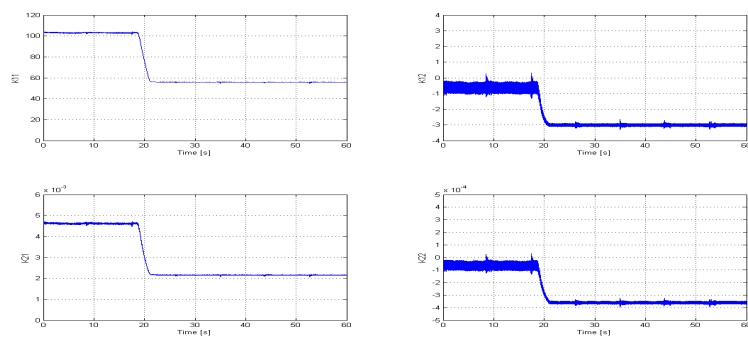


Figure C.9: Kalman filter 4: Kalman gains.

# Appendix D

## Test plan recycle system

The recycle model developed in chapter 3.4.1 was tested for different combinations of mass flow models and pipe lengths presented in tables D.1 to D.4.

<b>Test 1: Static wr and wf</b>	1	2	3	4	5	6
L1	10	20	30	30	10	40
L2	10	20	30	10	30	40
L3	X	X	X	X	X	X
L4	X	X	X	X	X	X

Table D.1: Test 1, 6 different length combinations tested.

<b>Test 2: Static wr and dynamic wf</b>	1	2	3	4	5	6
L1	20	20	20	10	20	30
L2	20	20	20	10	20	30
L3	50	100	150	30	30	50
L4	X	X	X	X	X	X

Table D.2: Test 2, 6 different length combinations tested.

<b>Test 3: Dynamic wr and static wf</b>	1	2	3	4
L1	20	20	20	10
L2	20	20	20	10
L3	X	X	X	X
L4	80	110	160	110

Table D.3: Test 3, 4 different length combinations tested.

<b>Test 4: Dynamic wr and wf</b>	1	2	3	4	5	6	7
L1	20	20	20	20	20	20	10
L2	20	20	20	20	20	20	10
L3	50	100	150	50	50	150	50
L4	110	110	110	80	160	160	110

Table D.4: Test 4, 7 different length combinations tested.

# Appendix E

## Testing of valve characteristics

In order to understand and develop a transfer function of the dynamics of the valves used in the laboratory set-up, different set-point changes in valve opening was applied to the throttle valve, and the step was then measured. The data was filtered using a Butterworth filter and matlab function *filtfilt*. All measurements are added to the disc together with a script for plotting the data.

The different steps are presented in table E.1. In figure E.1 the measured result of a step from 0 – 100% is seen, while figure E.2 shows the step from 100 – 0%. When opening the valve from closed to fully opened, a time delay of approximately 2.5 seconds and opening time of 6 seconds was the average. Closing the valve completely yielded a delay of 1 second and closing time of approximately 3 seconds. When going from 50% to either closed or fully opened, the time delay was drastically smaller at 0.3 seconds. The time to open from 50 – 100% was approximately 3 seconds, which was half of what it took to open from 0 – 100%

Test number	Step change	Number of tests
1	0-100	9
2	100-0	9
3	0-50	9
4	50-0	9
5	50-100	9
6	100-50	9

Table E.1: Test data gathered from valve.

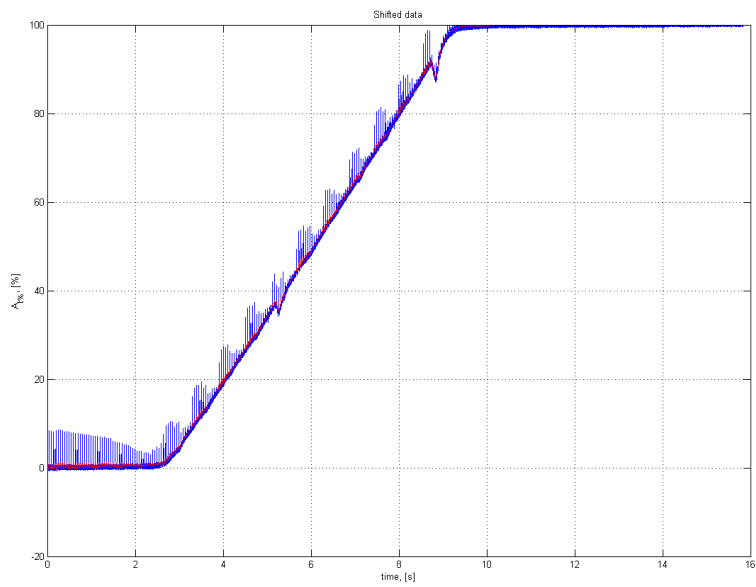


Figure E.1: Step in valve, 0 – 100%.

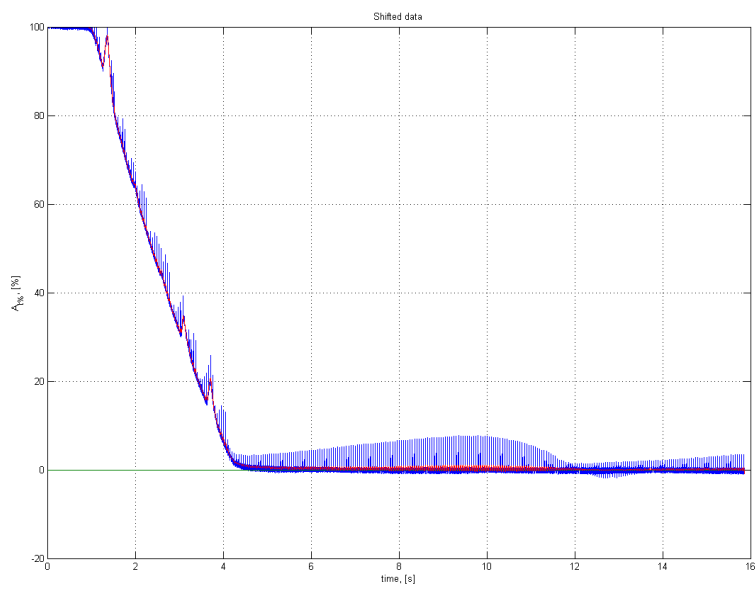


Figure E.2: Step in valve, 100 – 0%.

# Appendix F

## Contents of added disc.

This table serves as an overview of the contents on the added disc. The user of the disc is strongly advised to use the excel-table "Contents of cd" found on the root of the disc to obtain a full understanding of specific folders.

<b>Root folder</b>	<b>Sub folder</b>	<b>Description</b>
Compressor without recycling		Simulation model
Kalman Filters	data02032007 Run Kalman Filters	Measurement data Simulation model
Recycling directly downstream		Simulation model
Recycle From Plenum		Simulation model
Generic Component Model		Simulation model
Surge Avoidance Control	Mass Flow Reference Pressure Reference M and P Reference	Simulation model Simulation model Simulation model
Valve test data		Measurement data

Table F.1: Contents of cd